Design and Operation of Compressed Air Energy Storage (CAES) for Wind Power through Process Modelling and Simulation

A thesis submitted in partial fulfilment of the requirements for the degree of

Doctor of Philosophy

2018

Hui Meng

Supervisor: Prof Meihong Wang

Department of Chemical and Biological Engineering

Faculty of Engineering

The University of Sheffield

Acknowledgement

I would like to express my sincere gratitude to my supervisor Prof Meihong Wang for his support, patience, motivation and immense knowledge. His guidance and suggestions helped me in all the time of research, writing of this thesis and future development of career. I could not have imagined having a better supervisor for my PhD study.

My sincere thanks also go to Dr Olumide Olumayegun, Dr Xiaobo Luo and Dr Mathew Aneke for their insightful comments on my published journal papers. I would also like to thank all of the group members at the Process & Energy Systems Engineering Group and my friends at the University of Hull and the University of Sheffield.

I would like to thank my family for all their love and encouragement. My parents raised me with a love of science and supported me in all my pursuits. Most of all for my loving and encouraging wife Xiaoyan Liu, whose faithful support during the entire stages of my PhD study is so appreciated.

I am also grateful to the Great Britain-China Educational Trust (GBCET) for the support of the Chinese student awards.

Abstract

The compressed air energy storage (CAES) system, one of the grid-scale (>100MW) energy storage technologies, has been deployed in Germany and the USA. The round-trip efficiency of current commercial CAES plants is still low and needs to be improved. The CAES system will also play an important role in balancing electricity supply and demand because it can be integrated with renewable energy sources to overcome the intermittency problem. One unique feature of a CAES system integrated with wind power is that it is difficult to maintain constant operating conditions for CAES compression system due to fluctuating wind power output. The aim of this thesis is to study the approaches to improve the round-trip efficiency of CAES system, design and operation of the CAES system in the context of wind power and cost reduction when implementing the CAES system. This study is performed through process modelling, simulation and analysis.

In this study, an integrated system consisting of a CAES system and an organic Rankine cycle (ORC) was proposed to recover waste heat from the CAES system for improving the round-trip efficiency of the CAES system. Steady-state process models of the CAES system and the ORC were developed in Aspen Plus®. These models were validated using data from the literature. Process analysis was carried out using validated models regarding the impact of different organic working fluids (e.g. R123, R134a, R152a, R245fa, R600a) of ORC and expander inlet pressures of the ORC on system performance. It was found that integrating ORC with CAES system can be an effective approach to improve the performance of the CAES system. The round-trip efficiency was improved by 3.32-3.95%, compared to that of a CAES system without ORC.

The performance analysis of a CAES system in the context of wind power at design and off-design conditions were investigated through process simulation. Different operation strategies for fluctuating wind power outputs were proposed. Steady-state models for charging and discharging processes of the CAES system were developed in Aspen Plus® and validated. To enable off-design performance analysis, compressor and turbine characteristic curves were used during model development. A pseudo-dynamic model for cavern was developed in Excel. It was found that the CAES system at variable shaft speed mode has better performance than that at constant shaft speed mode because at variable shaft speed mode, it can utilise more excess wind energy (49.25 MWh), store more compressed air (51.55×10^3 kg), generate more electricity (76.00 MWh) and provide longer discharging time than at constant shaft speed mode.

Economic evaluation based on levelized cost of electricity (LCOE) was performed using Aspen Process Economic Analyser® (APEA). In terms of CAES system integrated with ORC, different working fluids in ORC and different power sources (e.g. wind and solar) associated with the CAES system were considered to estimate the LCOEs. It was found that the LCOEs for the integrated system were competitive with fossil-fuel fired power and even lower than offshore wind power and solar power. As for the CAES system in the context of wind power, it was found that the LCOE for the CAES system for wind power at variable shaft speed mode is lower than at constant shaft speed mode and the LCOEs at both modes are lower than solar and offshore wind power, conventional powers (e.g. natural gas combustion turbine) and especially the residential electricity price.

Results and insights presented in this PhD thesis will help to promote the commercial development of CAES technology.

Keywords:

CAES, Wind power, ORC, Process modelling, Process design, Process operation, Process integration.

Peer-reviewed Publications and Presentations

Part of this thesis has been published in the following peer-reviewed journals:

- **Meng, H.**, Wang, M., Aneke, M., Luo, X., Olumayegun, O. and Liu, X. (2018). Technical Performance Analysis and Economic Evaluation of a Compressed Air Energy Storage System Integrated with an Organic Rankine Cycle. *Fuel*, 211: 318–330.
- **Meng, H.**, Wang, M., Olumayegun, O., Luo, X. and Liu, X. (2018). Performance investigation and economic evaluation of compressed air energy storage (CAES) system integrated with wind power at design and off-design conditions. *Renewable Energy*. (Under Review)

The author contributed to the publication of the journal paper:

- Liu, X., Chen, J., Luo, X., Wang, M. and **Meng, H.** (2015). Study on Heat Integration of Supercritical Coal-Fired Power Plant with Post-Combustion CO_2 Capture Process through Process Simulation. *Fuel*, 158: 625–633.

Conference Presentation:

- **Meng, H.**, Wang, M., Olumayegun, O. (2018). Performance analysis at design and off-design conditions for a compressed air energy storage system integrated with wind energy. *12th European Conference on Coal Research and its Application (ECCRIA)*, Cardiff University, Cardiff, UK, 5-7 September 2018.

Table of Contents

List of Figures

List of Tables

Nomenclatures

E_T	The output power of Turbine (kWh)
E_C	Electrical energy taken from wind farm for driving the compressors (kWh)
E_f	Fuel input energy (kWh)
E_{ORC_1}	The power output of ORC during the charging period of the CAES system (kWh)
E_{ORC_2}	The power output of ORC during the discharging period (kWh)
E_{p_1}	The power consumption of ORC pump during the charging period (kWh)
E_{p_2}	The power consumption of ORC pump during the discharging period (kWh)
P_{EIP}	ORC expander inlet pressure (bar)
E_{output}	Net power output annually of the integrated system
P	The pressure of the cavern (Pa)
V	The volume of the cavern (m^3)
M_{Air}	The molar mass of the air (kg/kmol)
R	Ideal gas constant ($J\ K^{-1}\ mol^{-1}$)
T	The temperature in the cavern (K)
n	CAES plant lifetime (year)
i	Discount rate
r	Reference CAES system condition
s	Simulation result
re	Relative error
m_{Air}	The mass of the compressed air injected into the cavern (kg)

Greek Symbols

η_{sys}	System electric efficiency
η_{eff_1}	Round-trip efficiency of the CAES system
η_{eff_2}	Round-trip efficiency of the CAES system with system electric efficiency
$\eta_{CAES+ORC}$	Round-trip efficiency of the integrated system based on reducing the electricity taken from the grid
$\eta'_{CAES+ORC}$	Round-trip efficiency of the integrated system based on the round-trip efficiency of the CAES system

Abbreviations

ACAPEX	Annualised capital expenditure
AC	Alternating current
APEA	Aspen Process Economic Analyser®
CAPEX	Capital expenditure
CER	Charging electricity ratio
CRF	Capital recovery factor
CAES	Compressed air energy storage
DC	Direct current
FES	Flywheel energy storage
FOPEX	Fixed operation expenditure
HES	Hydrogen energy storage
HPC	High-pressure compressor
HPT	High-pressure turbine
HR	Heat rate
LCOE	Levelized cost of electricity
LHV	Lower heating value
LPC	Low-pressure compressor
LPT	Low-pressure turbine
ORC	Organic Rankine cycle
PHS	Pumped hydroelectric storage
SMES	Superconducting magnetic energy storage
TAC	Total annual cost
TES	Thermal energy storage
VOPEX	Variable operational expenditure

1. Introduction

This chapter will introduce the background and aim of this research. Section 1.1 summarises the up-to-date development status of global energy demand and greenhouse gases emissions, briefly introduces different energy storage technologies, compressors of the CAES system and wind turbines connected to the electricity grid. Section 1.2 presents the motivations for this study. Section 1.3 summarises the aim and objectives of this study. Section 1.4 justifies the predicted novel contributions. Section 1.5 explains the scope of this study. Section 1.6 introduces research methodology and the software tools used in this study. Finally, Section 1.7 gives the outline of the thesis.

1.1 Background

1.1.1 Energy demand and renewable energy

With the increase in global electrical energy demand, the annual amount of world electricity consumption reached 21,200 TWh in 2016 and the trend of global power consumption is still growing as shown in Figure 1-1 (Enerdata, 2017).

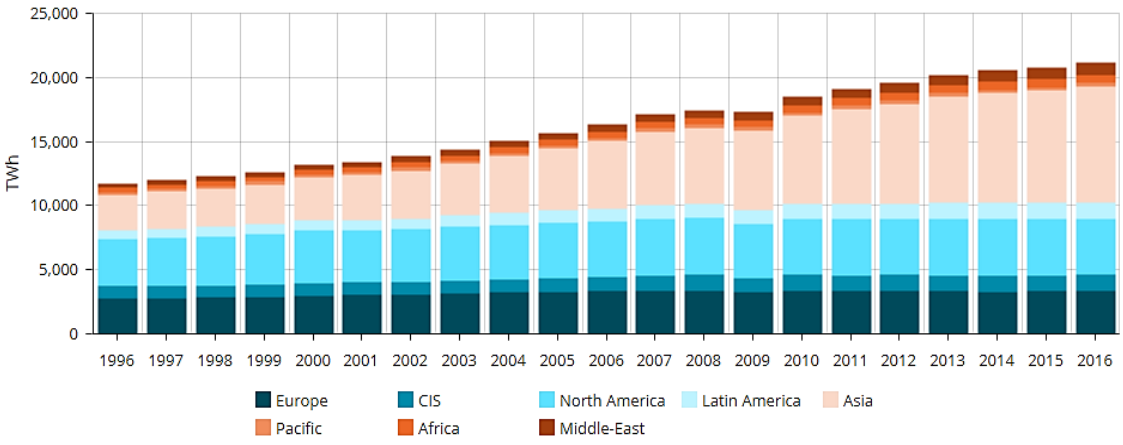

Figure 1-1. The situation of global electrical energy consumption from 1996 to 2016 (Enerdata, 2017).

Figure 1-2 shows that power generation by fossil fuels (e.g. coal, oil and natural gas) in conventional power plants contributed approximately 60% of world electrical energy supply in 2016 (IEA, 2017). As a result, massive CO_2 emissions released from these conventional power plants to the atmosphere has resulted in the problem of the greenhouse effect (Liu *et al.*, 2015).

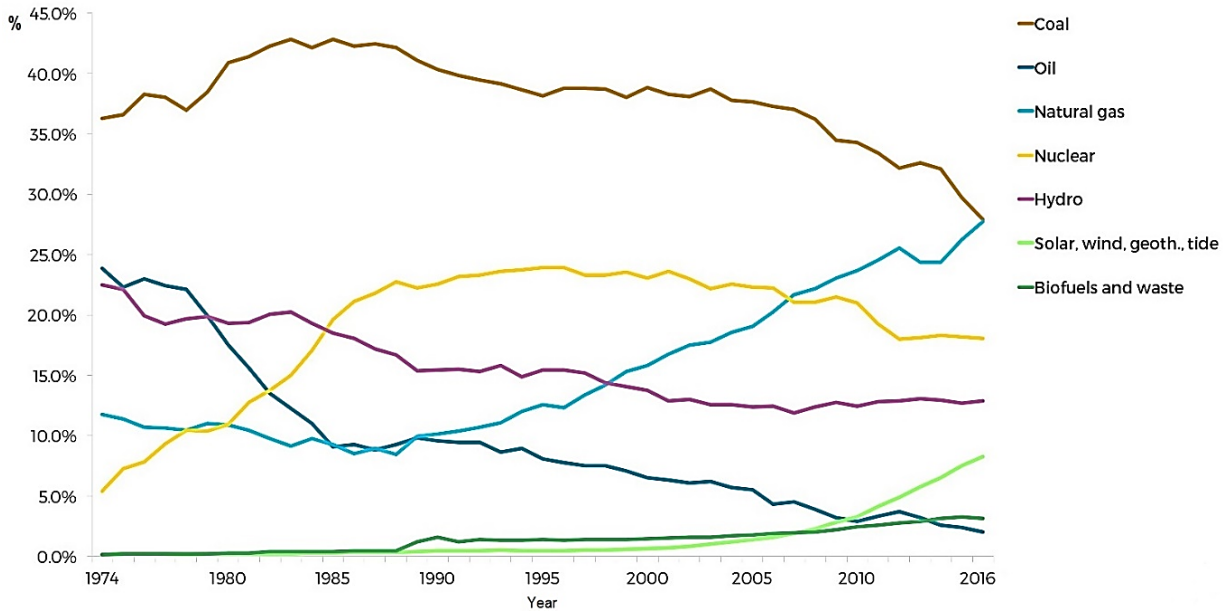

Figure 1-2. The situation of global electricity generation by different power sources from 1974 to 2016 (IEA, 2017).

To reduce the CO_2 emissions and also the high dependence on fossil fuels for power generation, renewable energy sources such as wind, solar and tide powers can be considered as alternative power generation sources (Skea and Nishioka, 2008; Ibrahim *et al.*, 2008; Castillo and Gayme, 2014). In recent years, renewable energy sources have increased to nearly 10% of the world power generation in 2016 (IEA, 2017). The capacity of wind power reached 3% of global electricity production in 2015 and it is expected to increase from 11.6% (3599 TWh) in 2030 to 14.8% (6145 TWh) in 2050 (Bouman *et al.*, 2016). However, the majority of renewable energy

sources have a common problem of intermittency. The increasing utilisation of renewable energy sources could lead to an imbalance between electricity generation and demand due to the intermittent nature of renewable energy sources, whose output mainly depends on local environmental conditions and unpredictable weather (Pan *et al.*, 2016; Arsie *et al.*, 2009). This brings a great challenge to ensure the stability and reliability of the electricity grid (Luo *et al.*, 2015; Ibrahim *et al.*, 2008; Sundararagavan and Baker, 2012). Wind power is one of the major renewable energy sources. Implementing energy storage technologies for wind power can overcome this problem and improve the stability and reliability of the electricity grid (Chen *et al.*, 2009; Beaudin *et al.*, 2014; Liu *et al.*, 2017; Sioshansi *et al.*, 2011).

1.1.2 Energy storage and energy storage technologies

1.1.2.1 Energy storage and benefits

The basic concept of energy storage is to store the energy and generate the energy for use when needed (Luo *et al.*, 2015; Chen *et al.*, 2009). The process of storing the energy can be regarded as the charging process, the process of releasing the energy can be regarded as the discharging process. Various working mediums used to store the energy can be regarded as the energy carriers (Aneke and Wang, 2016). Figure 1-3 presents the schematic concept of energy storage.

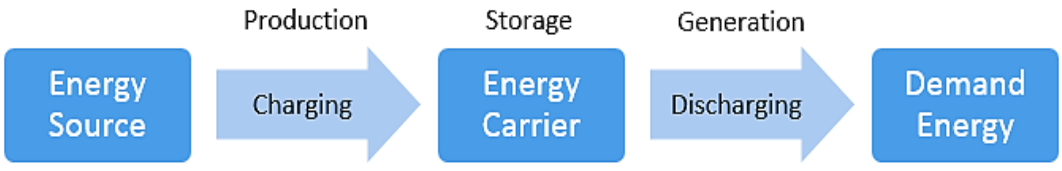

Figure 1-3. The schematic concept of energy storage (Aneke and Wang, 2016).

A key benefit of energy storage is better energy storage management, which can reduce the waste of energy and enhance the energy utilisation efficiency of power systems (Abedin and Rosen, 2012; Chan *et al.*, 2013; Aneke and Wang, 2016). A process of electrical energy storage is to convert electricity into a form of energy stored for converting back to electricity when needed (Chen *et al.*, 2009; Luo *et al.*, 2015). The electrical energy storage can be one of the most promising methods to address the problem of intermittent renewable energy sources and energy storage technologies have become increasingly important in balancing supply and demand of electricity to improve the quality and maintain stability of the grid network, as well as help in load shifting and peak shaving (Ibrahim *et al.*, 2008; Radcliffe, 2013; Pardo *et al.*, 2014; Castillo and Gayme, 2014; Kousksou *et al.*, 2014).

1.1.2.2 Classification of energy storage technologies

There are two suggested approaches to categorise the different energy storage technologies, depending on their functions and forms of stored energy (Chen *et al.*, 2009). The classification of energy storage technologies is shown in Figure 1-4. Energy storage technologies can be classified by the form of stored energy into mechanical, electrical, chemical and thermal energy storage technologies. According to the functional classification, energy storage technologies can be divided into technologies for energy management, and power quality and reliability. By comparison, the most widely adopted method of the classification for energy storage technologies is according to the form of stored energy (Chen *et al.*, 2009; Luo *et al.*, 2015; Aneke and Wang, 2016).

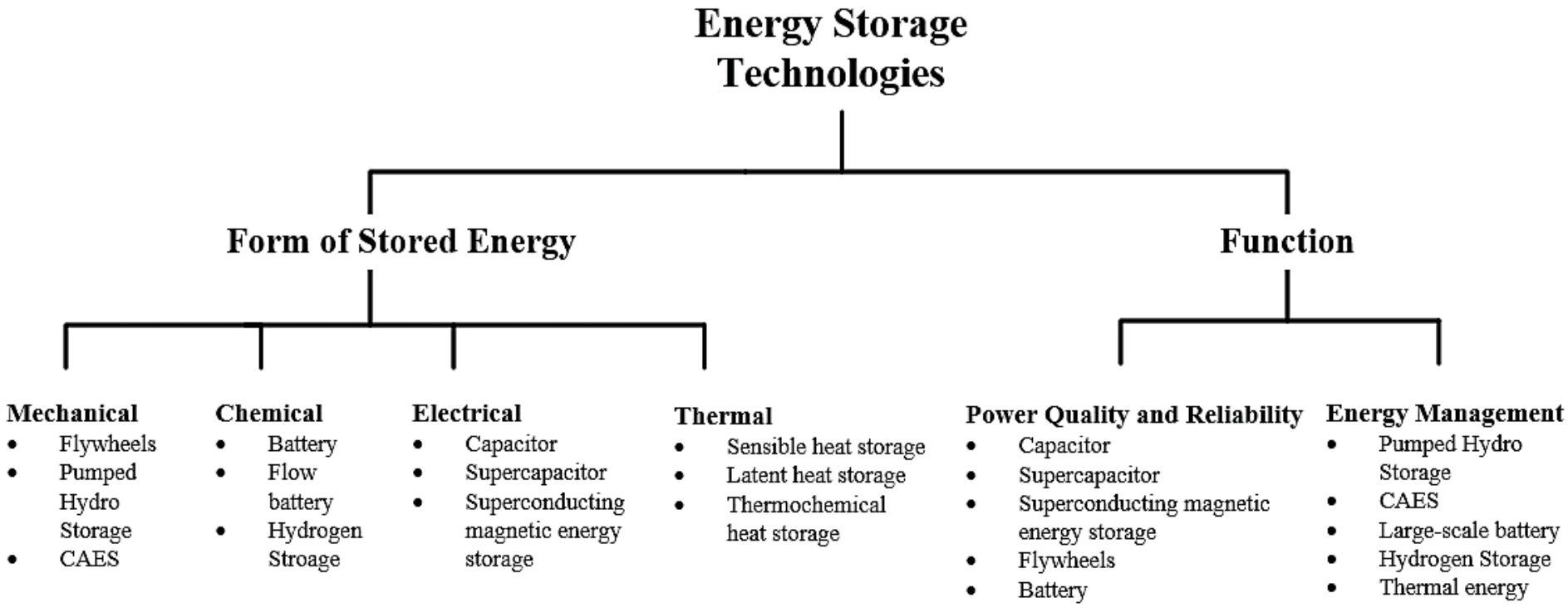

Figure 1-4. Classification of energy storage technologies (Chen *et al.*, 2009; Aneke and Wang, 2016; Luo *et al.*, 2015).

1.1.2.3 Brief introduction to energy storage technologies

1.1.2.3.1 Pumped Hydroelectric Storage (PHS)

PHS is a mature technology and widely implemented large-scale energy storage technology (more than 100 MWe). The schematic diagram of the PHS is shown in Figure 1-5.

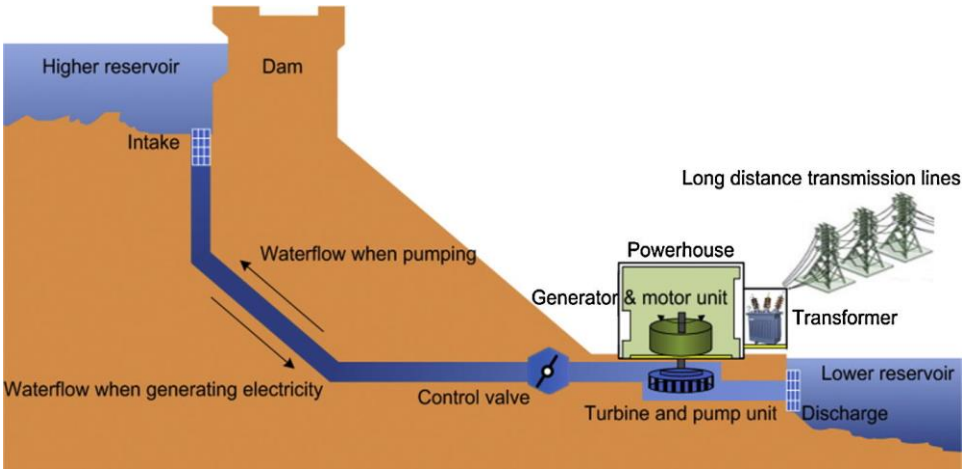

Figure 1-5. The schematic diagram of PHS (Luo *et al.*, 2015).

There are two reservoirs located at different elevations. During the period of the charging process, water is pumped from a lower reservoir to a higher reservoir using off-peak electricity. During the period of the discharging process, the water flows from the higher reservoir to the lower reservoir to drive the turbine and to generate electricity. The rated power of PHS power plants can be between 1MWe and 3,003 MWe, the round-trip efficiency is around 70-85% with more than 40 years lifetime (Chen *et al.*, 2009; Luo *et al.*, 2015; Aneke and Wang, 2016; Ibrahim *et al.*, 2008). Currently, there is more than 78,000 MWe capacity of PHS power plants in the world and the percentage of the PHS is over 99% of the worldwide large-scale energy storage construction (Aneke and Wang, 2016). One major limitation of PHS is the geographical requirement, including two large reservoirs at different

elevations. A long lead time (about 10 years) and high initial capital cost for construction, as well as environmental impacts, are constraints for the PHS development (Denholm and Kulcinski, 2004; Ferreira *et al.*, 2013; Luo *et al.*, 2015; Chen *et al.*, 2009).

1.1.2.3.2 CAES

In addition to PHS, CAES is another large-scale energy storage (more than 100 MW) technology. A schematic diagram of a CAES system is given in Figure 1-6.

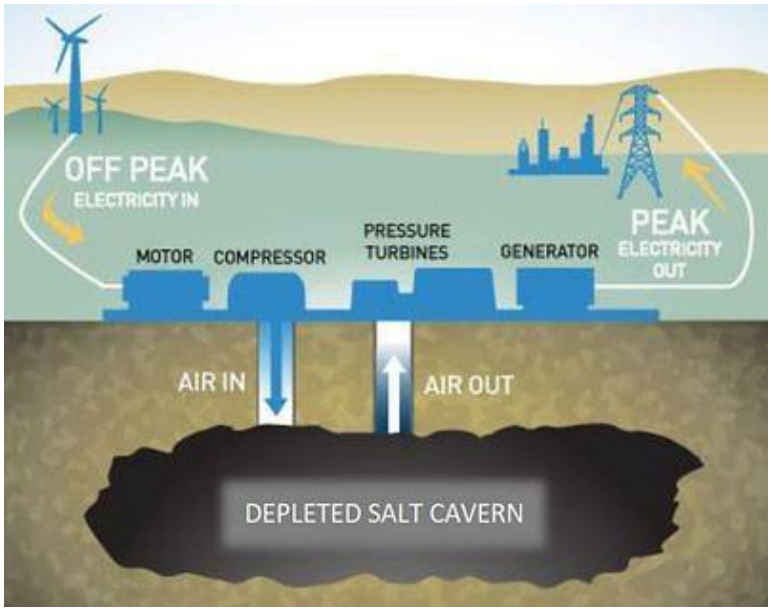

Figure 1-6. The schematic diagram of the CAES system (Ryan, 2017).

During the period of the charging process, the surplus off-peak electricity will be utilised to drive the compressors of the CAES system for compressing and injecting the air into the cavern. During the period of the discharging process, the compressed air stored in the cavern can be released and expanded in the turbines for generating electricity at peak time. Currently, there are two commercial CAES plants in the world, one is the Huntorf CAES plant established in 1978 with a rated power of 290 MWe and round-trip efficiency of around 42% in Germany, another is the McIntosh

CAES plant established in 1991 with a rated power of 110 MWe and round-trip efficiency of around 54% in the USA. The advantages of the CAES system include flexible size from kW to MW and it can be integrated with renewable energy sources to overcome the problem of intermittency. Nevertheless, the drawbacks of this system include the high initial capital cost and the limitation of the underground cavern. Details of the working principle of the CAES system will be described in Section 1.1.3.

1.1.2.3.3 Flywheel Energy Storage (FES)

An FES system consists of five key components: a flywheel, magnetic bearings, a motor/generator unit and a vacuum chamber (Amiryar and Pullen, 2017). The schematic diagram of the FES system is shown in Figure 1-7.

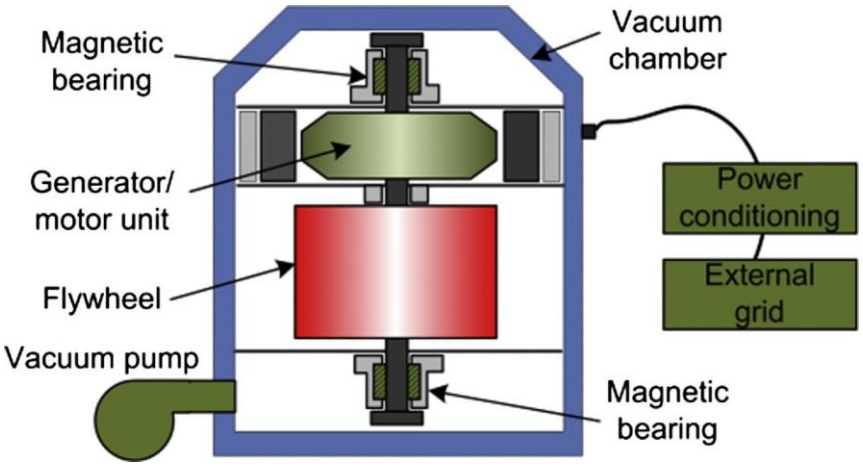

Figure 1-7. The schematic diagram of the FES system (Luo *et al.*, 2015).

During the period of the charging process, the electricity is utilised to accelerate the motor connected to the flywheel through the bearing, the shaft rotation can transfer the rotational momentum to the flywheel which can store the energy. During the period of the discharging process, the flywheel transfers the kinetic energy and converts it back to electricity using the generator connected to the shaft. FES can be

classified into two types based on the rotating speed: low-speed and high-speed FES. The rotating speed of the low-speed FES is less than 6000 rpm, the high-speed FES is up to approximately 100,000 rpm (Pena-Alzola *et al.*, 2011). The amount of energy stored depends on the rotating speed of the flywheel. The round-trip efficiency of the FES could be as high as 95%. It has a high power density, low maintenance cost, long lifetime and it is environmentally friendly (Luo *et al.*, 2015; Aneke and Wang, 2016). However, the FES is not good for long time energy storage and the frictional force could decrease the round-trip efficiency in the process of operation (Ibrahim *et al.*, 2008).

1.1.2.3.4 Conventional Battery

The conventional battery is the oldest way for electrical energy storage, which can store the electricity in the form of chemical energy. A rechargeable battery involves three key parts: the positive electrode (anode), the negative electrode (cathode) and the liquid, paste or solid electrolyte. These three sections constitute an electrochemical cell. During the process of discharging, the chemical reactions occur at the two electrodes and current flows through the external circuit from the anode to the cathode. During the charging process, the reaction will occur reversibly, the battery can be recharged by applying an external voltage across the electrodes (Ferreira *et al.*, 2013; Chen *et al.*, 2009). Most of the batteries can respond rapidly to load changes, which can improve the stability of the electricity grid or system. Batteries have a high energy efficiency (up to 95%), short lead time and easy installation (Kondoh *et al.*, 2000; Kluiters *et al.*, 1999; Luo *et al.*, 2015). However, the disadvantages of batteries include low energy densities, small power capacity, high maintenance costs and short lifetimes. Also, many batteries contain toxic

materials which have a negative impact on the environment (Chen *et al.*, 2009). There are different types of batteries in development, including lead acid, nickel cadmium, sodium sulphur, sodium nickel chloride and lithium-ion batteries (Luo *et al.*, 2015; Aneke and Wang, 2016).

- *Lead-acid (PbO_2) battery*

The lead-acid battery is the oldest rechargeable battery and is used widely for both household and commercial applications. The schematic diagram of the lead-acid battery is shown in Figure 1-8. The anode is made of PbO_2, the cathode is made of *Pb* and the electrolyte is sulfuric acid. The lead-acid battery has a rapid response time, low capital cost and high cycle efficiency with 63-90% (Hadjipaschalis *et al.*, 2009; Kondoh *et al.*, 2000; Luo *et al.*, 2015). The lead-acid battery can be used as backup power for telecommunication systems and energy management systems. For example, it has been implemented as power sources in the vehicle industries (Ferreira *et al.*, 2013; Luo *et al.*, 2015). The drawbacks of the lead-acid battery include low cycle time (up to about 2000) and low energy density (Baker, 2008).

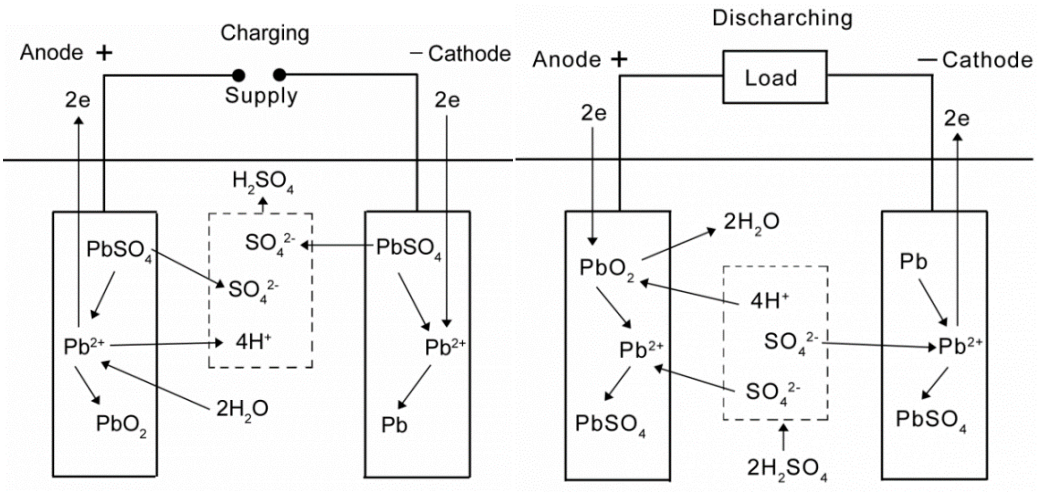

Figure 1-8. The schematic diagram of the lead-acid battery (ITACA, 2018).

- *Nickel-cadmium (NiCd) battery*

The NiCd battery is one of the most developed nickel-based batteries. It consists of a nickel hydroxide positive electrode plate, a cadmium hydroxide negative electrode plate and an alkaline electrolyte (Chen *et al.*, 2009). The NiCd battery has high energy density and low maintenance requirements. Nonetheless, the weakness of this kind of battery is the high capital cost which is about 10 times higher than the lead-acid battery and the toxic metals (cadmium and nickel) which could be harmful to the environment (Aneke and Wang, 2016; Ferreira *et al.*, 2013).

- *Sodium Sulphur (NaS) battery*

NaS battery is considered as one of the most promising batteries implemented for energy storage in the fields of electricity distribution grid system, wind power integration and high-value grid service (Luo *et al.*, 2015; Aneke and Wang, 2016). As shown in Figure 1-9, a NaS battery includes molten sodium at the negative electrode, molten sulphur at the positive electrode and employs beta-alumina as the solid electrolyte.

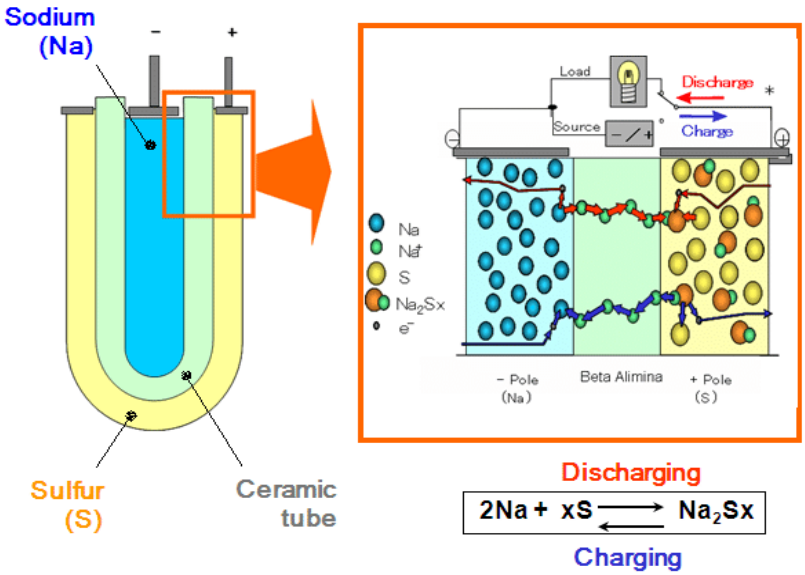

Figure 1-9. The schematic diagram of the NaS battery (Espinar and Mayer, 2011).

This battery needs to be operated at a high-temperature environment (e.g. 300-350˚C) during the periods of charging and discharging processes. The NaS battery can provide high energy density, high energy efficiency, long cycle life (~2500) and long discharge time (around 6 hours). The weaknesses of this kind of battery include a high operating temperature and a high capital cost. Sodium is combustible when it is exposed to water.

- *Sodium Nickel Chloride ($NaNiCl_2$) battery*

The $NaNiCl_2$ battery is similar to the NaS battery, it also needs a high operation temperature at around 270-350˚C. During the process of charging, NaCl salt and Ni can be converted into $NiCl_2$ and molten Na. The chemical reaction will be reversed during the process of discharging (Aneke and Wang, 2016). Compared with the NaS battery, the $NaNiCl_2$ battery has better safety characteristics, but the moderate energy density could be a weakness (Luo *et al.*, 2015). At present, this battery has been used in the electric vehicles and submarines (Ferreira *et al.*, 2013).

- *Lithium-ion (Li-ion) battery*

The Li-ion battery (refer to Figure 1-10) uses a lithiated metal oxide as the cathode and graphitic carbon with a layering structure as the anode (Chen *et al.*, 2009). This battery has been widely used for portable electronics and medical units. Compare with other batteries, the Li-ion battery is smaller, lighter and more powerful. The energy density is around 90-190 Wh/kg and power density is around 500-2000 W/kg (Hadjipaschalis *et al.*, 2009; Aneke and Wang, 2016). Moreover, it has high efficiency and low self-discharge rate. The drawbacks of the Li-ion battery include that the life cycle is easily affected by the temperature and the high capital cost also

limits the development in the large capacity applications (Aneke and Wang, 2016; Chen *et al.*, 2009).

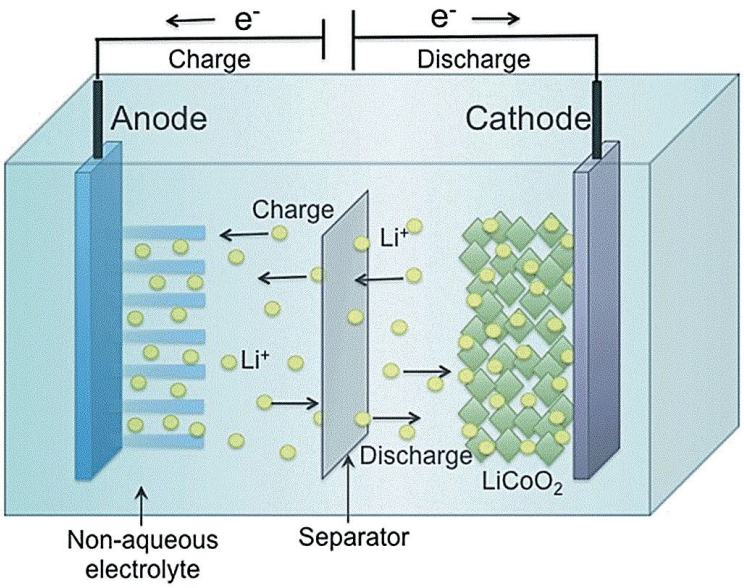

Figure 1-10. The schematic diagram of the Li-ion battery (Roy and Srivastava, 2015).

1.1.2.3.5 Flow Battery Energy Storage

Unlike the conventional batteries, the flow battery can store energy in two soluble redox couples which are located in the external tanks of liquid electrolyte. The electrolytes are pumped from the tanks to the cell stack which includes two electrolyte flow compartments and the cell stack is separated by the ion-selective membranes. Thus, the capacity of the flow battery is mainly determined by the size of the electrolyte tanks, the rated power is mainly determined by the size of the cell stacks (Ferreira *et al.*, 2013; Luo *et al.*, 2015). The operation of the flow battery is dependent on the reduction-oxidation reactions of the electrolyte solutions. During the period of the charging process, one of the electrolytes at the anode will be oxidised, another electrolyte at the cathode will be reduced. The electricity charged

can be transformed into the chemical energy of the electrolyte. The reaction process will be reversed for generating electricity during the period of the discharging process (Ferreira *et al.*, 2013).

The flow batteries have a high efficiency and short response time compared with other batteries. The weaknesses of the flow batteries include the low power density and the toxic characteristics of some materials (Ferreira *et al.*, 2013). Currently, there are two types of flow batteries available for the commercial applications, vanadium redox (VRB) (refer to Figure 1-11) and zinc bromic (ZnBr) (refer to Figure 1-12) batteries.

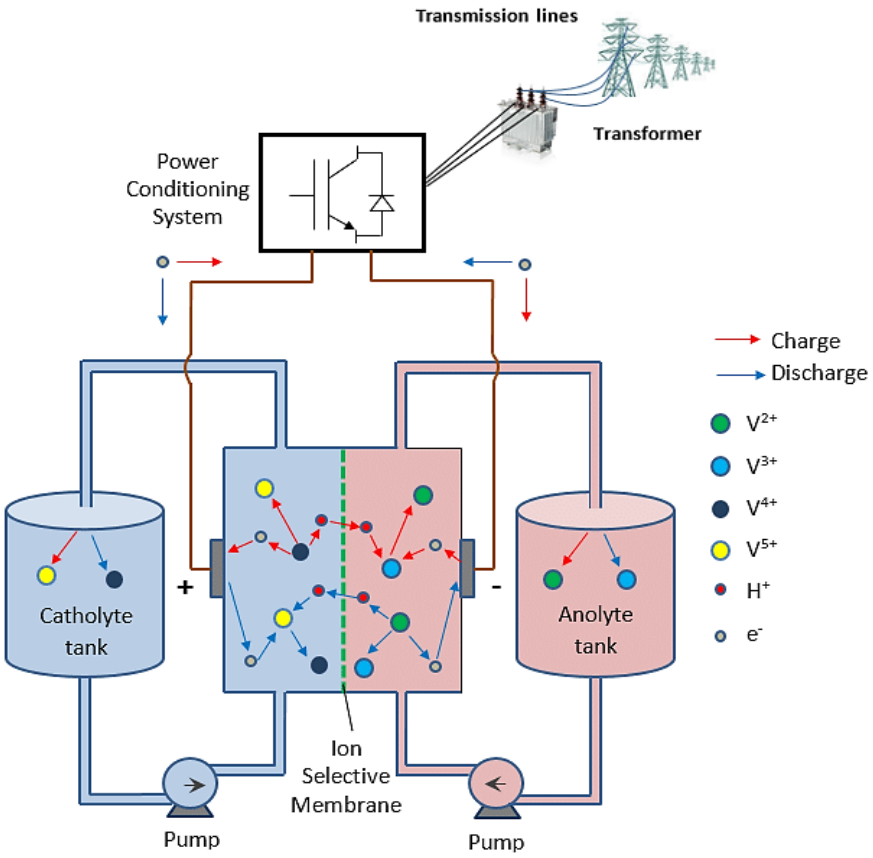

Figure 1-11. The schematic diagrams of VRB flow batteries (Nikolaidis and Poullikkas, 2017).

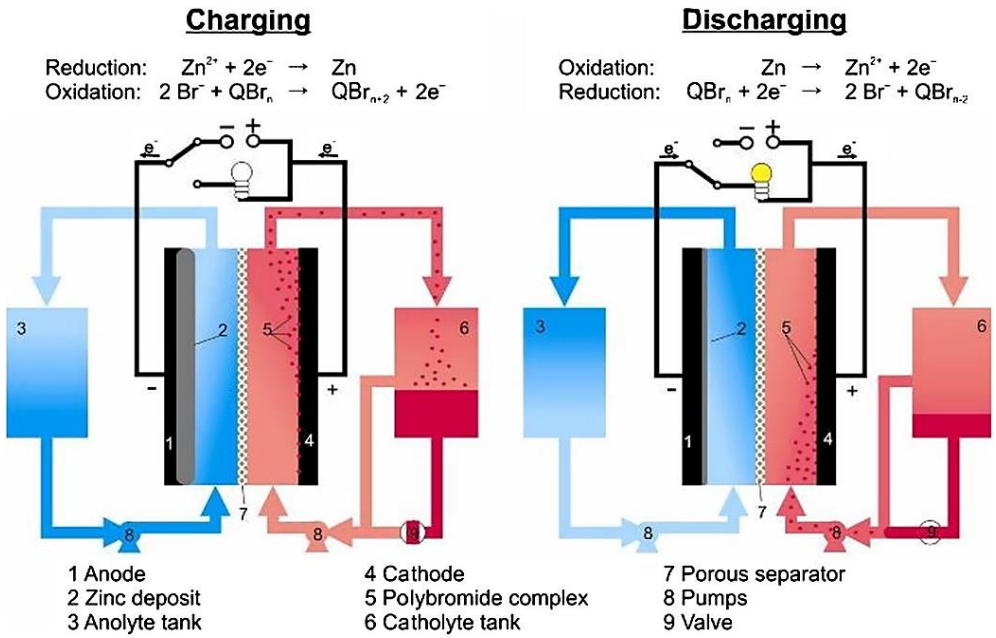

Figure 1-12. The schematic diagrams of ZnBr flow batteries (Akhil *et al.*, 2016).

The VBR is a mature flow battery system, it has a short response time, long cycle life (~10000 - 16000) and high efficiency (around 85%), but low energy density and high operating cost are the weaknesses which prevent its commercial development. The ZnBr flow battery has a high energy density (~30-65 Wh/L), but the cycle efficiency is low (approximately 65-75%) and the operating temperature range is narrow (Luo *et al.*, 2015).

1.1.2.3.6 Hydrogen Energy Storage (HES)

The HES is one of the most popular chemical energy storage technology because hydrogen is an efficient, clean and storable energy carrier (Carrasco *et al.*, 2006). As shown in Figure 1-13, during the period of the charging process, the off-peak electricity can be used to electrolyse water to generate hydrogen for later use. The hydrogen can be stored as different forms such as gas or liquid. During the period of discharging process, the stored hydrogen is used in the fuel cell and or burned directly to generate the electricity for the grid (Díaz-González *et al.*, 2012; Luo *et*

al., 2015). One major weakness of the HES is that the energy loss during the operation of a single cycle results in the low round-trip efficiency of the entire system (Schüth, 2012).

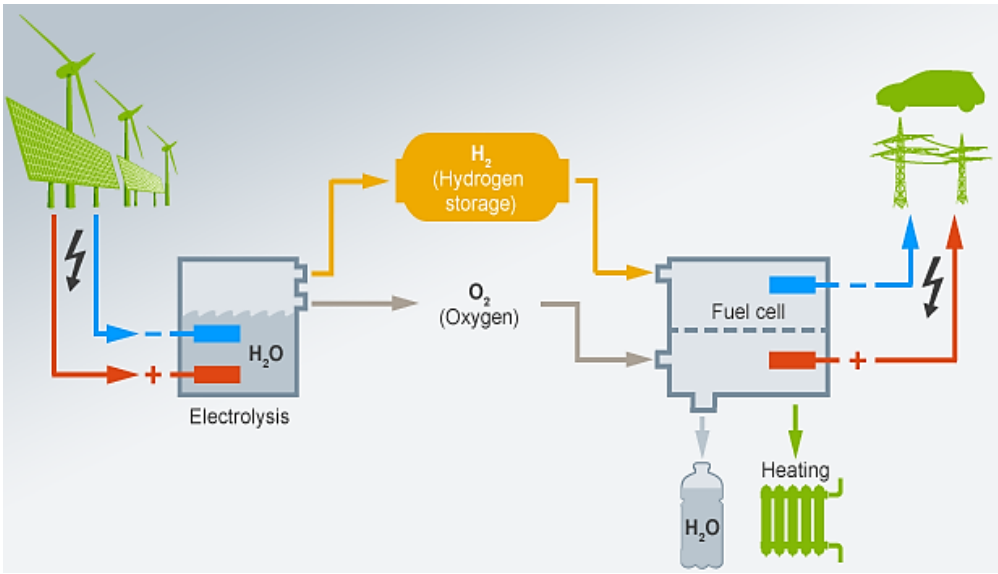

Figure 1-13. The schematic diagram of the HES (Ruiz, 2016).

1.1.2.3.7 Capacitor and Supercapacitor

A capacitor consists of two electrical conductors which are separated by a thin and nonconducting layer named a dielectric. When the capacitor is charged, the energy can be stored in an electrostatic field (Arepalli *et al.*, 2005; Chen *et al.*, 2009). Compared with the batteries, the capacitors have a higher power density and shorter charging time. Nevertheless, the development limitations of the capacitors are the finite capacity, low energy density and high energy dissipation because of the high self-discharge losses (Arepalli *et al.*, 2005; Chen *et al.*, 2009; Luo *et al.*, 2015). Supercapacitors, also called electric double-layer capacitors, include two conductor electrodes, a porous membrane separator and an electrolyte (refer to Figure 1-14).

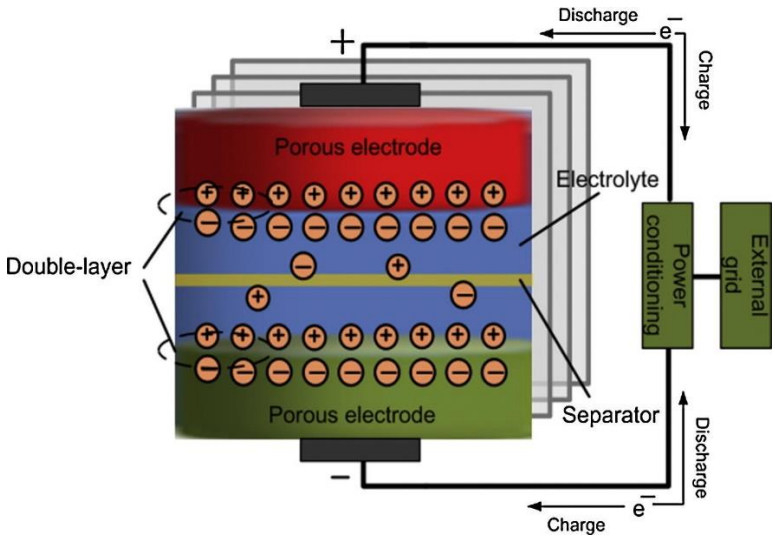

Figure 1-14. The schematic diagram of a supercapacitor (Luo *et al.*, 2015).

Compared with the capacitor and electrochemical battery, the supercapacitor has both the characteristics of electrochemical batteries and capacitors (Luo *et al.*, 2015). The supercapacitors store energy in the form of an electrolyte solution between two solid conductors instead of the general arrangement of a solid dielectric between the electrodes. The capacity of energy storage of the supercapacitor is much higher than the capacitor (Chen *et al.*, 2009). The supercapacitors have long cycle times (> 100,000 times) and high cycle efficiency (Smith *et al.*, 2008). Nonetheless, the self-discharge rate (around 5-40%) and the capital cost are high (Ibrahim *et al.*, 2008; Díaz-González *et al.*, 2012).

1.1.2.3.8 Superconducting Magnetic Energy Storage (SMES)

A SMES system includes three key components: a refrigerator and vacuum system, a power conditioning system and a superconducting coil/magnet unit. The schematic diagram of the SMES system is shown in Figure 1-15. The SMES system stores energy in the magnetic field created by the flow of the direct current (DC) in the superconducting coil, the temperature of the stored energy can be cooled to be lower

than its superconducting critical temperature. During the period of the discharging process, the stored energy can be released to the alternating current (AC) system using a power coverter module.

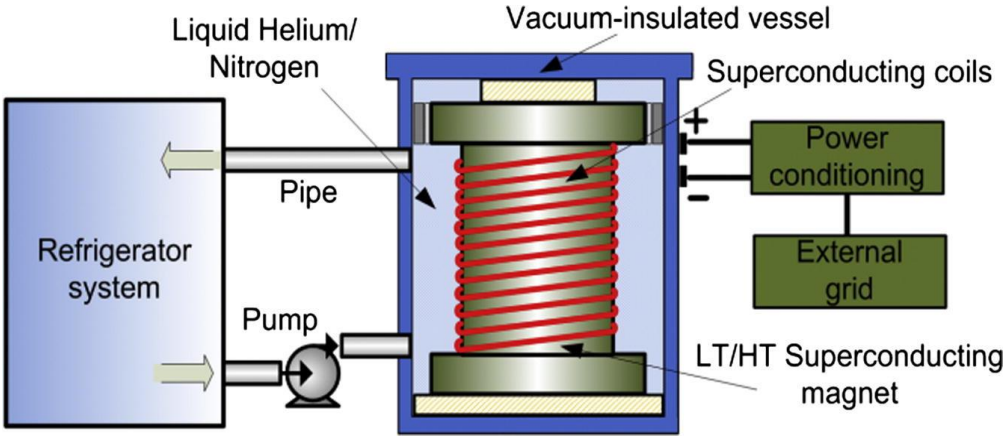

Figure 1-15. The schematic diagram of the SMES system (Luo *et al.*, 2015).

The DC will increase during the charging process of the SMES system. The advantages of SMES system include a high power density (~4000 W/L), rapid response time, high cycle efficiency (~95-98%) and long lifetime (up to 30 years) (Smith *et al.*, 2008; Chen *et al.*, 2009; Luo *et al.*, 2015; Schoenung, 2001). The drawbacks of the SMES system include high capital cost, high self-discharging rate (10-15%) and effects of the strong magnetic field (Schoenung, 2001; Beaudin *et al.*, 2014).

1.1.2.3.9 Thermal Energy Storage (TES)

The TES technology can store the heat energy in the tanks/ reservoirs which can be used to store electricity or recover waste heat using different methods. There are three key approaches including sensible heat storage, latent heat storage and thermochemical heat storage methods. The sensible heat storage stores energy through changing temperature of the material (e.g. molten salt), the latent heat

storage stores energy through the phase change of materials (e.g. paraffin), the thermochemical heat storage stores energy through the chemical structure changes of the materials (e.g. metallic hydrides: CaH_2; organic system: CH_4/H_2O) (Aneke and Wang, 2016; Ibrahim *et al.*, 2008; Sharma *et al.*, 2009). The self-discharge rate is low (about 0.05-1%), the storage reservoirs have a high energy density (80-500 Wh/L). However, the round-trip efficiency of TES is low (around 30-60%) (Ibrahim *et al.*, 2008; Chen *et al.*, 2009; Luo *et al.*, 2015).

1.1.2.4 Comparison of technical characteristics of energy storage technologies

Table 1-1. Comparison of technical characteristics of different energy storage technologies (Aneke and Wang, 2016; Luo *et al.*, 2015; Chen *et al.*, 2009; Zhao *et al.*, 2015; Hadjipaschalis *et al.*, 2009).

System	Energy density (Wh/L)	Power density (W/L)	Power rating (MW)	Discharging time	Suitable storage duration	Response time	Round-trip efficiency (%)	Capital cost ($/kW)
PHS	0.5-1.5	0.1-0.2	100-5000	1-24 hrs+	Hours-months	Minutes	70-85	600-2000
CAES	2-6	0.2-0.6	5-300	1-24 hrs+	Hours-months	Minutes	40-75	400-800
FES	20-80	5000	0-0.25	Up to 15mins	Seconds-minutes	< Second	85-95	250-350
PbO_2	50-80	90-700	0-20	Seconds-hours	Mintues-days	< Second	63-90	300-600
NiCd	15-80	75-700	0-40	Seconds-hours	Mintues-days	< Second	60-80	500-1500
NaS	15-300	120-160	0.05-8	Seconds-hours	Seconds-hours	< Second	70-90	1000-3000
$NaNiCl_2$	150-180	220-300	0-0.3	Seconds-hours	Seconds-hours	< Second	85-90	150-300
Li-ion	200-400	1300-10000	0-0.1	Mintues-hours	Mintues-days	< Second	90-97	1200-4000
VRB	20-70	0.5-2	0.03-3	Seconds-10 hrs	Hours-months	Seconds	65-85	600-1500
ZnBr	30-60	1-25	0.05-2	Seconds-10 hrs	Hours-months	Seconds	65-75	700-2500
HES	500-3000	0.2-20	0-50	Seconds-24 hrs+	Hours-months	Seconds-mintues	20-50	10000+
Capacitor	2-10	100000+	0-0.05	Up to 60 mins	Seconds-hours	< Second	60-70	200-400
Supercapacitor	10-20	40000-120000	0-0.3	Up to 60 mins	Seconds-hours	< Second	85-98	100-300
SMES	0.2-6	1000-4000	0.1-10	Up to 8s	Seconds-1 hour	< Second	95-98	200-300
TES	80-500	–	0.1-300	1-24 hrs+	Mintues-months	Not for rapid response	30-60	100-400

Some enegy storage technologies have unique charateristics which can be implemented in the particular energy storage applications. These unique characteristics can help in the selection of the proper energy storage technologies to be used in any given conditions. The details of technical characteristics of different energy storage technoilogies are summarised in Table 1-1.

1.1.3 Process description of the CAES system

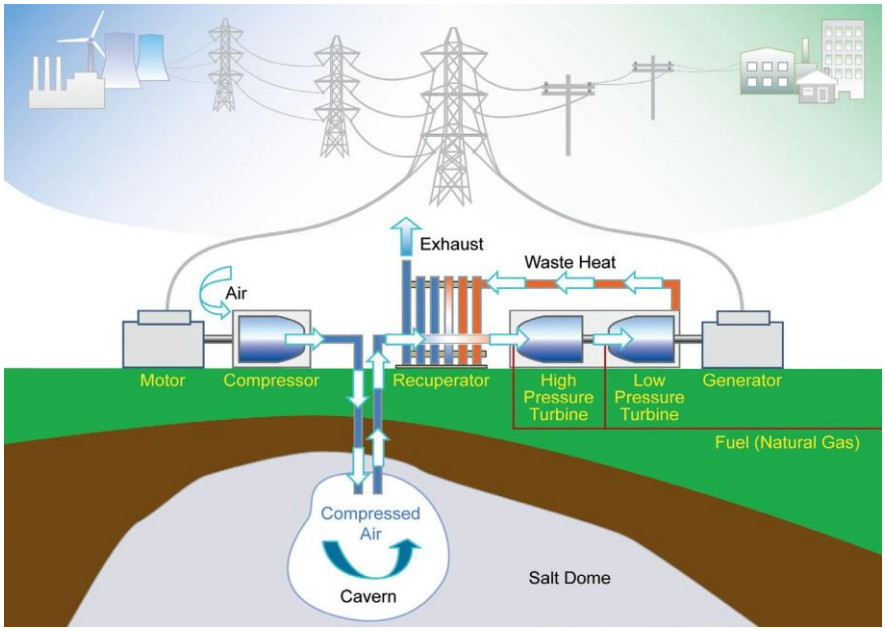

Figure 1-16. A schematic diagram of a CAES system (Butcher, 2010).

A CAES process (as shown in Figure 1-16) consists of three main subsystems: air charging, compressed air storage and compressed air discharging subsystems. In the charging subsystem, excess electricity at the off-peak time is utilised to compress air. The compressed air is injected into underground storage at high pressure. In the discharging subsystem, the stored compressed air in the cavern is extracted for generating electricity. The compressed air extracted is first preheated in the recuperator with recovered waste heat from the exhaust of the low-pressure turbine

before the waste heat is released to the atmosphere. The preheated air then passes into the combustion chambers where it is mixed with fuel (e.g. natural gas or methane) to be combusted. The high-temperature combustion product is expanded in the turbines to produce electricity (Chen *et al.*, 2013; Elmegaard and Brix, 2011; Luo *et al.*, 2014).

Currently, there are mainly two types of CAES system: the traditional CAES (also called diabatic CAES) and the adiabatic CAES (A-CAES). The traditional CAES is commercialised and has successfully been operated in the Huntorf CAES plant and the McIntosh CAES plant. Compared with the diabatic CAES system, the A-CAES (See Figure 1-17) can store the waste heat from the compression in the heat storage of charging process and re-use the waste heat to preheat the compressed air during the discharging process (Budt *et al.*, 2016). A higher efficiency of up to 70% could be achieved and there is no longer any need to burn extra fuel (such as natural gas) to heat the compressed air. However, the A-CAES is still under research and not commercialised in the industry (ESA, 2017; Budt *et al.*, 2016).

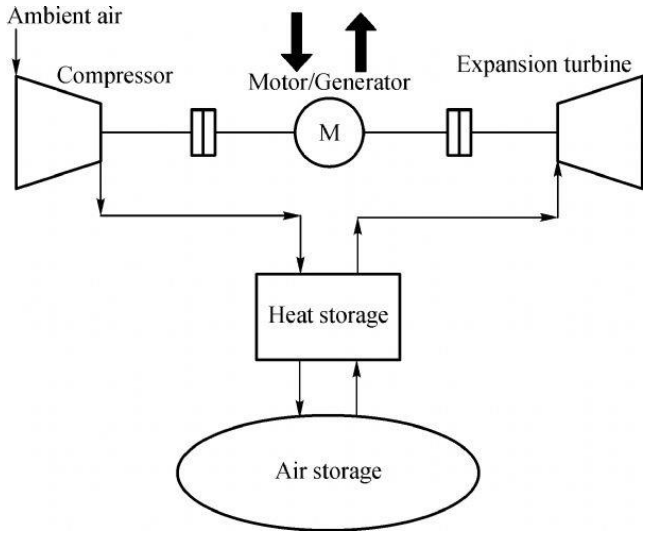

Figure 1-17. A schematic diagram of an A-CAES system (Ni and Chen, 2011).

1.1.4 Historical development of the CAES technology

The elementary idea of using compressed air to store the electrical energy traces back to the early 1940s (Kalhammer and Schneider, 1976). However, the development of the CAES technology was not rigorously pursued by the scientific research community and the industry due to lack of necessity and feasibility of a grid network connecting to energy storage technologies. It was not concerned until the 1960s when CAES technology attracted great interest due to the geographical limitations of PHS. The Brown Boveri Company (BBC) proposed the concept of the gas turbine air storage peaking plant. The CAES technology was further mentioned and began to rise through the mid-1970s (Kalhammer and Schneider, 1976). The Huntorf CAES plant, as the first CAES plant in the world, was operated by the BBC company in Germany in 1978 (Crotogino *et al.*, 2001). The details of this plant will be described in Section 2.3.1. With the successful operation of the Huntorf CAES plant and development of the CAES technology, the second generation A-CAES was investigated by Electric Power Research Institute (EPRI) (Budt *et al.*, 2016). Moreover, the Pacific Northwest National Laboratory (PNNL) asserted that A-CAES would be the most suitable and promising technology for energy storage (Zaloudek and Reilly, 1982). Nonetheless, the A-CAES project was postponed due to the successful establishment of the first CAES plant (e.g. McIntosh diabatic CAES plant) in the USA.

The McIntosh CAES plant was operated by PowerSouth Electric Cooperative in 1991 (PowerSouth Electric Cooperative, 2017). The description of this plant and comparison between the Huntorf and McIntosh CAES plants will be summarised in Sections 2.3.2 and 2.3.3. The operation of the McIntosh CAES plant had attracted

much interest from several US companies, such as Hawaiian Electric Co. and Tennessee Vally Authority. However, neither of them attempted to construct a commercialized plant (Budt *et al.*, 2016). In 2001, a Norton CAES project was planned for 2700 MWe (9×300 MWe) power output. However, this project has not been operated so far due to unfavourable low electricity prices. The Seneca CAES project was planned by NYSEG in the USA in 2012, but it was also cancelled because of economic conditions. The Apex Bethel Energy Centre planned a 317 MWe CAES project which started to be constructed in 2017 and expected to be operated in 2020 (Holloway, 2016; ApexCAES, 2017). A UK CAES project called 'Project-CAES Larne' was planned by Gaelectric Energy Storage (GES) in Northern Ireland in 2011. The rated power output of this project is 330 MWe (Budt *et al.*, 2016; Gaelectric, 2011). Details of this project will be described in Section 2.4.4.

Although many researches about the CAES technology are investigated, there is no more commercial CAES plant to be operated after the operation of the McIntosh CAES plant. Furthermore, the A-CAES technology is still under research. The EPRI only promotes the concepts of the CAES with few development efforts (Rice and Li, 2011). At present, the important features of the Huntorf and McIntosh CAES plants include black start capability and load shifting. Moreover, to overcome the intermittency problem of the renewable energy by integrating the CAES system with renewable energy can be another important driver for the development of the CAES technology. However, the CAES technology can be integrated with renewable energy sources was mentioned without being of importance. The CAES technology is now playing a more important role in overcoming the intermittency problem of

renewable energies (Lund and Salgi, 2009; Budt *et al.*, 2016). In 2003, the European research on the project of A-CAES aimed to develop an A-CAES plant with the high round-trip efficiency of 70% but still has not been realised so far. The main concerns for the A-CAES system are the design of adiabatic compressors and materials of high-temperature TES (Budt et al., 2016; Luo et al., 2014). At the beginning of the 21st century, the research and development of the CAES technology have been spread to many aspects such as process design and optimisation, process integration and efficiency improvement.

1.1.5 Air compressor and its implementation in CAES system

The function of compressors of the CAES system is to provide sufficient air to store the compressed air in the cavern. The compressor can increase the pressure of the compressed air with the required mass flowrate and pressure for storage. The compressor is to supply bleed air for different purposes. The bleed air can be taken from any of the various pressure stages of compressors (AIRCAV, 2008). There are two main types of compressors implemented in the CAES plant, axial compressor and centrifugal compressor.

1.1.5.1 Axial compressor

The axial compressor (shown in Figure 1-18) includes two main components: a rotor and a stator. The air passes along the compressor through rows of rotating and stationary blades. The blades can convert the kinetic energy to pressure, and a balancing drum is built in order to offset the axial thrust (Arfalk, 2017). The advantages of the axial compressor include: high peak efficiency, small area of the front and high pressure ratio because of the increased number of stages with negligible losses. The drawbacks of axial compressor include the narrow rotational

speed range, complex structure, high cost and high starting power consumption (AIRCAV, 2008).

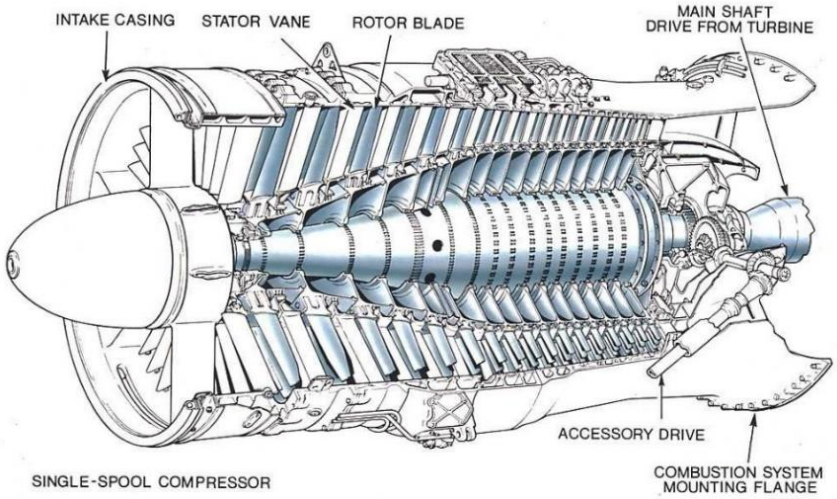

Figure 1-18. The schematic diagram of the axial compressor (Kala, 2011).

1.1.5.2 Centrifugal compressor

The centrifugal compressor (see Figure 1-19) comprises impeller (rotor), diffuser (stator) and casing.

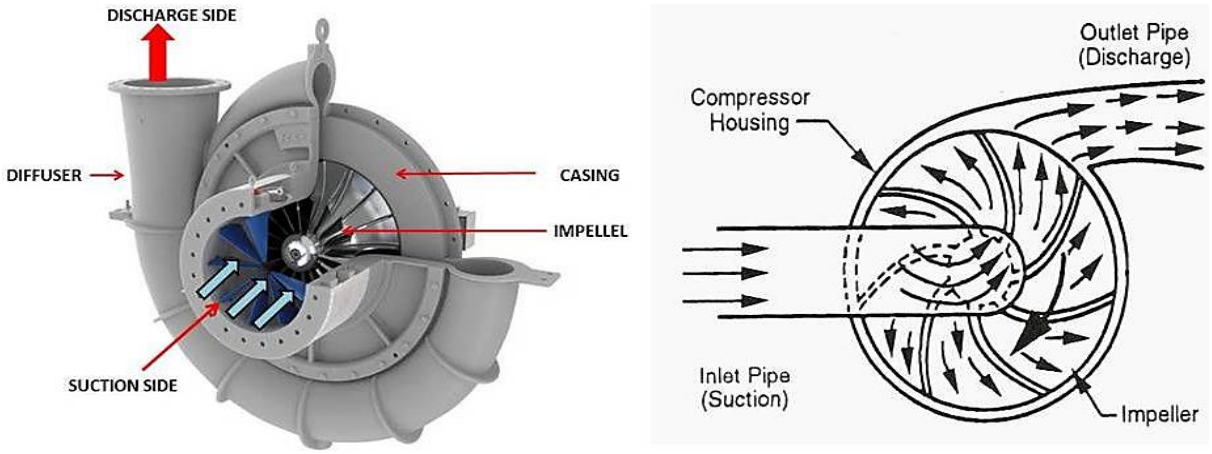

Figure 1-19. The schematic diagram of the centrifugal compressor (mech4study, 2017).

The air enters the suction side of a rotating impeller with radial blades and is pushed toward the centre by centrifugal force. This radial movement of the air can lead to the rise of pressure and generate kinetic energy. Before the air enters the impeller, the kinetic energy can be also converted into pressure by the diffuser and volute (Arfalk, 2014; AIRCAV, 2008). The advantages of the centrifugal compressor include: high pressure ratio (per stage), wide rotational speed range, low cost and low starting power consumption. The disadvantages include: large area of the front and the impracticality of more than two stages due to non-ignorable losses between stages (AIRCAV, 2008).

1.1.5.3 Implementation of compressors in the CAES system

A combination of low-pressure axial compressors and high-pressure centrifugal compressors was used in the Huntorf CAES plant (Wang, et al., 2017; Riaz, 2010; Hoffeins, 1994). The pressure of the cavern of the CAES system can reach over 70 bar, so the multi-stage compressors need to be considered. The axial compressor implemented in the first stage of compression process is typically used in an application with the requirement of low differential pressure (head), high volume air flowrate and higher efficiency (around 85%) (EnggCyclopedia, 2012).

The wide range of pressure rise from 6 bar to over 70 bar after the first-stage compression mainly depends upon high rotational speed of impeller and its size. Nevertheless, the maximum allowable speed could be limited by strength of structural materials of impeller blades. This limitation on maximum achievable pressure rise can be overcome using high shaft speed centrifugal compressors, which can compress air to the required pressure using multi-stage centrifugal compressors operating in series (EnggCyclopedia, 2012).

1.1.6 Linking of wind electricity to the electricity grid

1.1.6.1 Wind turbine

A wind turbine is a device which can convert kinetic energy of wind into electrical energy. The main components of a wind turbine include: tower, rotor, blades, main shaft, gearbox system, yaw mechanism and generator (as shown in Figure 1-20) (Ragheb, 2014). The energy in the wind turns the blades around a rotor which is connected to the gearbox and the main shaft. The shaft can spin the generator to produce electricity (DOE, 2018).

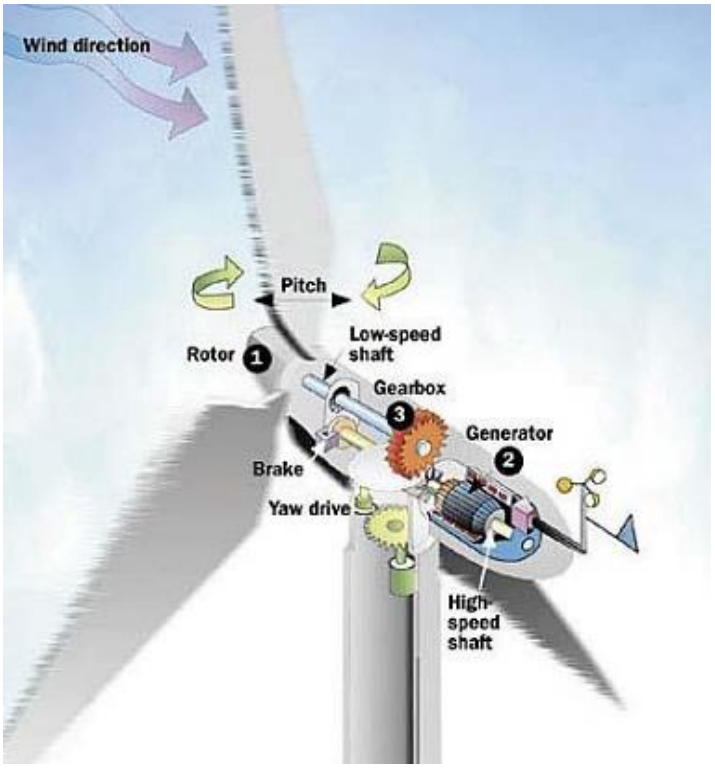

Figure 1-20. The schematic diagram of a wind turbine (Ragheb, 2014).

1.1.6.2 Wind turbines connected to the electricity grid

In Figure 1-21, the wind turbine converts wind energy into electrical energy. The electricity will be delivered to the electricity supply system. The output electricity

of the wind turbine to the supply system is transmitted to the different levels of voltage systems. The majority of wind turbines are connected to the medium-voltage grid (1-35kV), the large offshore wind farms will be connected to the high-voltage grid (more than 35kV) (DM Energy, 2011). The generator of a wind turbine produces AC electricity. The power converter can convert AC to direct current (DC) with a rectifier, then convert back to AC with an inverter. The purpose of converting AC to DC and then back to AC again is to match the frequency and phase of the electricity grid (DM Energy, 2011; DOE, 2018).

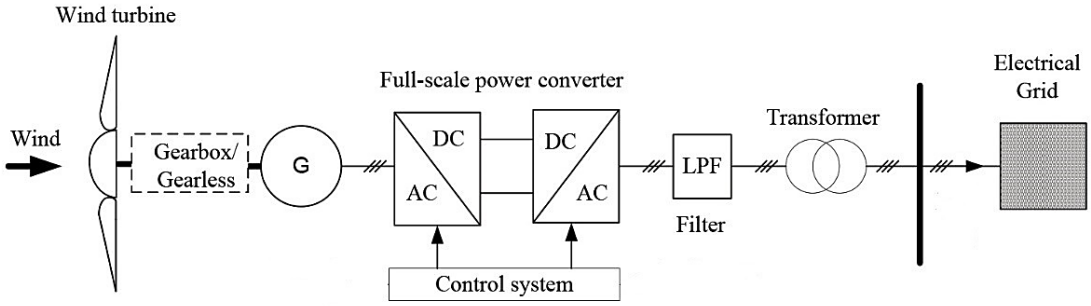

Figure 1-21. The schematic diagram of wind turbines connected to the grid (Kalyani *et al.*, 2016).

1.2 Motivations for this study

1.2.1 Grid-scale capacity

At present, only PHS and CAES technologies can be applied in large or grid-scale (>100MW) application. The PHS technology is mature and has been implemented widely in many countries around the world. However, geographical constraints for the PHS technology requiring two large reservoirs at different elevations and also the environmental issues limit its commercial deployment (Chen *et al.*, 2009; Kousksou *et al.*, 2014; Denholm and Kulcinski, 2004; Denholm and Holloway,

2005). Thus, the CAES technology could become an attractive alternative for large or grid-scale energy storage applications.

1.2.2 Round-trip efficiency

With regards to waste heat from charging and discharging processes in the CAES system, the temperatures of inter-coolers (around 95 ˚C to 130˚C), after-cooler (around 130˚C) and exhaust from recuperator (around 121˚C) are high enough to be recovered for power generation using an organic Rankine cycle (ORC). CAES system integrated with ORC for waste heat recovery will also improve the round-trip efficiency of the CAES system. Therefore, the CAES system integrated with the ORC to recover waste heat from the charging and discharging processes of the CAES system is to be investigated and analysed through process simulation for improving system performance.

1.2.3 Use of renewable energy sources

Wind power as one of the major renewable energies is intermittent, whose output mainly depends on local environmental conditions and unpredictable weather. The CAES technology as one grid-scale energy storage technology can be an attractive and promising option to mitigate the intermittency problem of large-scale wind power generation to improve the stability and reliability of the grid. Figure 1-22 shows that CAES system can utilise excess off-peak wind electricity to store and discharging electricity during the period of high demand. For example, from 1 am to 4 am and from 6 am to 10 am, the external electricity demand is low, the excess off-peak electricity will drive air compression and the cavern pressure increases. From 11 am to 1 pm, the external electricity demand becomes higher, the stored air will be expanded to drive turbines for electricity generation.

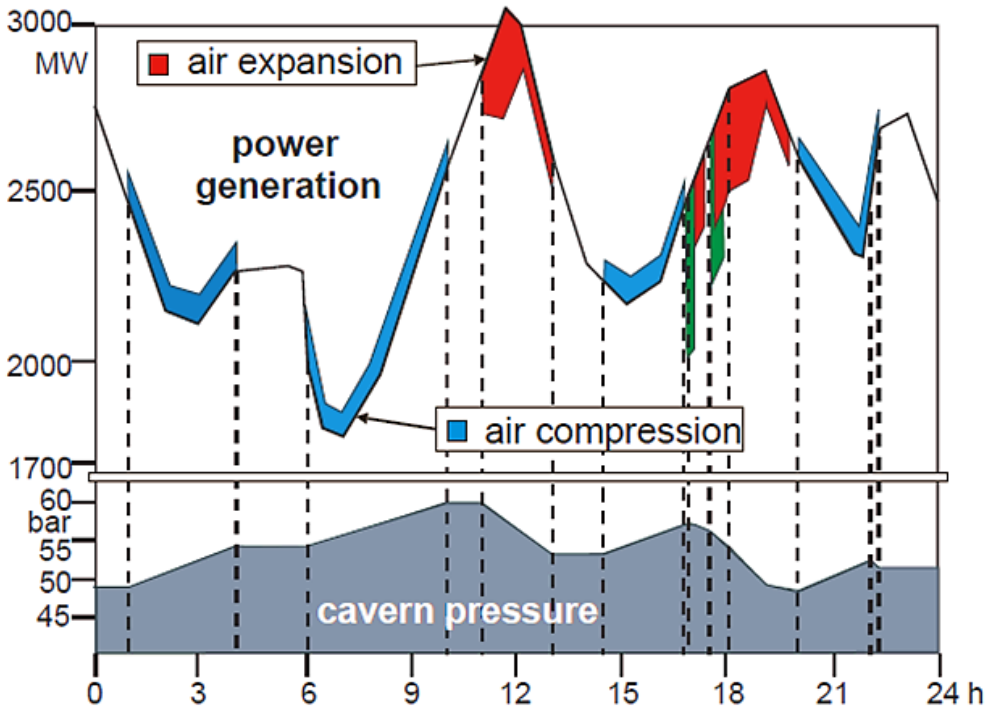

Figure 1-22. Operation of the CAES system integrated with wind power within 24 hours (Crotogino *et al.*, 2001).

One unique feature of a CAES system in the context of wind power is that it is difficult to maintain constant operating conditions for the CAES compression system due to fluctuating wind power output. Thus, the performance of a CAES system in the context of wind power at design and off-design conditions will be investigated and analysed through process simulation.

1.3 Aim and objectives of this research

The aim of this thesis is to study the approaches to improve the round-trip efficiency of CAES system, design and operation of the CAES system for wind power and cost reduction when implementing the CAES system. This study is performed through process modelling, simulation and analysis. To achieve the aim, the following objectives have been identified:

- To provide a comprehensive review and critical assessment of previous researches on round-trip efficiency improvement, design and operation of the CAES system.
- To develop and validate process models for the CAES system and ORC in Aspen Plus®:
    - Steady-state models for charging process of the CAES system
    - Steady-state models for discharging process of the CAES system
    - Steady-state model for ORC
- To carry out process analysis of the CAES system integrated with ORC and to explore different factors which can influence round-trip efficiency of the CAES system.
- To develop and validate improved models of the CAES system for wind power in Aspen Plus®:
    - Improved models for the compressors and turbines based on their charateristic curves.
    - Pseudo-dynamic model for the storage cavern of the CAES system
    - Improved model of the CAES system for wind power
- To perform process analysis of the CAES system for wind power at design and off-design conditions involving the different modes: constant and variable shaft speed modes of the compressors.
- To perform economic evaluations of different systems, consisting of the CAES system integrated with the ORC and the CAES system for wind power at design and off-design conditions.

1.4 Novel contributions

In a stand-alone CAES system, there is a large amount of low-grade waste heat from heat exchangers (e.g. intercooler, aftercooler and recuperator). ORC is a widely used technology for recovery of low-grade heat. On the other hand, most of the studies on process modelling and simulation of the CAES system in the context of wind electricity were for the system analysis at design condition. The off-design performance of the CAES systems for wind power is yet to be investigated. The novel contributions of this thesis include:

- For the CAES system integrated with ORC
  - Steady-state models were developed and model validations were carried out for the CAES system and ORC respectively.
  - A new scheme for waste heat recovery using ORC technology was proposed for the CAES system.
  - Technical performance of the integrated system of the CAES system with ORC was evaluated through process simulation using the validated models.
  - Economic evaluation of the integrated system was carried out using Aspen Process Economic Analyser® (APEA).
- For the CAES system in the context of wind power
  - Improved steady-state models were developed for compressors and turbines of the CAES system based on characteristic curves in Aspen Plus® and Fortran, a pseudo-dynamic model for the cavern was developed in Excel.

- Models for the CAES system in the context of wind power at design and off-design conditions were developed.
- Different operation strategies for the CAES system integrated with wind power were proposed for different wind power output conditions.
- Technical performance analysis of the CAES system in the context of wind power at design and off-design conditions was investigated, also two different modes (constant and variable shaft speed modes) at off-design conditions were evaluated.
- Economic evaluation for the CAES system for wind power at design and off-design conditions was carried out using APEA.

1.5 Scope of this study

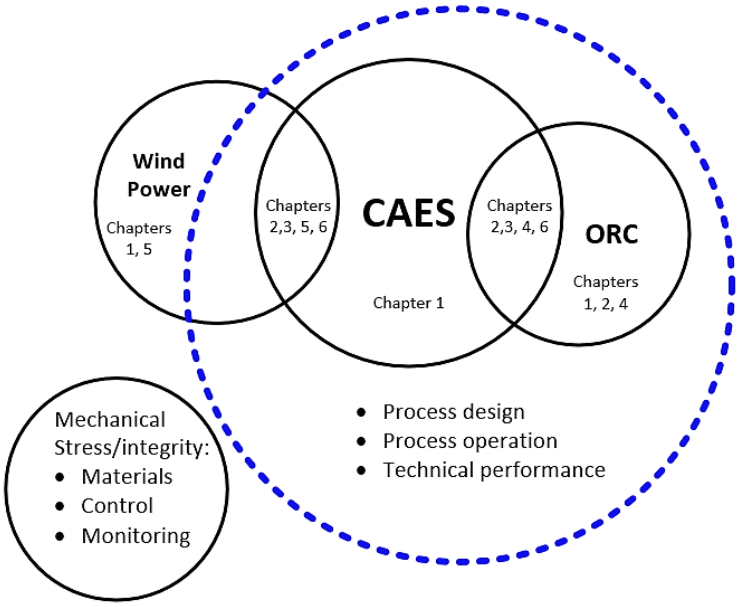

Figure 1-23. Overview of the scope of this thesis.

Figure 1-23 shows the scope of this thesis, the blue dashed line (- - - - -) is the boundary of this thesis. This thesis focuses on the CAES system. Firstly, it is the CAES system integrated with ORC to improve the round-trip efficiency of the CAES system. Secondly, it is the CAES system in the context of wind power to

curtail the intermittency problem of wind power. However, this thesis does not include model development of wind farm and components between the CAES system and wind turbines. This thesis also does not include the integrated system of the CAES system with ORC for wind power which will be mentioned in Section 7.2 for future research and the consideration of mechanical stress or integrity of the system (e.g.materials, control and monitoring).

1.6 Research methodology and software tools used in this study

1.6.1 Research methodology

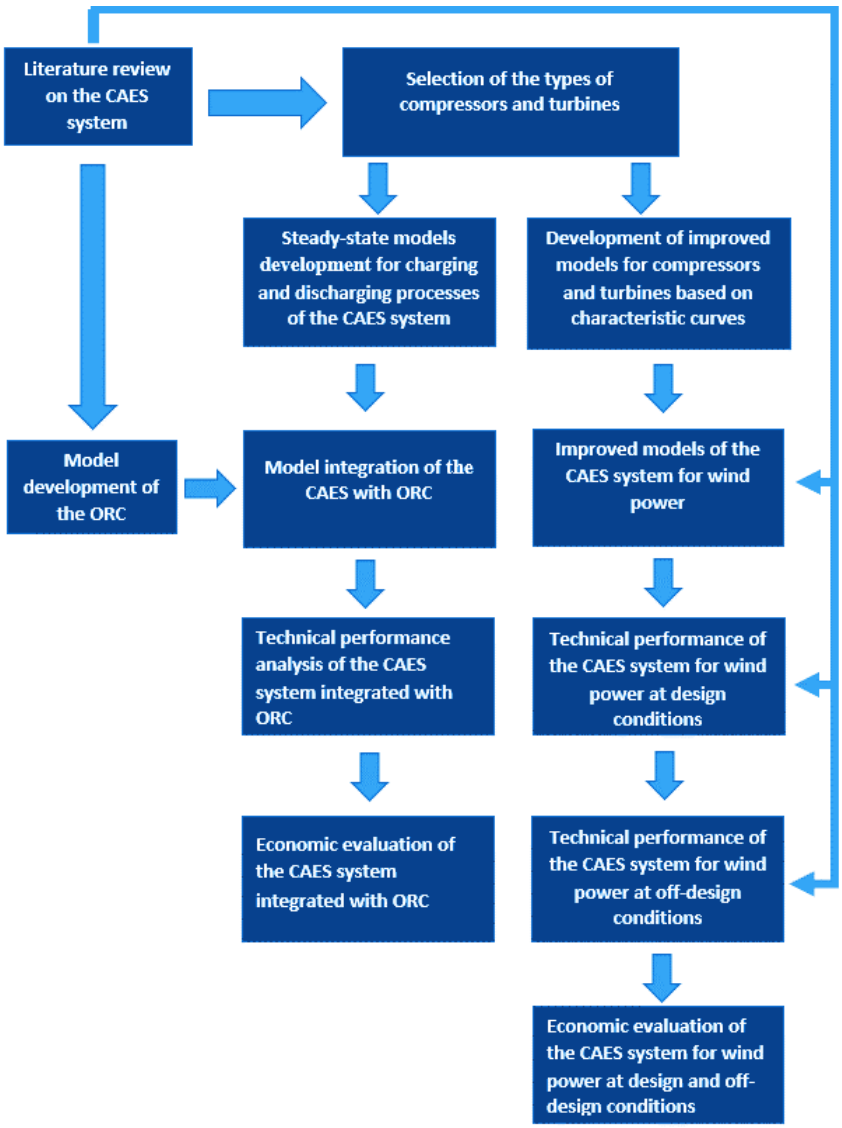

Figure 1-24. Overview of research methodology.

Although two CAES plants have been commercialised, there are still many challenges regarding the performance improvement, waste heat recovery and integration with renewable energy sources. Figure 1-24 shows the research methodology implemented in this thesis to achieve the aim and objectives of this study as presented in Section 1.3.

1.6.2 Software tools used in the study

1.6.2.1 Aspen Plus®

ASPEN is an acronym for Advanced System for Process Engineering and is based on a flowsheet simulation. Aspen Plus® developed by Aspen Technology, Inc. was an engineering software used for model development study (AspenTech, 2018a). Aspen Plus® was implemented for modelling and simulation of the CAES system throughout this thesis. Its advantages include (AspenTech, 2018a; Al-Malah, 2016; Luo, 2016):

- Aspen Plus® has different physical property methods and comprehensive property databank, which can support modelling, process simulation and optimisation.
- Aspen Plus® is a professional engineering software for the chemical industry. It can prove physical properties and reaction models for chemicals, electrolytes, solids and polymers.
- Use integrated modelling for batch and continuous processes from innovation through operations.

1.6.2.2 Aspen Process Economic Analyzer® (APEA)

The APEA is cost estimating software to calculate the capital expenditures and operating expenses for a process system (AspenTech, 2018b). In this study, the software tool was used to evaluate different costs (e.g. capital cost, operating cost and levelized cost of electricity (LCOE)) of the CAES system and integrated system. The major characteristics of APEA include (AspenTech, 2018b; Luo, 2016):

- APEA adopts a bottom-up method for cost evaluation depended on the historical data from real projects except for some special equipment or unit.
- APEA can re-map and re-size each equipment or unit of a system model created by Aspen Plus®. However, the model created by Aspen Plus® cannot be directly implemented in the APEA because some equipment or units exceed the design parameters of the real plants (e.g. flowrate, area and volume) and APEA can re-evaluate each equipment from the real data from the database.

1.7 Outline of the thesis

Chapter 2 reviews an up-to-date assessment of the research activities and development of the CAES technology. The development of the experimental studies and commercial deployment projects is described. The research activities on the modelling and simulation of the CAES system and the integrated system of the CAES system with other systems (e.g. ORC and renewable energy sources) are discussed. Finally, the economic evaluation and performance criteria for the CAES system are also reviewed.

Chapter 3 presents the basic working principle of ORC, model development and model validations of the CAES system and ORC. The characteristic curves for compressors and turbines of the CAES system are also discussed. The improved models and model validations for the compressors and turbines and a pseudo-dynamic model for cavern of the CAES system are developed. The improved model of the CAES system for wind power is developed based on the improved models of the compressors and turbines and the pseudo-dynamic model of the cavern.

Chapter 4 describes the working principles of the integrated system of the CAES system with ORC. The integration of the CAES system with ORC is discussed and the saturation curves and operating point of ORC are also presented in this chapter. Technical performance analysis of the CAES system integrated with ORC is investigated with the discussion of the effects of different factors (e.g. ORC working fluid and expander inlet pressure).

Chapter 5 presents working principle and operation strategies of the CAES system for wind power. Type selection of compressors and turbines of the CAES is discussed. Technical performance investigation of the CAES system for wind power at design and off-design conditions including two different modes (e.g. constant and variable shaft speed modes) are also discussed and analysed.

Chapter 6 proposes economic evaluation for the CAES system integrated with ORC and the CAES system in the context of wind power. The methodology for using APEA is described. The economic evaluation for the CAES system integrated with the ORC is discussed with the effects of different ORC working fluids, variable power sources and comparison of LCOEs for different power sources. The economic evaluation for the CAES system in the context of wind power at design and off-

design conditions is investigated with the effects of different modes and comparison in LCOE of different power sources.

Chapter 7 summarises conclusions for this study and the recommendation for future work.

2. Literature Review

The aim of this chapter is mainly to summarise state-of-the-art research activities on CAES technologies. The chapter will present relevant concepts, features, relevant projects and plants about the CAES techniques. The past research approaches, recent progress and advancement of the CAES system will be reviewed in this chapter. Moreover, this chapter will also present the CAES system integrated with renewable energy sources, economic evaluation, environmental impact and performance criteria on the CAES system.

2.1 Lab experimental rigs on CAES for wind power and relevant studies

2.1.1 Lab experimental rigs on a unidirectional hybrid system and relevant studies

2.1.1.1 Lab experimental rigs

A new hybrid system of a CAES system integrated with wind turbines (refer to Figure 2-1) through mechanical power transmission has been developed by a research team at the University of Warwick (Sun *et al.*, 2015). A scroll expander was implemented to serve as an "air-machinery energy converter" which transmitted excess driving power generated by the stored compressed air from the CAES system to the wind turbine shaft for smoothing the fluctuating wind power (Sun *et al.*, 2015). This experimental test rig was developed by the research team. Figure 2-2 shows the experimental test rig of a small-scale CAES system integrated with a wind turbine.

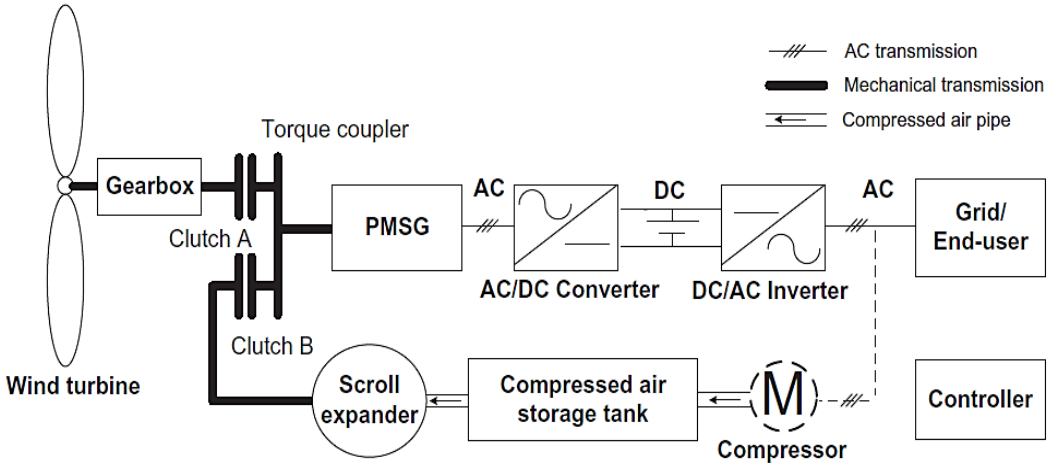

Figure 2-1. The schematic diagram of the unidirectional hybrid system (Sun *et al.*, 2015).

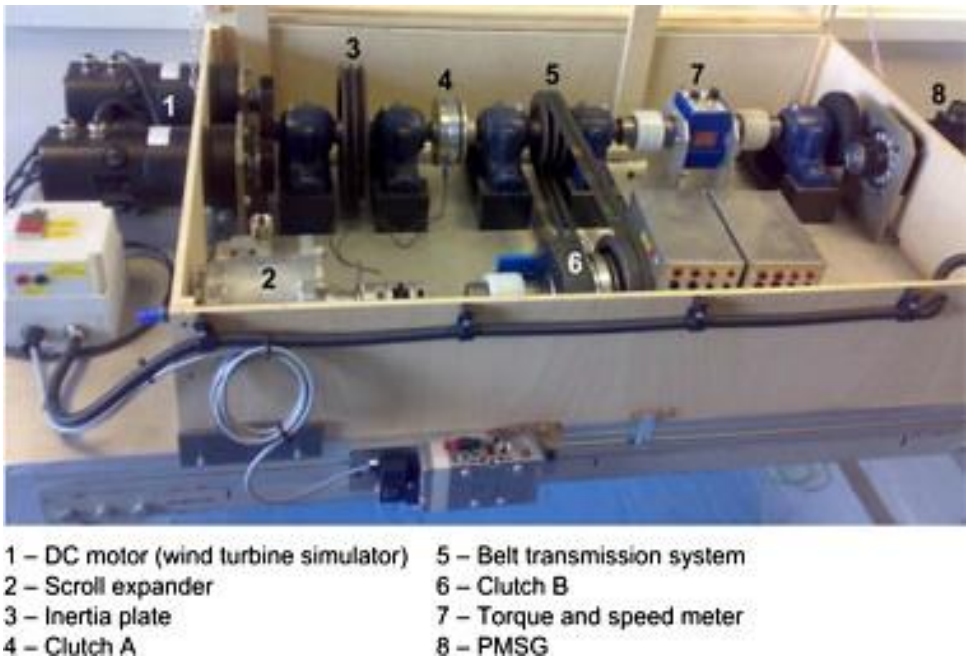

Figure 2-2. The experimental test rig of the unidirectional hybrid system (Sun *et al.*, 2015).

Table 2-1 lists the major components and the corresponding parameters of this experimental rig including motor, permanent magnet synchronous generator (PMSG), scroll-expander, tank, valve and so on.

Table 2-1. The main components of lab rigs of the unidirectional hybrid system (Sun *et al.*, 2015).

Name	Serial number/description	Manufacturer
DC motor	SN:M4-2952X-2100t-000	Callan Tech.
PMSG	SN:SGMSS-20A	Yaskawa Elec.
Scroll expander	Modified from scroll compressor TRSA090	Sanden
Air tank	Max 6 bar due to univ. safety regulation	BOC UK
Controller	Model: RTI1104	dSPACE
Clutch A	SN:CS-10-31G, 24V	Mikipulley
Clutch B	SN:101-10-15G, 24V	Mikipulley
DC power supply	90Vdc, 0-10Adc, for DC motor	TRM Elec.
DC amplifier	SN:10/100, 24-100Vdc, 0-10Adc	TRM Elec.
Voltage transducer	SN:LV 25-P,±10V	LEM
Current transducer	SN:LTSR 15-NP,±15A	LEM
Pressure sensor	SN:SDE1-D10-G2-W18-L-PU-M8	FESTO
Flow meter	SN:MS6 SFE-F5-P2U-M12	FESTO
Pressure regulator	SN:VPPM-6L-L-1-G18-0L10H-V1N	FESTO
Pneumatic valve	SN:MYPE-5-1/4-010-B, 0-10 bar	FESTO
Torque sensor	SN:RWT 310, 0-2000 RPM	Sensor Tech.
Temperature sensor	K-type thermocouple	RS UK

2.1.1.2 Relevant studies

The mathematical model of the hybrid system of the CAES system integrated with wind turbine developed by the Matlab/Simulink was given and the limitation of the model was that the extreme low wind speed or no wind conditions were not properly represented (Sun *et al.*, 2015). The corresponding control strategies of this hybrid system were also presented in another literature (Sun *et al.*, 2011; Sun *et al.*, 2015). The simulation results were compared with the experimental test results, which showed good agreement.

The maximum round-trip efficiency of this integrated system was around 55%. For this hybrid system, the process is to covert the energy of compressed air to mechanical energy for the wind turbine. Energy losses are inevitable, such as operation loss of the scroll expander. Furthermore, the limitation of this experimental study is using two DC motors to replace the wind turbine and can only

investigate the low wind speed condition due to the condition of laboratory and university safety regulations (Sun *et al.*, 2015).

2.1.2 Lab experimental rigs on a bidirectional hybrid system and relevant studies

2.1.2.1 Lab experimental rigs

Krupke et al. (2017) proposed a bidirectional hybrid system of a CAES system integrated with wind turbine (as shown in Figure 2-3) based on the experience from the unidirectional hybrid system in Section 2.1.1. The major components of lab experiment rigs of this hybrid system include motor, generator, scroll-expander/compressor, storage tank and pressure valve.

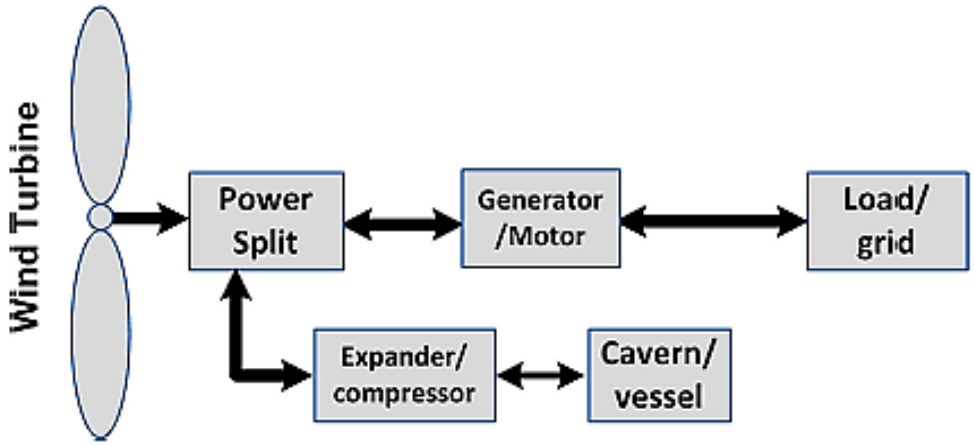

Figure 2-3. The schematic diagram of the bidirectional hybrid system (Krupke *et al.*, 2017).

Compared with the unidirectional hybrid system in Section 2.1.1, the main difference is that this bidirectional hybrid system not only enables a turbomachinery device (e.g. scroll-compressor or scroll-expander) of a CAES system to connect the wind turbine for smoothing the fluctuating wind power, but also the turbomachinery

device can serve as a compressor or expander for servicing the charging and discharging processes of a CAES system (Krupke *et al.*, 2017).

2.1.2.2 Relevant studies

As for this bidirectional hybrid system, a dynamic mathematical model was presented. The models for each of system components were discussed. However, for the whole system, only the discharging process of the CAES system was discussed and analysed in which the scroll-device serve as the expander. The charging process of the CAES system was not presented in which the scroll-device serve as the compressor. Moreover, the round-trip efficiency of this bidirectional hybrid system was only about 37% due to the losses of massive energy in the process such as air leakage, friction and transmission losses (Krupke *et al.*, 2017).

2.2 Pilot CAES plants

2.2.1 CAES system with thermal energy storage (TES)

(a) Front view of the pilot plant

(b) Side view of the pilot plant

Figure 2-4. The pilot CAES plant with TES (Wang *et al.*, 2016).

A pilot plant of a CAES system with TES called TICC-500 (see Figures 2-4) was designed with power rating 500 kWe and designed round-trip efficiency of 33.3% in collaboration between Tsinghua University and Chinese Academy of Science. It has been tested and operated since 2014 (Wang, 2017; Wang *et al.*, 2016). The process diagram of the pilot plant is shown in Figure 2-5. This pilot plant uses water as working fluid for thermal energy storage of the CAES system.

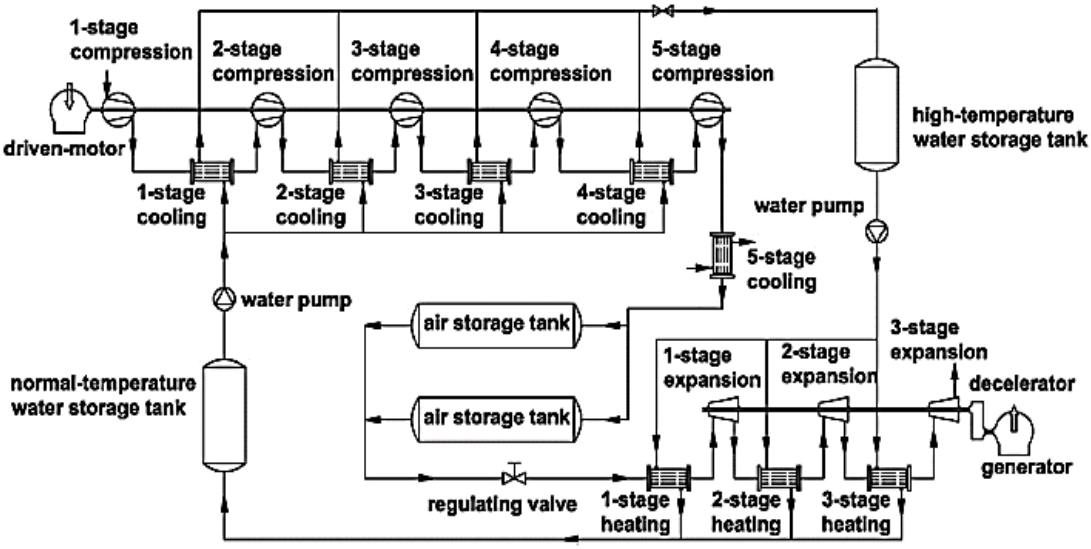

Figure 2-5. The diagram of pilot CAES plant with TES (Wang *et al.*, 2016).

Wang *et al.* (2016) analysed the performance of the system with key factors including power consumption and output, air temperature and pressure of the storage tank with charging and discharging time. However, the average round-trip efficiency of the pilot plant was only 22.60% in the experimental study (Wang *et al.*, 2016). The reason was that the unstable operating condition of compressors caused by the pressure variation in the storage tank resulted in more power consumption in the charging process of the CAES system. Moreover, the power output was affected by the insufficient mass flow of compressed air expanded in the turbines and the efficiency of the recovered waste heat in TES was less than the design condition

(Wang *et al.*, 2016). Additionally, the more remarkable suggestions for improving round-trip efficiency of the CAES integrated with TES can be high-temperature TES (more than 600˚C) and the heat-resistant materials of the compressor (Hartmann *et al.*, 2012).

2.2.2 Supercritical CAES (SC-CAES) plant

From Guo *et al.* (2016), a 1.5MW SC-CAES pilot plant (refer to Figure 2-6) was designed by Macaoenergy Industry Park Development Co. Ltd and Institute of Engineering Thermo-physics of the Chinese Academy of Science in 2013. The system performance has been tested and reached the designed conditions in Bijie, China. The SC-CAES system does not consume fossil fuel and does not need a large volume of cavern for storing compressed air, it can recover the waste heat from compression process and present high round-trip efficiency using the special properties of supercritical air (Guo *et al.*, 2016). The schematic diagram of the SC-CAES plant is shown in Figure 2-7. Currently, the project has been operating for more than 3000 hours and the average round-trip efficiency is 55% (Macaoenergy, 2013; Wang, 2017).

Figure 2-6. A 1.5MWe SC-CAES pilot plant (Wang, 2017).

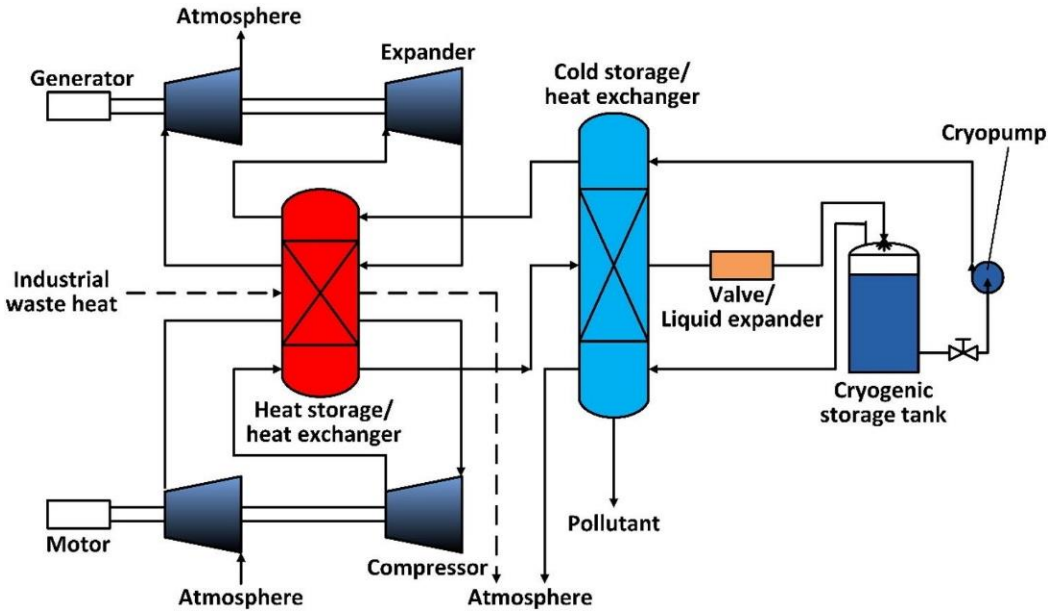

Figure 2-7. The schematic diagram of the SC-CAES pilot plant (Guo *et al.*, 2016).

2.2.3 Advanced CAES pilot plant

Based on the experience of the 1.5 MWe SC-CAES project, a 10 MWe rated power advanced CAES project (refer to Figure 2-8) was developed in Guizhou of China by the Energy Storage R & D centre, Chinese Academy of Science in 2016.

Figure 2-8. A 10 MWe advanced CAES pilot plant (Wang, 2017).

This system is mainly for scientific research and demonstration including wide-load compressors, high-load turbines and heat exchangers. This system has been in operation since 2017 (Energy Storage R&D Center, 2016).

2.3 Commercial CAES plants

Currently, there are two commercial CAES plants in the world. One is the Huntorf CAES plant in Germany, another one is the McIntosh CAES plant in the USA. Details of these two plants will be described in the following sections.

2.3.1 Huntorf CAES plant

The Huntorf CAES plant in Germany designed by BBC Mannheim, as the first commercial CAES plant in the world, has been in operation since 1978 (refer to Figure 2-9) (Chen *et al.*, 2013; Crotogino *et al.*, 2001). The initial Huntorf CAES plant was 290MWe output power for 2-hour discharging duration, which was upgraded to 321 MWe output power for 3-hour discharging duration in 2006 (He *et al.*, 2017; Barnes and Levine, 2011).

Figure 2-9. The Huntorf CAES plant in Germany (Bullough, 2004).

The compressed air is stored in two salt caverns (total volume around 310,000 m^3) with 43-70 bar regular operational pressure and depth of 600-800m (Robb, 2011; Aneke and Wang, 2016; Crotogino *et al.*, 2001). The round-trip efficiency of the Huntorf CAES plant is around 42% (the plant requires 0.8kWh electricity and 1.6kWh fuel energy for an output of 1kWh electricity), also this plant can operate with remarkable performance with ~90% availability and ~99% starting reliability (Chen *et al.*, 2009; Luo *et al.*, 2014; Succar and Williams, 2008; Pimm, 2011). This plant has been operated for 40 years and the initial function of the Huntorf CAES plant was to provide black-start power to the nuclear power plant and generate more electricity at peak time (peak shaving). Currently, the CAES plant is also operated to integrate with wind power to curtail the intermittent problem of wind power output and balance supply-demand of the electricity grid (Barnes and Levine, 2011).

2.3.2 McIntosh CAES plant

The McIntosh CAES plant designed by Dresser-Rand has been operated since 1991 in McIntosh, Alabama, USA (refer to Figure 2-10). Some operating conditions of this plant (e.g. temperature and pressure) were similar to the Huntorf CAES plant. The McIntosh CAES plant can generate 110MWe output power for 26-hour discharging duration. The storage capacity of a single salt cavern is over 560,000 m^3 with the regular operational pressure of 45-74 bar and a depth of around 450m (PowerSouth Electric Cooperative, 2017; Aneke and Wang, 2016). The round-trip efficiency of the McIntosh CAES plant is around 54% (the plant requires 0.69 kWh electricity and 1.17 kWh fuel energy for an output of 1kWh electricity), and it can operate with remarkable performance with ~92.1% starting reliability and ~99.5% running reliability (Barnes and Levine, 2011; Luo *et al.*, 2014; Pimm, 2011).

Figure 2-10. The McIntosh CAES plant (Seltzer, 2017).

The unique and major improvement of the McIntosh CAES plant is the use of a recuperator to recover waste heat from the turbine exhaust to preheat the compressed air. Recovering waste heat by the recuperator can increase the round-trip efficiency of the McIntosh CAES plant from 42% to 54% and also reduce fuel consumption by 22-25%, compared with the Huntorf CAES plant (Luo *et al*., 2014; Barnes & Levine, 2011). However, adding the recuperator could delay the system start-up time (van der Linden, 2007; Barnes and Levine, 2011).

2.3.3 Comparison between the two commercial CAES plants

A specific comparison in the two CAES plants is given in Table 2-2. The two commercially operated CAES plants are diabatic, which have no TES device for heat storage. However, the multi-stage intercoolers implemented in the two CAES plants can reduce exergy losses during the charging process (Crotogino *et al.*, 2001). The implementation of a recuperator in the McIntosh CAES plant for waste heat recovery can also limit the exergy losses (PowerSouth Electric Cooperative, 2017).

Table 2-2. Comparison between the Huntorf and McIntosh CAES plants (Venkataramani *et al.*, 2016; PowerSouth Electric Cooperative, 2017; Crotogino *et al.*, 2001).

Components & Streams	**Huntorf CAES**	**McIntosh CAES**
Operation time	1978	1991
Rated power output (MW)	290 (upgrade to 321)	110
Maximum charging electricity (MW)	60	50
Charging time (hours)	8	40
Discharging time (hours)	2-3	26
Round-trip efficiency (%)	42	54
Number of caverns	2	1
Type of cavern	Salt	Salt
Volume of caverns (m^3)	310,000	560,000
Depth of caverns (metres)	600-800	450
Regular operation pressure in the cavern (bar)	43-72	45-74
Fuel in the combustors	Gas	Gas / Oil
Air mass flowrate in charging process (kg/s)	108	90
Air mass flowrate in discharging process (kg/s)	417	156

2.4 Planned CAES projects

2.4.1 Iowa CAES project

A CAES project was planned by the Iowa Association of Municipal Utilities in 2003, the rated power of the CAES plant was 270 MWe with $400 million investment.

This plant was planned to be operated in 2015 (Haugen, 2012; Schulte *et al.*, 2012). This plan was to integrate the CAES system with the Iowa 75 to 100 MWe wind farms announced in 2006 (Barnes and Levine, 2011). Nevertheless, CAES plant was terminated after eight years due to limitations of geology (Schulte *et al.*, 2012). It is evidenced that Iowas' sandstone aquifer was not suitable for storing compressed air because the stored air in Iowa's aquifers cannot be fast released to reach the requirement of air flowrate to generate electricity in the discharging process of the plant (Haugen, 2012; Luo *et al.*, 2014).

2.4.2 ADELE A-CAES project

The first grid-scale A-CAES project (refer to Figure 2-11) was designed by RWE POWER, General Electric, Ed. Züblin AG and its subsidiary Ooms-Ittner-Hof GmbH (OIH), and German Aerospace Center (DLR) in Germany.

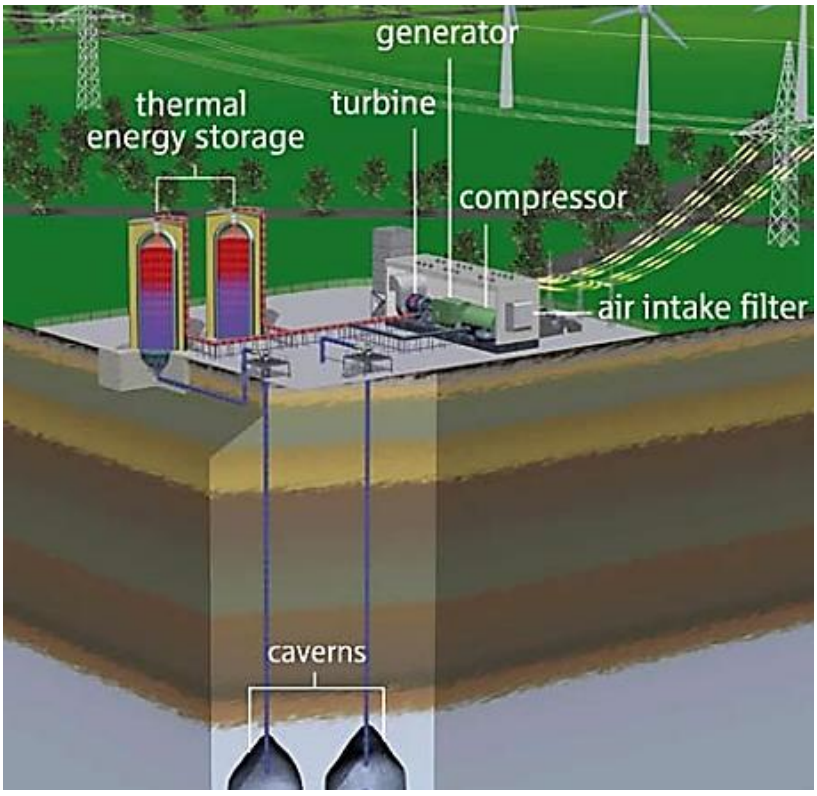

Figure 2-11. The planning layout of the ADELE project (RWE, 2013).

This A-CAES project was called ADELE with high round-trip efficiency target of around 70% (RWE, 2013). The aim of the project was to integrate the CAES system with wind power for smoothing the fluctuating wind power. The novelty of A-CAES system is to recover waste heat from the compression process and to expand compressed air without CO_2 emissions. The project was planned to have 360 MWh energy storage and 90 MWe rated power output. However, there are still some technical challenges to be solved. For example, the design of high pressure and temperature compressor with the consideration of lubrication and the special materials of high-temperature TES withstanding thermal and mechanical stress (Luo *et al.*, 2014; Budt *et al.*, 2016). Currently, this project is still under research and construction because of technical challenges and uncertain business conditions (Wang, 2017; Luo *et al.*, 2016).

2.4.3 Norton CAES project

The Norton energy storage project was announced by FirstEnergy Generation Corp in 2009. The project was planned to install and generate 268 MWe electricity (FirstEnergy Generation Corp, 2009). With 9.6 million m^3 storage of the compressed air in the cavern, the Norton Energy Storage Project has the potential to be produced approximately 2,700 MWe (9×300 MWe) electricity (FirstEnergy Generation Corp, 2009; Luo *et al.*, 2014). The aim of this project is to integrate the CAES with renewable energies to overcome the intermittency problem of renewable energy (FirstEnergy Generation Corp, 2009). In 2013, FirstEnergy Generation Corp delayed the construction of this project because of the low electricity price and low demand (Luo *et al.*, 2014; Budt *et al.*, 2016).

2.4.4 Larne CAES Project

A project called 'Project-CAES Larne' was investigated by Gaelectric's energy storage division, Gaelectric Energy Storage (GES) in 2011 and GES began to construct a CAES system potentially in the Larne of North Ireland. The aim of this project is also to integrate the CAES system with renewable energies sources (e.g. wind, solar and bioenergy) which will generate up to 1000 MW of renewable power in Larne area by 2020 (Gaelectric, 2011). The power output of this CAES project is 330 MWe including two 165 MWe units with two 1400-1700m underground caverns (Budt *et al.*, 2016; Gaelectric, 2011). Project-CAES Larne will bring significant benefits to the operation of the wider Northern Ireland transmission grid. Additionally, the project will be a vital demonstration project for further development of CAES technology at other sites in the UK (Gaelectric, 2011).

2.4.5 Texas CAES project

The Apex Bethel Energy Centre planned a CAES project located in Anderson County, within Texas' ERCOT power market. This project was constructed in 2017 and expected to operate in 2020 with 317 MWe rated power output (ApexCAES, 2017; Holloway, 2016). The aim of this project is to provide black start, peak load shift, frequency regulation and integration with renewable energy. The company Chamisa Energy announced that this CAES project can be integrated with wind power in Texas to curtail the intermittency problem of wind energy, which can ensure the reliable and stable power flow to the grid (Holloway, 2016).

2.4.6 Columbia Hills CAES plant and Yakima Minerals hybrid CAES plant

The Columbia Hills CAES plant and the Yakima Minerals hybrid CAES plant were designed by Bonneville Power Administration (BPA) and Pacific Northwest

National Laboratory (PNNL) in the USA (McGrail *et al.*, 2013). The Columbia Hills CAES system represents a conventional CAES system design as shown in Figure 2-12 and the rated power is around 207 MWe. PNNL calculated through process simulation that the total capital cost for this plant was about $1,112/kW and the LCOE was about 6.41cents/kWh (McGrail *et al.*, 2013).

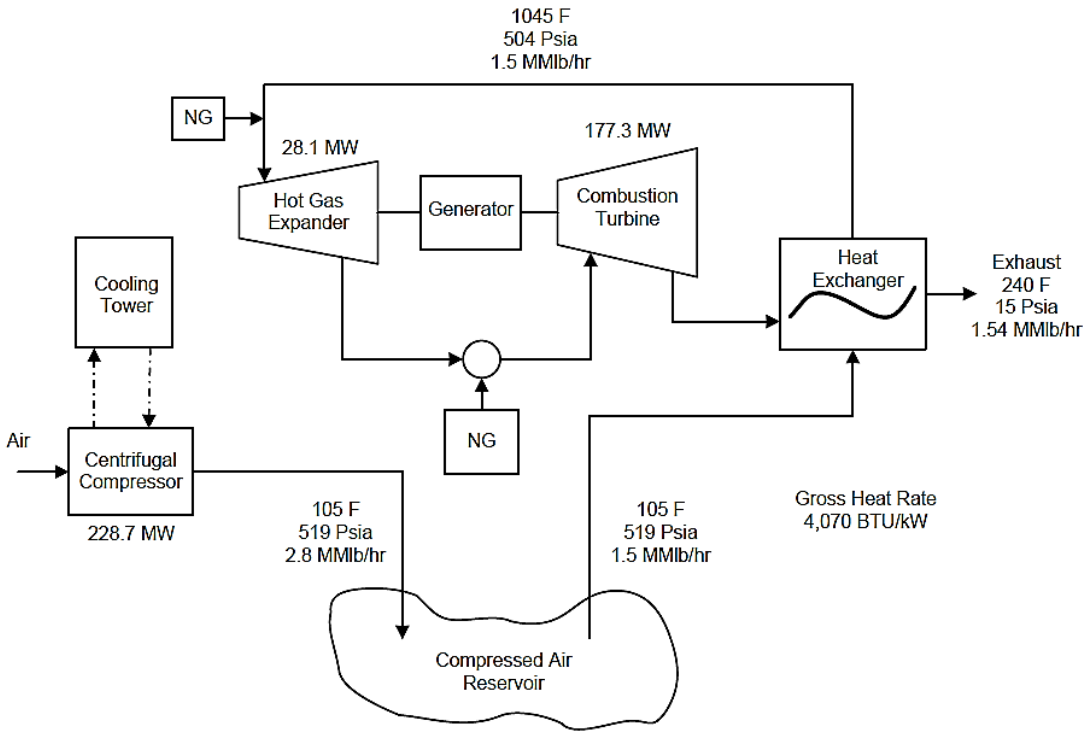

Figure 2-12. The schematic diagram of the Columbia Hills CAES plant (McGrail *et al.*, 2013).

The Yakima Minerals hybrid CAES plant utilises both CAES technology and the geothermal heat source to generate electricity (McGrail *et al.*, 2013). The schematic diagram of the hybrid plant is presented in Figure 2-13. Apart from the conventional CAES technology used in this hybrid plant, the waste heat from compression would be recovered and stored in molten salt. The geothermal heat would be utilised to preheat the compressed air in the discharging process of the CAES system and the

waste heat in molten salt will provide additional heat for low-pressure turbine. This hybrid CAES plant which does not consume fossil fuel is environmentally friendly. The rated power is around 83 MWe, the total capital cost and LCOE are $2,738/kW and 11.84 cents/kWh respectively (McGrail *et al.*, 2013).

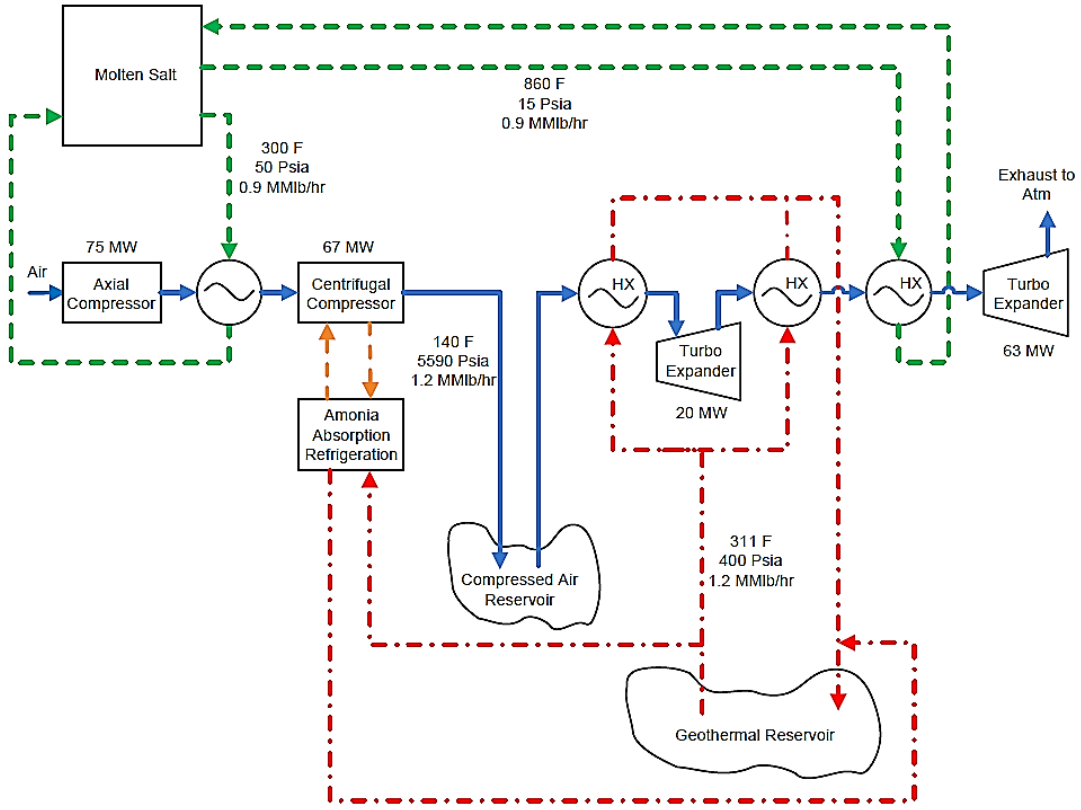

Figure 2-13. The schematic diagram of the Yakima Minerals hybrid CAES plant (McGrail *et al.*, 2013).

2.4.7 Summary

As for the aforementioned planed CAES projects, some of projects have been cancelled or delayed, some of projects have been under plan or construction because of different situations. The details of different planned CAES projects are summarised in Table 2-3.

Table 2-3. Summary of different planned CAES projects (Haugen, 2012; Schulte *et al.*, 2012; Budt *et al.*, 2016; FirstEnergy Generation Corp, 2009; Gaelectric, 2011; Holloway, 2016; McGrail *et al.*, 2013).

CAES projects	Rated power (MWe)	Reasons of cancel or termination
Iowa	270	Limitation of geology: sandstone aquifer
ADELE	90	Technical challenges and uncertain business conditions
Norton	268	Delayed the construction: low electricity price and demand
Larne	330	Under construction
Texas	317	Under construction
Columbia Hills	207	Under plan
Yakima Minerals	83	Under plan

2.5 Performance improvement of CAES and system optimisation

Many publications studied performance improvement and system optimisation of the CAES system by different methods, such as preventing heat loss during the CAES charging process. The round-trip efficiency of a CAES system is highly affected by the heat loss from the charging process or exhaust of turbines because these waste heat can be recovered. This section will provide an overview of the study on performance improvement and system optimisation to understand the process investigation and analysis.

2.5.1 Methods for performance improvement and system optimisation

There are different possible approaches for performance improvement of the CAES system. Najjar *et al*. (2006) developed a CAES system with humidification (CASH) system by storing compression heat in hot water to increase the power output and round-trip efficiency. It found that the round-trip efficiency of the CASH system is

about 3.9% higher than the CAES system. Yoshimoto *et al*. (2005) proposed a CAES system integrated with an advanced combined cycle and analysed the system performance and economic evaluation for the integrated system through modelling and simulation. The study investigated the optimal operation simulation of the integrated system in competition with the PHS system. Liu *et al*. (2014) proposed that a CAES system integrated with combined cycle system (CAES-CC), which was based on a conventional CAES system integrated with a steam turbine cycle by waste heat boiler, can recover waste heat from intercoolers and aftercooler as hot standby in the steam turbine to improve the flexibility of the integrated system. It was also found that the round-trip efficiency of the CAES-CC system is increased by ~10% compared with that of the conventional CAES system through process simulation.

A new process of CAES system (See Figure 2-14) based on the ET11NM gas turbine was suggested by Alstom (Elmegaard and Brix, 2011). The process was designed such that the first high-pressure turbine can expand the compressed air from the cavern without combustion process. The difference compared with a conventional CAES system is that the position of first combustion burner was changed and installed after the low-pressure turbine. The advantage of this system is the mitigation of the NO_x pollutions generated by the process of combustion at low pressure and the round-trip efficiency was around 57% (Elmegaard and Brix, 2011).

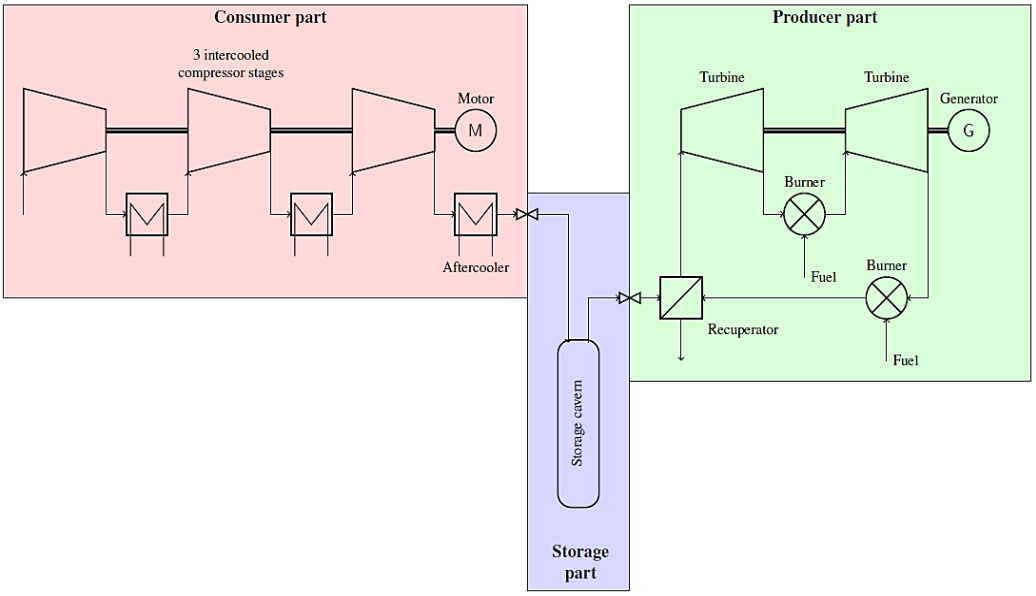

Figure 2-14. The schematic diagram of a CAES system by Alstom (Elmegaard and Brix, 2011).

Several approaches for performance improvement and methods of avoiding the heat loss of the CAES system were proposed. Currently, many researchers have focused on the A-CAES system, because the TES implemented in the CAES system not only can recover the waste heat to improve the round-trip efficiency of the system, but also avoid utilising the fossil fuel (RWE, 2013; Barnes and Levine, 2011; Luo *et al.*, 2016).

2.5.2 A-CAES system

A thermodynamic model for the A-CAES system was developed in Mozayeni *et al.* (2017) to analyse the system performance. This study found that the pressure of compressed air storage cavern has a significant impact on the energy stored in the thermal storage and electricity generated by the turbines of the A-CAES system. It also found that the overall energy conversion efficiency is affected by the varying isentropic efficiency of the compressor and turbine (Mozayeni *et al.*, 2017). In Guo *et al*. (2017), a thermodynamic model of an A-CAES system was developed and

implemented in Matlab/Simulink software. It was found that higher heat transfer coefficient between atmosphere and air, which lead to more compressed air in the cavern and more expanded air in discharging process, can improve the energy density of the compressed air in the storage cavern. The pressure of the cavern also had positive effects on the energy density, but it had no significant impacts on the round-trip efficiency of the A-CAES system (Guo *et al.*, 2017).

Luo *et al*. (2016) developed a mathematical model of A-CAES based on the condition of the Huntorf CAES plant and found that the isentropic efficiency of compressor and turbine, and the heat transfer rates of heat exchangers have an obvious influence on the round-trip efficiency of the A-CAES system. The storage temperature of the TES plays a significant role in the round-trip efficiency of the A-CAES system (Budt *et al.*, 2016; Wolf and Budt, 2014). Zhang *et al*. (2013) also investigated the effect of the TES on the round-trip efficiency of the A-CAES system and found that when power efficiency reaches maximum, a proportion of thermal energy is still remained in TES vessel and the utilisation of the thermal energy is influenced by the appropriate selection of pressure of cavern. Sciacovelli *et al*. (2017) developed a specific A-CAES system integrated with packed bed TES to improve the system performance. Also, a mathematical model of an A-CAES system integrated with packed beds was developed and the round-trip efficiency of the system can achieve more than 70% when TES efficiency rise above 90%. However, it found that the main heat loss is from the turbomachinery rather than from the packed beds (Kosi *et al.*, 2015; Barbour *et al.*, 2015). Additionally, Wolf (2011) developed an A-CAES system with a low-temperature TES, in order to avoid

the design of a huge packed bed TES. The efficiency range of the integrated system is 62-69% with the consideration of humid air effect.

According to most of the studies on the A-CAES system through modelling and simulation, the round-trip efficiency can reach around 70%. Jubeh *et al*. (2012) proposed the model of A-CAES system compared with diabatic CAES systems and found that the round-trip efficiency of the A-CAES system can get to 74%. Barbour *et al*. (2015) announced that the round-trip efficiency of the continuous operation of A-CAES system using packed beds can be more than 70% through process simulation. A small-scale A-CAES system was designed and simulated with the round-trip efficiency of 72% (Grazzini and Milazzo, 2008). A planned A-CAES project with round-trip efficiency target of 70% was developed by ADELE. This project still has some challenges to overcome, the high-temperature compressor and the materials for TES are needed to withstand the thermal and mechanical stress (Budt *et al.*, 2016; Barbour *et al.*, 2015; Dreißigacker *et al.*, 2013).

However, some studies found the round-trip efficiency of the A-CAES system to be lower than 70%. Sciacovelli *et al*. (2017) analysed the dynamic performance of A-CAES plant with packed bed TES and the round-trip efficiency of the plant is in the range of 60-70% when the TES system needs to operate with the storage efficiency more than 90%. Hartmann *et al*. (2012) investigated round-trip efficiency on A-CAES systems through a simulation study and found that the round-trip efficiency of a polytropic configuration is around 60% and that of an ideal isentropic configuration can reach 70%. Wolf and Budt (2014) suggested a low-temperature A-CAES system with the round-trip efficiency in the range of 52%–60%, and a brief economic analysis was also investigated. The round-trip efficiency of this low-

temperature A-CAES system is lower than that of high-temperature A-CAES. Nevertheless, this low-temperature A-CAES system has fast start-up characteristics (less than 5 minutes) and a wide range of load ability (Wolf and Budt, 2014). Pickard *et al*. (2009) investigated that the round-trip efficiency was roughly 50% or better for a bulk A-CAES system (1 GW day). Pickard *et al*. (2009) also suggested that the A-CAES system still have difficulties with commercialisation, because there is obvious inefficiency in the TES and the A-CAES has never been tested rigorously and its round-trip efficiency should be competitive with the commercial energy storage plants (e.g. the round-trip efficiency of PHS plant is around 75%).

With regards to the round-trip efficiency of A-CAES system to be more than 70% in most of publications, the reasons could be some particular conditions or different models implemented. Actually, the charging and discharging processes, the TES process, other parameters or complex conditions can affect the system performance and yield different calculation results.

2.5.3 ORC for performance improvement

ORC has a beneficial impact on the energy efficiency through waste heat recovery (Quoilin *et al.*, 2013; Vélez *et al.*, 2012). Integrating an ORC with a system to convert waste heat into electrical energy could enable this system to achieve better performance (Quoilin *et al.*, 2013; Liu *et al.*, 2004; Bronicki *et al.*, 1996; Kutscher, 2001). The major advantages of the ORC include low mechanical stress, high efficiency of the turbine, low operation cost and long plant life (Desai and Bandyopadhyay, 2016). Also, Liu *et al*. (2013) presented that the payback time of some pollutant gases CO_2, CH_4 and NO_x in the ORC for waste heat recovery life

cycle can be shorter, compared with the grid emission of other five types of power generation modes.

ORC technology has been investigated since the 1880s, it could be implemented to recover low grade energy from different power systems, such as industrial waste heat solar energy, biomass, geothermal energy, fuel cells and ocean thermal energy (Tchanche *et al.*, 2011; Vélez *et al.*, 2012; Wang *et al.*, 2013; Wang *et al.*, 2013; Quoilin *et al.*, 2013; Dai *et al.*, 2009). ORC application with 0.2-2MW output power has been validated in several industrial plants installed in the USA, Germany, Italy, Netherlands, Austria and Sweden (Tchanche *et al.*, 2011; Vélez *et al.*, 2012). Several commercial ORC projects have been established in the world with the power output range from kW to 10MW using different working fluids and operating temperatures (Vélez *et al.*, 2012; Freeman *et al.*, 2015).

The selection of appropriate working fluids in ORC is crucial because it can have significant effects on the system performance (Tchanche *et al.*, 2011). A number of studies have reported that the selection of working fluids of ORC depends on the heat recovery applications and multiple criteria, such as low-toxicity, low-flammability, high flash point, pressure, curve of saturation and low cost etc. (Desai and Bandyopadhyay, 2016; Vélez *et al.*, 2012; Chen *et al.*, 2010; Tchanche *et al.*, 2011; Man Wang *et al.*, 2013). Pezzuolo *et al*. (2016) analysed different working fluids of ORC recovering heat from different heat sources through process simulation in MATLAB environment. The analysis results on different working fluids for an ORC integrated with solar energy were summarised in Desai *et al*. (2016). It was found that ORC plant using R113 and R245fa as working fluid has the very low cost and high cost of electricity, respectively. It also concluded that

comparing with ORC, steam Rankine cycle has higher LCOE due to the low isentropic efficiency of a saturated steam turbine (Pezzuolo *et al.*, 2016).

2.6 CAES system integrated with renewable energy sources

2.6.1 CAES system integrated with wind power

There is a problem of intermittency in renewable energy sources, such as wind and solar energy, it is difficult to generate a constant power output and balance supply and demand of the grid. In order to improve flexibility and supply smooth power output from renewable energy sources, wind power integrated systems were investigated such as wind-diesel-CAES hybrid system and CAES-Wind system (Sedighnejad, 2011; Ibrahim *et al.*, 2010; Ibrahim *et al.*, 2008). In recent years, many researchers focus on the CAES system integrated with wind power to overcome this problem because wind electricity generation has experienced a massive growth in many countries. The CAES system has already been considered to facilitate wind power and to curtail the fluctuation of wind power output (Cavallo, 2007; Krupke *et al.*, 2017; Arsie *et al.*, 2009). Elmegaard *et al.* (2005) and Salgi and Lund (2008) evaluated a CAES plant in a region with high penetration of wind power into the energy market. The study investigated effects of integrating CAES with the Western Danish energy system, where about 20% of electricity is provided by wind farms and the results showed that the optimal penetration of wind power for maximum operation of the CAES system is approximately 55% in Denmark (Salgi and Lund, 2008).

Cavallo (2007) concluded that a CAES system integrated with wind power can be a viable strategy for the wind farm. The operation, control and management strategies

of CAES system integrated with wind power have been proposed using mathematical models (Marano *et al.*, 2012; Kahrobaee and Asgarpoor, 2013; Hasan *et al.*, 2012; Lobera and Foley, 2012; Saadat *et al.*, 2015). As reviewed in Section 2.1.1, Sun *et al*. (2015) presented a unidirectional hybrid CAES-wind turbine system using a scroll expander to drive the wind turbine through a mechanical transmission system for smoothing the wind power output. As reviewed in Section 2.1.2, Krupke *et al*. (2017) showed a bidirectional hybrid CAES-wind turbine system, a single stage of turbomachinery (scroll-compressor/scroll-expander) of the CAES system connects to the shaft of the wind turbine for smoothing the fluctuating wind power. However, the experimental study for the efficiency of this integrated system was only 37% due to the loss of massive heat. The difference between the two hybrid systems has been discussed in Section 2.1.2.2. Chen *et al*. (2016) developed a mathematical model of a CAES system integrated with the hydraulic wind power and the performance study of this integrated system was analysed by process simulation. It was found that a CAES system can improve the quality and stability of the grid, also it can maintain the stable and constant power provision at fluctuating wind speeds and high demand for electricity.

Li *et al*. (2015) proposed a mathematical model of a CAES system integrated with a vertical axis wind turbine (VAWT). It was concluded that the integrated system with the control strategy enables the round-trip efficiency to increase by 5.21% and the time at the protection mode was decreased by 22 hours in four weeks. In addition, the integrated system can overcome the fluctuating power output from VAWT and generate 30kW stable power flow. Ibrahim *et al*. (2010) studied the CAES system integrated with wind-diesel hybrid systems to optimise its cost and performance.

The proposed design of the integrated system requires repowering of current facilities including an increase of power output, engine lifetime and efficiency for reduction of 20-25% fossil fuel consumption and greenhouse gas emissions, also saving the cost of system maintenance and replacement (Ibrahim *et al.*, 2010). In spite of the limitation of low average wind speed in the case study, significant cost savings may be achieved by the implementation of the CAES system. Nonetheless, this study only explored the energy-based cost and does not include the energy cost based on the cost of investment and new facilities (e.g. wind turbines and the CAES system). Most of the mathematical models and simulations of CAES systems reported in the literature were for the system analysis at design condition.

2.6.2 CAES system integrated with photovoltaic power

Simpore *et al*. (2016) suggested an integrated system of the CAES with photovoltaic power to overcome the intermittency problem of photovoltaic electricity in Reunion, France. The limitation of this study is that the integrated system was not connected to the grid network due to the limitation of the location condition. A model for the integrated system was developed to evaluate its feasibility. The process analysis by simulation study on key parameters of the system was investigated and the simulation results including the round-trip efficiency, the load coverage ratio and the energies were discussed for achieving better system performance. Marano *et al*. (2012) investigated a dynamic model for a hybrid system of a wind farm, a photovoltaic system and a CAES system on a daily cycle for energy, economics and environmental impacts. This study was also to determine the optimal management strategy with the target to maximise the profits and minimise the cost. It was found that the CAES system integrated with the power grid can improve the economic

viability of renewable sources. Moreover, the operating cost can be reduced by about 80% with respect to the conventional solution and the CO_2 emissions can be reduced by 74%.

2.7 Economic evaluation and environmental impact

2.7.1 Economic evaluation

Marano *et al*. (2012) analysed the operating cost of the CAES system integrated with a wind farm and a photovoltaic plant. Economic analysis including capital cost, sizing of compressor and turbine, LCOE of the CAES system and also CAES system integrated with wind power has been investigated in the literature (Bosio and Verda, 2015; Huang *et al.*, 2017; Denholm and Sioshansi, 2009; Greenblatt *et al.*, 2007; Mason and Archer, 2012). Safaei *et al*. (2013) carried out the economic evaluation of the distributed CAES system for different lengths of pipes from the charging process to the storage cavern and optimised for various gas prices and capital cost on the pipes. It was concluded that the distributed CAES system with a short distance was more economical than the conventional large-scale CAES system.

Abbaspour *et al*. (2013) developed a mixed integer non-linear programming for the CAES system integrated with wind power on profit maximisation and cost minimisation scenarios in case studies., it was found that the CAES system can enhance 43% operational profits and reduce 6.7% total cost. However, this study does not consider the aspect of capital costs. Swider (2007) investigated an electricity market model for estimating the effects of wind electricity generation on the operation of the CAES system and its economic value of the investment. The objective of this model was to minimise the cost of the integrated system and the

study found that the CAES system can be economic for the large capacity of the wind farm in Germany. Karellas and Tzouganatos (2014) investigated a steady state analysis of four different micro-CAES systems (single and two-stage compression with and without a recuperator) from the aspects of energy and exergy efficiency using IPSEpro simulation software and the hydrogen energy storage system was dynamically simulated by the HOMER energy software. It was found that the capital costs of the CAES system are higher than the hydrogen storage system. However, the operation and maintenance costs of the hydrogen system are higher than the CAES system.

2.7.2 Environmental impact

Some investigations focused on the environmental impacts of the CAES system. The potential environmental benefits of implementation of the CAES system were evaluated, it was found that greenhouse gas emissions from PHS integrated with nuclear and renewable energy sources are lower than that from battery energy storage or CAES system. However, when integrated with the fossil fuel source system, the CAES system releases significantly lower greenhouse gas emissions than PHS or battery energy storage (Denholm and Kulcinski, 2004). Bouman *et al*. (2013; 2016) analysed the environmental impacts of CAES systems coupled with offshore wind power through life cycle assessment and concluded that the environmental impacts of the CAES systems are lower than that of conventional power plants. The power provided by the CAES system can only be utilised when the wind electricity is insufficient to meet the power demand. In Denholm *et al*. (2005), implementing the CAES system to generate additional electricity during low wind power can mitigate the greenhouse gas emissions to a range of 66-104g CO_2-

eq/kWh, which is less than 20% of emissions from fossil fuel systems and the life-cycle emission rates of NO_X and SO_2 can be much lower than fossil fuel systems.

2.8 Performance criteria for CAES system

The process performance of a power plant can be readily presented by the round-trip efficiency which can be calculated by the ratio of power output of the power plant to chemical energy in the fuel consumed (Barnes and Levine, 2011). The CAES system is different from the conventional power plants because two different types of energy inputs are utilised in the system. Electricity is used to drive compressors during the charging period and chemical energy in the fuel combusted is released in the combustor during the discharging period (Elmegaard and Brix, 2011). This situation is difficult to describe the performance of the CAES system by a clear and definite index, which depends on the specific application for the CAES system. Therefore, two performance indices including the heat rate and charging electricity ratio should be also considered for different energy input before discussing the performance index of the CAES system.

2.8.1 Heat rate

The heat rate (HR) is the amount of fuel consumed to generate one kilowatt-hour (kWh) of electricity for the CAES system. Equation (2-1) is described as (Barnes and Levine, 2011):

$$HR = \frac{E_f}{E_T} \tag{2-1}$$

HR is a functional parameter for designing many power system. However, HR could be affected by the heat recovery system in the design process. The implementation

of a recuperator can recover the waste heat from the LPT to preheat the compressed air released from the cavern. The HR for the CAES system without the recuperator can be around 5500 to 6000 kJ/kWh lower heating value (LHV). For example, the HR of the Huntorf CAES plant is 5870 kJ/kWh LHV. The HR for the CAES with the recuperator can be around 4200 to 4500 kJ/kWh LHV. For example, the HR of the McIntosh CAES plant is 4330 kJ/kWh LHV. Comparing the CAES plants with the conventional power plants, HR of a conventional gas turbine (about 9500 kJ/kWh LHV) could be twice higher than the CAES plant. This is because almost two-thirds of the power output in the conventional gas turbine will be utilised to drive the compressor. However, the electricity consumption in the charging process and the electricity generation in the discharging process of the CAES system are separate and independent operations. Thus, HR of the CAES system can be much lower than other power plants (Barnes and Levine, 2011).

2.8.2 Charging electricity ratio

The charging electricity ratio (CER) for the CAES system is the ratio of the power consumption of compressors to the power output of turbines of the CAES system. Equation (2-2) is described as (Barnes and Levine, 2011):

$$CER = \frac{E_C}{E_T} \tag{2-2}$$

The CER could be affected by the piping and throttling losses, especially the compressor and turbine efficiencies. Turbine efficiency is very important for the LPT because most of the enthalpy drop occurs in the LPT and almost three-quarters of power output is generated by the LPT. The increase of turbine inlet temperature

can promote the efficiency of the turbine and the electrical efficiency of the CAES system (Barnes and Levine, 2011).

2.8.3 Round-trip efficiency

The CAES system is different from other power plants because two types of input energy are utilised in the system. Electricity is used to drive compressors during the charging period and chemical energy in the fuel is released into the combustor during the discharging period. There are two different Equations (2-3) & (2-4) to calculate the round-trip efficiency of the CAES system. A broad overview of these two methods has been described in (Budt *et al.*, 2016; Liu *et al.*, 2014; Elmegaard and Brix, 2011).

Round-trip efficiency_1

$$\eta_{eff\_1} = \frac{E_T}{E_C + E_f} \tag{2-3}$$

In equation (2-3), both input energy E_C and E_f are regarded as total input energy and this approach was commonly applied in most of the literatures (Budt *et al.*, 2016; Elmegaard and Brix, 2011; Liu *et al.*, 2014; Mohammadi *et al.*, 2017). However, this equation could be still argued because the total input energy includes two different types of energy, electricity to drive compressors and chemical energy from the fuel consumed (Elmegaard and Brix, 2011; Budt *et al.*, 2016).

Round-trip efficiency_2

$$\eta_{eff\_2} = \frac{E_T}{E_C + \eta_{sys} \cdot E_f} \tag{2-4}$$

In Equation (2-4), the chemical energy contribution of fuel consumed in the combustors is considered due to the combustion system electric efficiency η_{sys}. The value of η_{sys} can be determined by different gas firing conversion power systems. In general, the reference system for electric efficiency could be around 30% (Liu *et al.*, 2014; Elmegaard and Brix, 2011). This equation can be regarded as how much electricity is indeed consumed in the system to generate the electricity output of the CAES system.

2.9 Summary

This chapter assessed various research aspects of the CAES system including lab experimental rigs and relevant studies, commercial plants and planned commercial projects, performance improvement and system optimisation (mainly through modelling and simulation), integrated system with renewable energy sources, economic evaluation, environmental impact and performance criteria for CAES system. It can be concluded by the following points:

- The commercial CAES plants and planned commercial CAES projects were reviewed in this chapter. The data from commercial CAES plants and the Columbia Hills CAES system will be used for model development and validations in Chapter 3 and process analysis in Chapters 4 and 5.
- The round-trip efficiency of a CAES system is still low due to the dissipation of waste heat produced from the compression process of compressors and exhaust waste heat of the turbine. ORC technology as one of low-grade heat recovery systems could be a good choice for recovering the waste heat of the CAES system for efficiency improvement.

- As for the CAES system integrated with renewable energy sources, especially wind power. It is necessary to study how to design and operate the CAES system for wind power at both design and off-design conditions since the wind electricity output varies all the time.
- With regards to performance criteria for CAES system, Equation (2-3) was commonly applied in most of the literature, this equation using the certain and measurable input energy can be more persuasive for comparison in the round-trip efficiency of the CAES systems because most of the literature adopted this equation to evaluate the round-trip efficiency. Therefore, Equation (2-3) will be applied in this study for the round-trip efficiency of the CAES system.

3. Model Development and Model Validations

3.1 Introduction

In this chapter, the development of the steady-state models for the charging and discharging processes of the CAES system and ORC will be presented in Sections 3.2 and 3.3 respectively. In Section 3.4, the improved models of main components (e.g. compressors and turbines) will be also considered and developed based on the characteristic curves of compressors and turbines because these components have a significant impact on the performance of the CAES system for wind power at design and off-design conditions. Therefore, this chapter will describe the methodology for development and validations of these models.

3.2 Model development and validations of CAES system

3.2.1 Model development of charging and discharging processes of CAES system

The CAES model was divided into two sections: charging and discharging sections. The main components of the CAES system include compressors, intercoolers, aftercooler, recuperator, combustors and turbines. Steady-state models for the charging and discharging processes of the CAES system were developed and simulated in Aspen Plus® V8.4 with input parameters based on industrial operation consideration. The compressors and turbines were simulated based on isentropic efficiency using *Compr* block in Aspen Plus®. Isentropic efficiencies and mechanical efficiencies of compressors and turbines were specified to improve the accuracy of the prediction (Luo, 2016; Canepa *et al.*, 2013). The intercoolers and

aftercooler were simulated with *Heater* blocks, which was selected by heat transfer between process stream and cooling utility. The outlet temperature and pressure were required for implementing this block in the CAES model.

In the discharging process, the combustor was simulated with *RGibbs* reactor block. The flow rate of air is chosen so as to ensure complete (equilibrium) combustion of the natural gas. The *RGibbs* block calculates the equilibriums by the Gibbs free energy minimisation thereby avoiding the complicated calculations of reaction stoichiometry and kinetics. This will simplify the required input parameters for the block. Phase equilibrium and chemical equilibrium was selected as the calculation option for the combustors and the required inputs were temperature and heat duty of the combustor. The recuperator was simulated with a *HeatX* block because two process streams for heat transfer were specified. The flow direction in the recuperator was chosen to be counter-current flow. The selected input parameters and options for exchanger specifications were design option, exchanger duty and minimum temperature approach. PENG-ROB (Standard Peng-Robinson cubic equation of state) method was implemented for the property calculation for the CAES model (Liu *et al.*, 2014). Different components of the CAES system and corresponding blocks in Aspen Plus® has been summarised in Table 3-1.

Table 3-1. The CAES components and corresponding blocks in Aspen Plus®.

Components	**Blocks**
Compressors / Turbines	*Compr*
Intercoolers / Aftercooler	*Heater*
Combustors	*RGibbs*
Recuperator	*HeatX*

3.2.2 Model validation of the Huntorf CAES plant

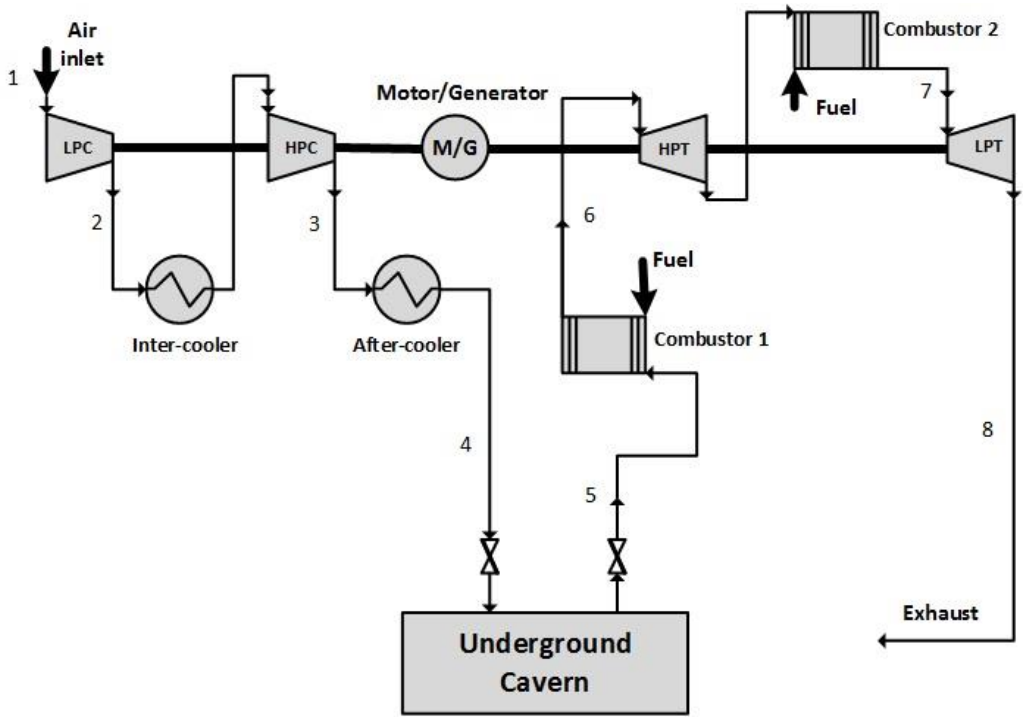

Figure 3-1. A schematic diagram of the Huntorf CAES system (Elmegaard and Brix, 2011).

The plant data used for the Huntorf CAES model validation was obtained from Crotigino *et al*. (2001), Liu *et al*. (2014) and Hoffein (1994). The flowsheet of the Huntorf CAES system is shown in Figure 3-1. Table 3-2 gives the input process conditions and parameters for the Huntorf CAES plant model.

In Table 3-3, the simulation results were compared with the Huntorf CAES plant data (Hoffeins, 1994). The results show that relative errors are 1.72% and 3.05%. However, only two variables (e.g. consumption power of compressors and output power of turbines) were compared with simulation results due to lack of detailed data in the literatures (Crotogino *et al.*, 2001; Hoffeins, 1994; Liu *et al.*, 2014; Kaiser, 2015; Elmegaard and Brix, 2011).

Table 3-2. Input process conditions and parameters for the Huntorf CAES plant (Crotogino *et al.*, 2001; Liu *et al.*, 2014; Hoffeins, 1994).

Stream Numbers	**Process Conditions**			
	Process Point Description	**Pressure (bar)**	**Temperature (˚C)**	**Flowrate (kg/s)**
1	Ambient conditions	1.013	10	108
2	Outlet 1st compressor	6		108
3	Outlet 2nd compressor	46		108
4	Aftercooler outlet / Cavern inlet	46	50	108
5	Throttle outlet	42		417
6	Inlet 1st turbine	42	550	417
7	Inlet 2nd turbine	11	825	417
8	Outlet 2nd turbine	1.13		417
	Compressor isentropic efficiency		75%*	
	Turbine isentropic efficiency		85%*	

* The efficiencies were calculated regressively from the dataset by the author

Table 3-3. Comparison between simulation results and the data of the Huntorf CAES plant.

Variables	**Plant Data** (Hoffeins, 1994)	**Simulation Results**	**Relative Errors (%)**
Consumption Power of Compressors (MW)	60	61.03	1.72
Output Power of Turbines (MW)	290	298.84	3.05

3.2.3 Model comparison of the Columbia Hills CAES plant

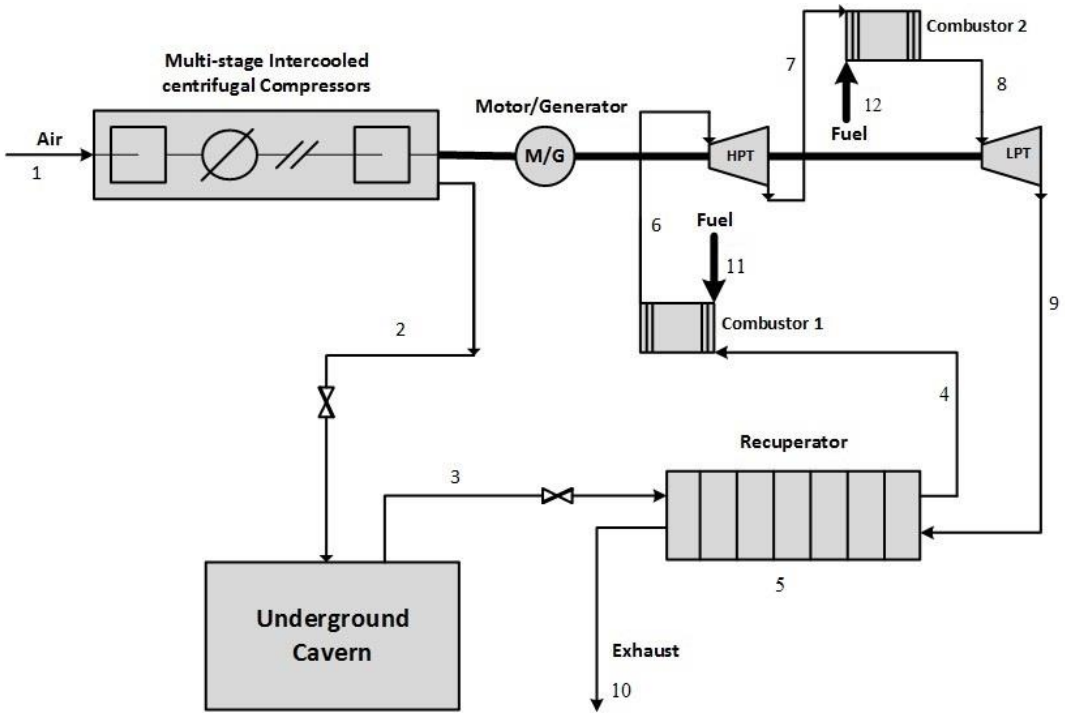

Figure 3-2. The schematic diagram of the Columbia Hills CAES plant (McGrail *et al.*, 2013).

The flowsheet and simulation data of the Columbia Hills CAES plant were obtained from a technical report by PNNL (McGrail *et al.*, 2013). Figure 3-2 shows the process configuration of the Columbia Hills CAES plant. The main difference between the Columbia Hills CAES system and the Huntorf CAES system is a recuperator which can recover the heat from the exhaust of the turbine for preheating compressed air. The charging process of the Columbia Hills CAES plant is implemented with a multi-stage centrifugal compressor with six intercooled stages (McGrail *et al.*, 2013). Using intercooled centrifugal compression stages can reduce the gross energy demand of the machine and therefore improves efficiency. However, this increases the capital cost when compared to the Huntorf CAES plant. The simulation results will be compared with the data from literature (McGrail *et*

al., 2013). Table 3-4 gives the input process conditions and parameters of the Columbia Hills CAES plant.

Table 3-4. Input process conditions and parameters of the Columbia Hills CAES plant (McGrail *et al.*, 2013).

Stream Numbers	**Process Conditions**			
	Process parameters	**Pressure (bar)**	**Temperature (˚C)**	**Flowrate (kg/s)**
1	Ambient conditions	1.03	15	353
2	Aftercooler exit / Cavern inlet	115.65		353
3	Throttle outlet	35.78	40.56	189
11	Inlet natural gas of 1st combustor	44.82	32.22	0.527
12	Inlet natural gas of 2nd combustor	24.13	32.22	4.111
6	Inlet 1st turbine/Outlet of 1st combustor	34.40		
7	Outlet 1st turbine	18.27		
8	Inlet 2nd turbine/Outlet 2nd combustor	17.93		
9	Outlet 2nd turbine	1.03		
5	Heat duty of recuperator (MW)	105.51		
	Air charging time (Hours)		3	
	Compressed air discharging time (Hours)		6	
	Pressure ratio of the compressor		1.96177*	
	Compressor isentropic efficiency		75%*	
	Turbine isentropic efficiency		93%*	

* The pressure ratio and efficiencies were calculated regressively from the dataset by the author

In Table 3-5, the process simulation results are compared with the literature data. The results showed that the relative errors are less than 0.7% except for the error prediction of exhaust temperature of the recuperator which is 4.64%.

Table 3-5. Simulation results compared with literature data from Columbia Hills CAES plant.

Stream Number	**Parameters / Variables**	**Literature Data** (McGrail *et al.*, 2013)	**Simulation Results**	**Relative Errors (%)**
2	Temperature of Aftercooler exit / Cavern inlet (˚C)	40.56	40.56	0.00
4	Cold stream outlet temperature of recuperator (˚C)	562.78	560.12	0.47
6	Temperature of inlet 1st turbine / outlet of 1st combustor (˚C)	676.67	673.89	0.41
7	Temperature of outlet 1st turbine (˚C)	546.11	544.02	0.38
8	Temperature of inlet 2nd turbine / outlet 2nd combustor (˚C)	1331.67	1330.65	0.08
9	Temperature of outlet 2nd turbine (˚C)	601.72	605.15	0.57
10	Exhaust temperature of recuperator (˚C)	115.56	120.92	4.64
	Consumption Power of Compressors (MW)	228.67	230.22	0.68
	Output Power of Turbines (MW)	205.39	205.76	0.18

3.3 Model development and validation of ORC

3.3.1 Process description of ORC

ORC works on the principle of using an organic fluid with a boiling point less than that of water as the working fluid. Recovering low-grade waste heat (T<370˚C) from other systems by integrating ORC can improve the performance of the entire system (Quoilin *et al.*, 2013; Liu *et al.*, 2004; Bronicki *et al.*, 1996; Kutscher, 2001).

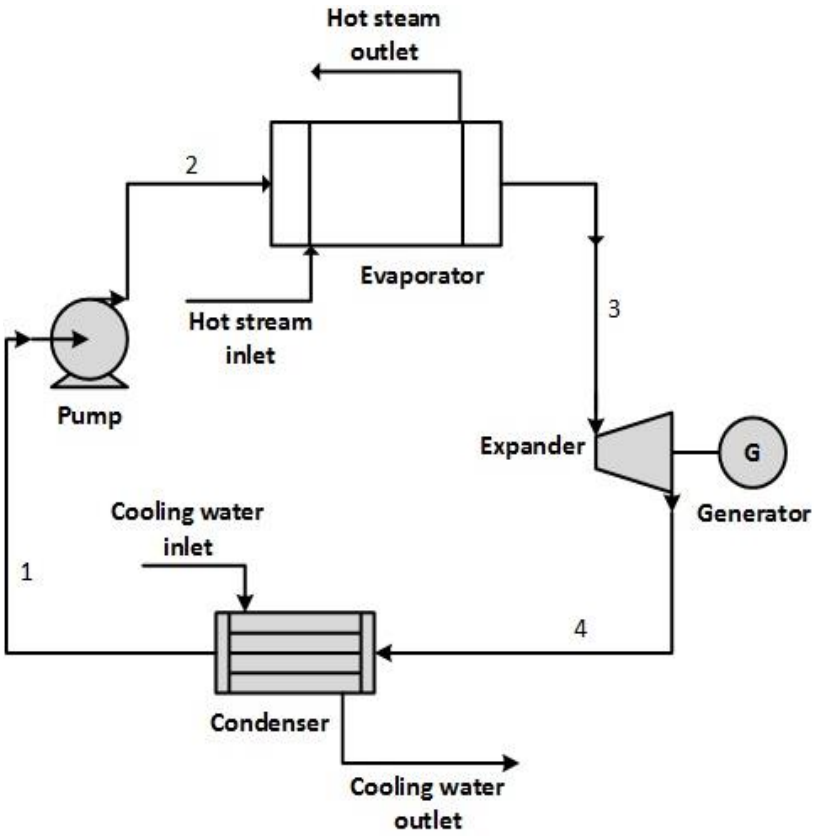

Figure 3-3. A schematic diagram of an ORC (Aneke *et al.*, 2011).

The main components of an ORC as shown in Figure 3-3 include evaporator, expander, condenser and pump. The working fluid leaving the condenser is compressed by a pumped back to the evaporator for recovering waste heat. The working fluid will be evaporated. The evaporated vapour passes into the expander to generate electricity by rotating the shaft, which is connected to the generator. Finally, the exhaust from the expander will be condensed from vapour to liquid in the condenser using cooling water (Wang *et al.*, 2013).

3.3.2 Model development of ORC

The modelled components of the ORC include pump, evaporator, expander and condenser. The pump was simulated with *Pump* block in Aspen Plus® and discharge pressure was supplied as an input parameter. The expander was simulated as

isentropic turbines using *Compr* block. The requirement for this block is the same as the compressor or turbine in the CAES model. The evaporator and condenser were simulated with *HeatX* block which is the same as the requirement of the recuperator in the CAES model. The flow direction and input parameters specification type were chosen to be countercurrent and design respectively. Minimum temperature approach was specified as an input parameter for both the evaporator and the condenser. Different components of the ORC and corresponding blocks in Aspen Plus® have been summarised in Table 3-6.

Table 3-6. Summary of components of the ORC and corresponding blocks in Aspen Plus®.

Components	**Blocks in Aspen Plus®**
Pump	*Pump*
Expander	*Compr*
Evaporator / Condenser	*HeatX*

3.3.3 Model validation of ORC

The flowsheet (refer to Figure 3-3) and plant data for validation of the ORC model were obtained from the Chena Geothermal Power Plant (Aneke *et al.*, 2011). The organic working fluid of the ORC is R134a (1,1,1,2-tetrafluoroethane). It is a common refrigerant implemented in a wide range of refrigeration and air conditioning applications, including medium and high-temperature refrigeration and industrial applications (‘R134a’). Table 3-7 gives the input process conditions and parameters of ORC.

Table 3-7. Input process conditions and parameters of ORC (Aneke *et al.*, 2011).

Parameters / Variables	**Plant Data**
Hot stream inlet mass flowrate (kg/s)	33.39
Hot stream inlet temperature (˚C)	73.33
R134a mass flowrate (kg/s)	12.17
Cooling water inlet mass flowrate (kg/s)	101.68
Cooling water inlet temperature (˚C)	4.44
Turbine inlet / outlet pressure (bar)	16.00 / 4.00
Pump efficiency	90%
Expander efficiency	80%

Table 3-8. Simulation results compared with ORC data from the Chena Geothermal Power Plant.

Parameters / Variables	**Literature data** (Aneke *et al.*, 2011)	**Simulation results**	**Relative Errors (%)**
Hot stream outlet temperature (˚C)	54.44	55.27	1.52
Cooling water outlet temperature (˚C)	10.00	9.82	1.80
Output power of Expander (kW)	250.00	252.56	1.02
Evaporator heat transfer rate (kW)	2580.00	2735.33	6.02
Condenser heat transfer rate (kW)	2360.00	2482.32	5.18

The simulation results were compared with the plant data for model validation as shown in Table 3-8. All the relative errors were less than 6.02% and the simulation results matched the real plant data.

3.4 Development of improved models for compressors, turbines and cavern of CAES system and model validations

When the CAES system is applied for wind power, the compressors and turbines of the CAES system cannot always operate at design condition due to the fluctuating wind power output. Therefore, it is necessary to develop the improved models for compressors and turbines based on their characteristic curves in order to analyse the off-design conditions of the CAES system in the context of wind power.

3.4.1 Characteristic curves for compressors and turbines

Figures 3-4 and 3-5 indicate the characteristic curves for the compressors and the turbines of the CAES system (Briola *et al.*, 2016). They will be used to obtain their corresponding performance at different operating points for model development and process simulation. Figures 3-4 (a) and (b) present the characteristic curves of the LPC (the axial compressor) and HPC (the centrifuge compressors), and show the relationship between mass flow rate and pressure ratio at different shaft speeds. Figures 3-5 (a) and (b) present the characteristic curves of the LPT and HPT, and the relationship between the pressure ratio and the mass flow rate at different turbine speeds.

Different shaft speeds of the compressors or the turbines were normalised as the different dimensionless velocities. For example, when the dimensionless velocity equals 1 ($v = 1$), the CAES system will operate at design shaft speed. When the dimensionless velocity is above or below 1 ($v > 1$ or $v < 1$), the CAES system will operate at off-design shaft speeds. The optimal efficiency lines in Figures 3-4 and

3-5 show the optimal efficiencies operated at different shaft speeds for the compressors and turbines of the CAES system.

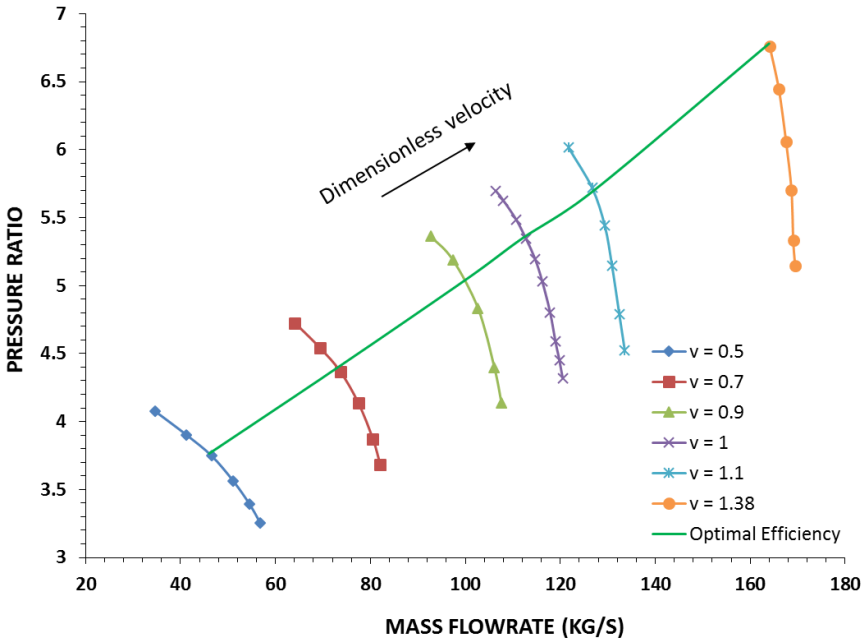

(a)

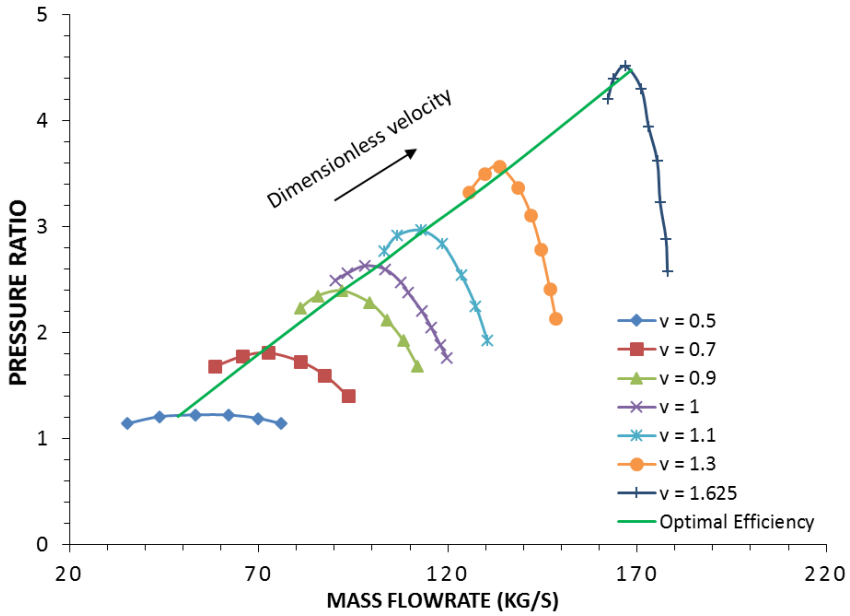

(b)

Figure 3-4. Characteristics curves of (a) LPC and (b) HPC of the CAES system (Briola *et al.*, 2016).

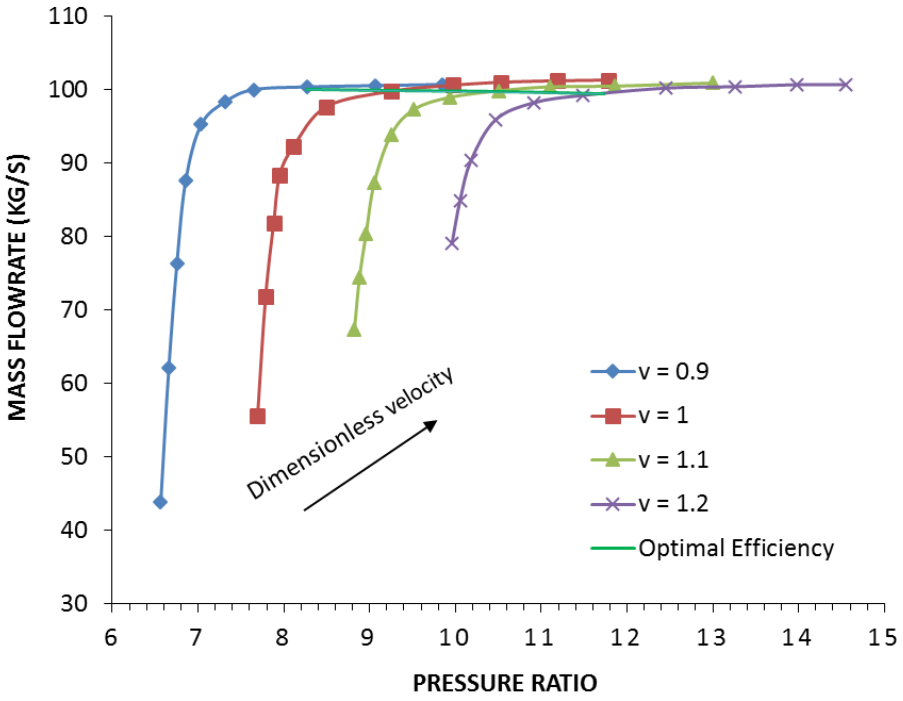

(a)

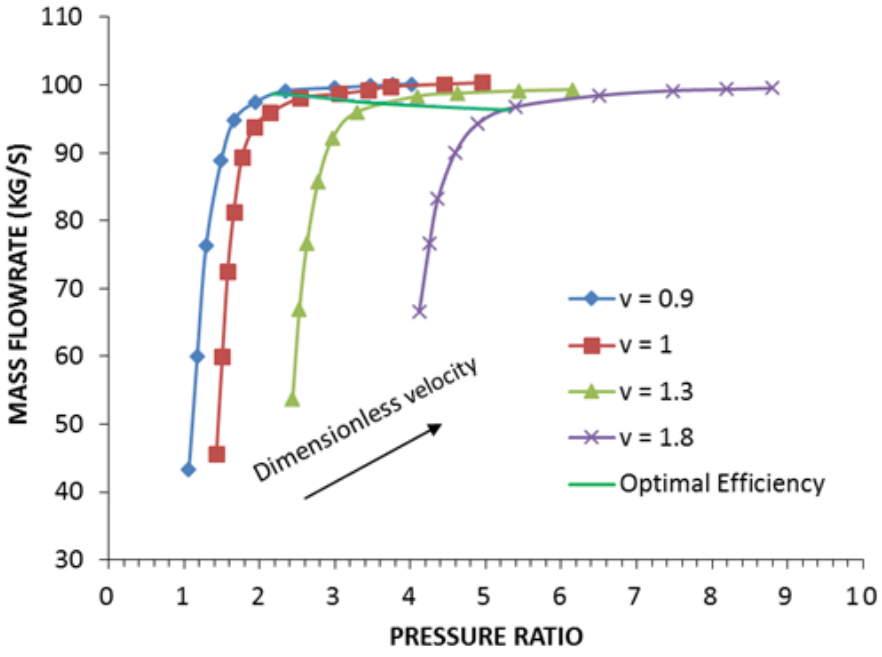

(b)

Figure 3-5. Characteristics curves of (a) LPT and (b) HPT of the CAES system (Briola *et al.*, 2016).

3.4.2 Development of improved models for compressors and turbines

The performance characteristic curves of the compressors shown in Figure 3-4 and the turbines shown in Figure 3-5 were used to obtain their corresponding performance at different operating points. These operation points from performance curves were entered into the Aspen Plus® models of the compressors and turbines to simulate their off-design performance through *Performance Rating*. As for the compressor models, there are several characteristic curves at different shaft speeds for two types of compressors in Figure 3-4, The parameters including pressure ratio and mass flowrate were chosen in the *Performance and Flow Variables*. The data at different operating points can be filled in the *curve data*. As for the turbine models, there are four characteristic curves at different shaft speeds for the two turbines in Figure 3-5. The procedures of model development for the turbines is almost the same as that of the compressor. As for the optimal efficiency operated at off-design conditions, the model of the optimal efficiency for different shaft speed curves can be developed in Fortran which can be connected to the Aspen Plus®. The results will be carried out by Fortran calculator and used for the Aspen Plus® model.

3.4.3 Model validations for compressors and turbines of the CAES system

The data of the reference CAES system used for model validation was from Briola *et al*. (2016). The flowsheet of the CAES plant is shown in Figure 3-6. The reference CAES system conditions (*r*), simulation results (*s*) and the relative errors (*re*) for the compressors and turbines of the CAES system have been summarised in Tables 3-9, 3-10 and 3-11.

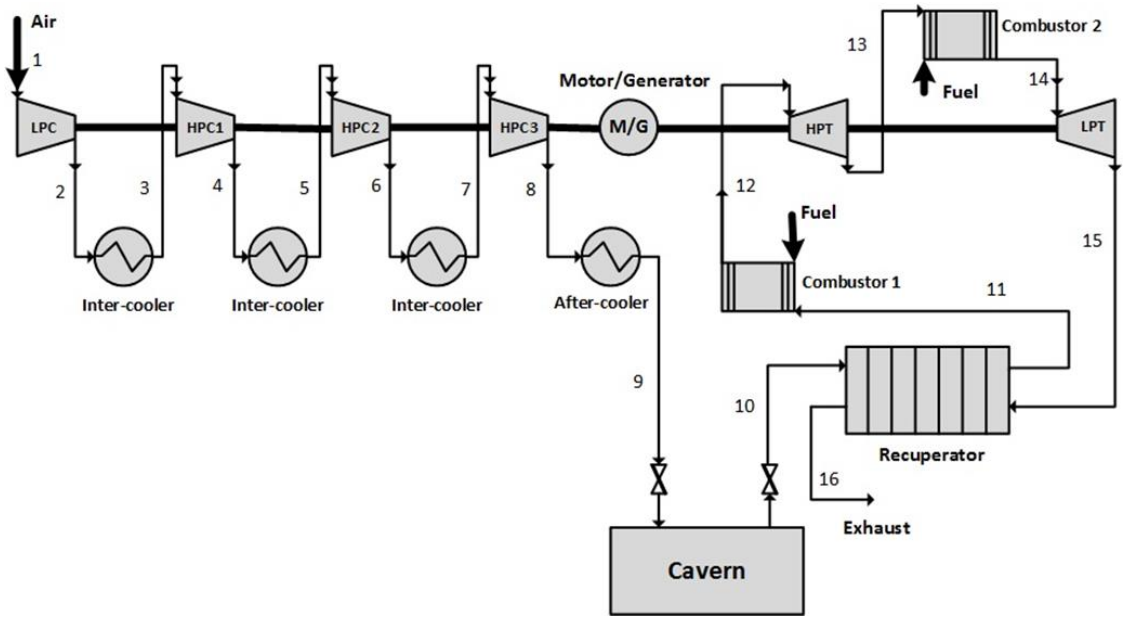

Figure 3-6. The schematic diagram of the CAES system (Briola *et al.*, 2016).

In Tables 3-9, 3-10 and 3-11, the simulation results for the compressors and turbines were compared with the reference CAES system condition. The results from process simulation showed that all of the relative errors are less than 2.3% with a good agreement.

Table 3-9. The reference conditions (*r*), simulation results (*s*) and relative errors (*re*) for LPC.

		LPC			
	Variables	**Stream No.**	***r***		
Input parameters	**P_{in} (bar)**	1	1		
	T_{in} (K)	1	283		
	m (kg/s)	1	108		
	Pressure ratio		5.9		
Results	**P_{out} (bar)**	**Stream No.**	***r***	***s***	***re***
		2	5.9	5.9	0.0%
	Power consumption (MW)	**Power consumption of LPC**			
		r	***s***	***re***	
		23.8	24.37	2.3%	

Table 3-10. The reference conditions (*r*), simulation results (*s*) and relative errors (*re*) for HPC.

		HPC 1				**HPC 2**				**HPC 3**			
	Variables	**SN***	***r***			**SN**	***r***			**SN**	***r***		
Input parameters	**P_{in} (bar)**	3	5.8			5	13.1			7	30.7		
	T_{in} (K)	3	323			5	323			7	323		
	m (kg/s)	3	108			5	108			7	108		
	Pressure ratio		2.35				2.37				2.37		
Results	**P_{out} (bar)**	**SN**	***r***	***s***	***re***	**SN**	***r***	***s***	***re***	**SN**	***r***	***s***	***re***
		4	13.3	13.6	2.2%	6	31.2	31.3	0.03%	8	72	72.8	1.1%
	Power consumption (MW)	**The total power consumption of HPC 1-3**											
		r				***s***				***re***			
		35.6				34.93				1.9%			

* SN: Stream Number

Table 3-11. The reference conditions (*r*), simulation results (*s*) and relative errors (*re*) for HPT and LPT.

		HPT				**LPT**			
	Variables	**SN**	***r***			**SN**	***r***		
Input parameters	**P_{in} (bar)**	12	43			14	11.3		
	T_{in} (K)	12	823			14	1098		
	m (kg/s)	12	410			14	410		
	P_{out} (bar)	13	11.5			15	1		
Results	**T_{out} (K)**	**SN**	***r***	***s***	***re***	**SN**	***r***	***s***	***re***
		13	624	626	0.3%	15	673	681	1.17%
	Power output (MW)	**The power output of HPT**				**The power output of LPT**			
		r	***s***		***re***	***r***	***s***		***re***
		90	89.24		0.85%	200	201.19		0.59%

3.4.4 Pseudo-dynamic model for cavern of CAES system

The model of the cavern was developed in Excel as a pseudo-dynamic model (refer to Equation 3-1) based on the Ideal Gas Law (PV= nRT) (Poling *et al.*, 2001).

$$PV = \frac{m_{Air}}{M_{Air}} \cdot RT \tag{3-1}$$

A dynamic process varies with time with considerable change in terms of value. A pseudo-dynamic process is also time dependent but change is slow (e.g. the pressure of cavern was changed hourly). The pseudo-dynamic approach enables approximate simulation of various dynamics in accordance with their actual timescales, the accuracy and practicality will be improved (Nakashima *et al*., 1992). In Figure 3-7, assuming the cavern pressure changes hourly in this study. During the charging period, the pressure of the cavern will increase with increasing mass of the compressed air injected into the cavern. On the contrary, the pressure of the cavern will decrease when the compressed air expanded during the discharging period.

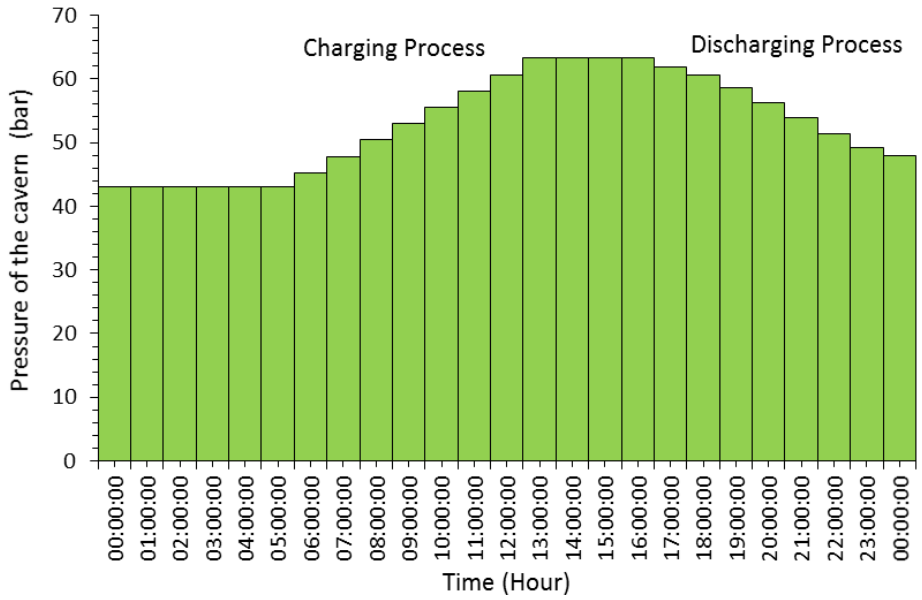

Figure 3-7. The pressure condition of the carven during charging and discharging processes of the CAES system for wind power.

As for the cavern model, during the charging period, the cavern pressure was updated hourly in Excel according to the mass flowrate of the incoming compressed air. Similarly, during the discharging period, the cavern pressure was also changed hourly according to the air mass flowrate to out of cavern.

It is noted that modelling of the cavern was assumed to follow the Ideal Gas Law which relates pressure, temperature, and volume of the ideal gas. However, the Ideal Gas Law is accurate only at relatively low pressures and high temperatures. To account for deviation from the ideal situation, another factor called the gas compressibility factor need to be considered. Therefore, the Non-Ideal Gas Law could become: $PV = Z \cdot nRT$ (Z is the gas compressibility factor, n is number of moles of gas present) (The Engineering Toolbox, 2018).

Table 3-12. Compressibility factor for air (The Engineering Toolbox, 2018).

Compressibility factor for Air - Z -														
Temperature *[K]*	Pressure *[bar absolute]*													
	1	5	10	20	40	60	80	100	150	200	250	300	400	500
75	0.005	0.026	0.052	0.104	0.206	0.308	0.409	0.510	0.758	1.013				
80		0.025	0.050	0.100	0.198	0.296	0.393	0.489	0.726	0.959	1.193	1.414		
90	0.976	0.024	0.045	0.094	0.187	0.278	0.369	0.468	0.678	0.893	1.110	1.311	1.716	2.111
100	0.980	0.887	0.045	0.090	0.178	0.264	0.350	0.434	0.639	0.838	1.040	1.223	1.594	1.954
120	0.988	0.937	0.886	0.673	0.178	0.256	0.337	0.413	0.596	0.772	0.953	1.108	1.509	1.737
140	0.993	0.961	0.921	0.830	0.586	0.331	0.374	0.434	0.591	0.770	0.911	1.039	1.320	1.590
160	0.995	0.975	0.949	0.895	0.780	0.660	0.570	0.549	0.634	0.756	0.884	1.011	1.259	1.497
180	0.997	0.983	0.966	0.931	0.863	0.798	0.743	0.708	0.718	0.799	0.900	1.007	1.223	1.436
200	0.998	0.989	0.977	0.954	0.910	0.870	0.837	0.814	0.806	0.855	0.931	1.019	1.205	1.394
250	0.999	0.996	0.991	0.982	0.967	0.955	0.946	0.941	0.945	0.971	1.015	1.070	1.199	1.339
300	1.000	0.999	0.997	0.995	0.992	0.990	0.990	0.993	1.007	1.033	1.067	1.109	1.207	1.316
350	1.000	1.000	1.000	1.001	1.004	1.008	1.012	1.018	1.038	1.064	1.095	1.130	1.212	1.302
400	1.000	1.001	1.003	1.005	1.010	1.016	1.023	1.031	1.053	1.080	1.109	1.141	1.212	1.289
450	1.000	1.002	1.003	1.006	1.013	1.021	1.029	1.037	1.061	1.091	1.118	1.146	1.209	1.278
500	1.000	1.002	1.003	1.007	1.015	1.023	1.032	1.041	1.065	1.091	1.118	1.146	1.205	1.267
600	1.000	1.002	1.004	1.008	1.016	1.025	1.034	1.043	1.068	1.092	1.117	1.143	1.195	1.248
800	1.000	1.002	1.004	1.008	1.016	1.024	1.032	1.041	1.062	1.084	1.106	1.128	1.172	1.215
1000	1.000	1.002	1.004	1.007	1.014	1.022	1.029	1.037	1.056	1.074	1.095	1.113	1.152	1.189

In this study, the regular operating pressure of the cavern is between 43bar and 66bar and the temperature of the compressed air in the cavern is assumed constant at 50˚C (323.15K). From summary of compressibility factor for air in Table 3-12, it was found that there is no much influence on the compressibility factor of the air between 40bar and 70bar at constant temperature of 50˚C (323.15K), the compressibility

factors of the air are approximately 0.998 (40bar) and 1.000 (70bar) at 325K. Therefore, modelling compressed air in the cavern model can be based on the ideal gas in this thesis.

3.5 Improved model of the CAES system for wind power

The improved models for the compressors and turbines were developed based on the characteristic curves in Figures 3-4 and 3-5 in Section 3.4.1 and the details have been described in Section 3.4.2. The model is capable of predicting the components' performance of the CAES system at the design and off-design conditions. The model of the cavern was developed in Excel and the specific description for the model development of the cavern has been given in Section 3.4.4. The models of other components (e.g. combustors, recuperator, intercoolers and aftercooler) of the CAES system are same as the model development of charging and discharging processes of the CAES system in Section 3.2.1.

3.6 Conclusions

In this chapter, the models developed in Aspen Plus® for the CAES system, ORC and main components (e.g. compressors and turbines) and model validations were carried out with input parameters based on industrial operation considerations. The main conclusions for this chapter are summarised as follows:

- The steady-state models for the charging and discharging processes of the CAES system were developed in Aspen Plus®. The model validations based on the Huntorf CAES plant and model comparison based on the Columbia Hills CAES plant were carried out successfully.

- The working principle of ORC was described and the steady-state model for ORC was developed in Aspen Plus®. The model validation for ORC was also presented based on the real plant flowsheet and data.
- The improved models for compressors and turbines developed based on the characteristic curves and model validations were carried out. The pseudo-dynamic model for the cavern was developed in the Excel.
- The improved model for the CAES system based on the improved models of the compressors, turbines and cavern was developed. This improved model of the CAES system will be used in Chapter 5 for the process analysis of the CAES system in the context of the fluctuating wind power output at design and off-design conditions

4. Technical Performance Analysis of a CAES System Integrated with ORC

4.1 Introduction

With regards to waste heat from charging and discharging processes in the CAES system, the temperatures of intercoolers (around 95 to 130˚C), aftercooler (around 130 ˚C) and exhaust from recuperator (around 121 ˚C) are high enough to be recovered for power generation using an ORC. The CAES system integrated with ORC for waste heat recovery will also improve the round-trip efficiency of the CAES system. Therefore, the integration of the ORC to recover waste heat from the charging and discharging processes of the CAES system is investigated and analysed through process simulation for improving system performance. In this chapter, the electricity is assumed to take from electricity grid at off-peak time and electricity generated by the CAES system integrated with ORC will be supplied to the electricity grid at peak time.

4.2 Process description

4.2.1 Process description of the CAES system integrated with ORC for waste heat recovery

The schematic diagram of the proposed CAES system integrated with the ORC is shown in Figure 4-1. The organic working fluid of the ORC has two flow path options for heat recovery in the integrated system because charging and discharging operations do not occur simultaneously. During the charging operation of the CAES system in off-peak period, the organic working fluid in the ORC will flow through

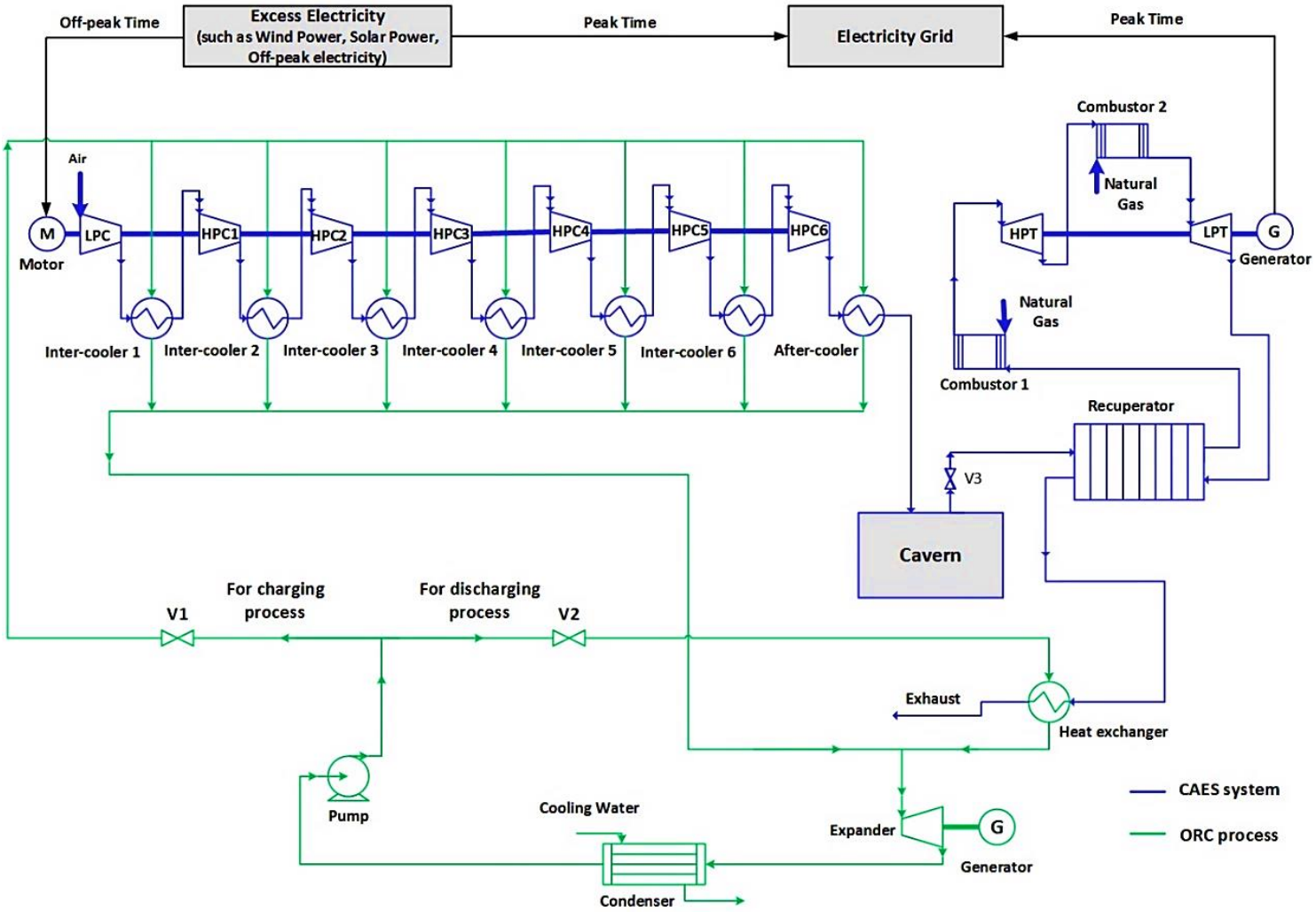

Figure 4-1. The schematic diagram of the CAES system integrated with

the valve V1 to recover waste heat from the intercoolers and aftercooler of the compressors to generate electricity to reduce the electrical energy taken from the electricity grid for driving the compressors. During the discharging operation of the CAES system in the peak period, the organic working fluid will flow through the valve V2 to recover waste heat from the exhaust gas leaving the recuperator to generate more electricity for the improvement of system performance. Therefore, an ORC integrated with the CAES system can recover waste heat during both charging and discharge operations. This can improve the efficiency as well as reduce the operating cost of the system. Similar as Columbia Hills CAES system from the PNNL technical report, 3 hours per day of the charging operation and 6 hours per day of the discharging operation were specified in this study (McGrail *et al.*, 2013).

4.2.2 Integration of the CAES system with ORC

With regards to the successful operation of a commercial size system, the design and operating procedures are based on experimentation, process simulation and demonstration with a small-scale operation (Sulaiman, 2018). The scale-up for the large-scale chemical process system is very important and need to be considered. It was noticed that the volume of the initial state of air is huge before compressed by the compressors due to the large mass flowrate of the air (353 kg/s). The volume of the initial state of the air exceeds the volume of the compressors from industrial mechanism and manufacturer. Therefore, there will be three compressors for LPC, two compressors for HPC1 in real applications, although the schematic diagram (refer to Figure 4-1) shows only one compressor for LPC or HPC1. There is only one compressor for HPC2-HPC6 respectively because the volume of compressed air has been reduced after air compression by LPC and HPC1.

An ORC would have different operating points during charging and discharging operations because of the different flow rates, operating pressures and temperatures. This will affect the design of the ORC components, especially the ORC expander. Hence, there will be two ORC expanders in real applications, although the process diagram (refer to Figure 4-1) shows only one ORC expander. Two expanders will be engaged during the charging operation period. However, one of the expanders will be withdrawn during the discharging operation because the recovered waste heat during the discharging period is less than that during the charging period.

All of the components of the CAES system integrated with ORC are also taken into consideration for the economic evaluation of the integrated system in Chapter 6. The APEA will be used to evaluate each of the components of the integrated system depended on the database from the real industrial plants and manufacturers.

4.2.3 Saturation curves and operating point of ORC

In conventional steam Rankine cycle, water is used as the working fluid is used to recover waste heat. However, the temperature of waste heat could not be high enough to superheat water. When outlet stream of the steam expander contains more than 15% saturated liquid, this could damage expander blades and reduce the efficiency of the expander (Desai and Bandyopadhyay, 2009). The dry organic working fluid (e.g. R123 and R134a) does not have this problem because the dry organic working fluid does not need to be superheated and the outlet stream of the ORC expander can be always saturated vapour. The wet organic working fluids (e.g. R717 and water) could require superheating (Desai and Bandyopadhyay, 2009; Vélez *et al.*, 2012; Tchanche *et al.*, 2011; Escalante *et al.*, 2017). Figure 4-2 shows

the Temperature-Entropy (T-s) diagram of ORC which includes the following processes:

1-2: pressure increase in the compression process by the pump;

2-3-4: heat absorption process in the vapour evaporator;

4-5: expansion process through ORC expander;

5-6-1: heat rejection process in the condenser.

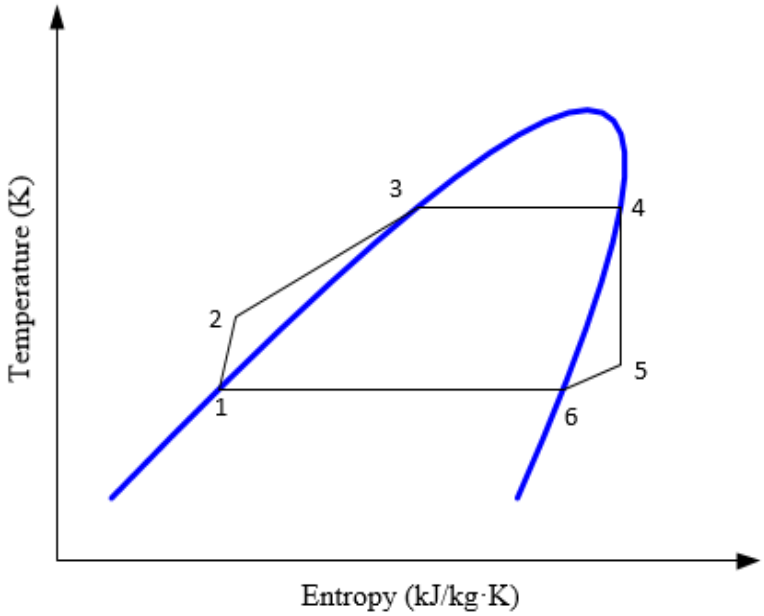

Figure 4-2. The T-s diagram of ORC.

The thermo-physical properties of these refrigerants should be considered because the ORC working fluids have a significant impact on the ORC performance (Wang et al., 2013). Also, different working fluids have different operating points in the ORC. For example, Figure 4-3 illustrates the Pressure-Enthalpy (P-h) diagram for ORC working fluid R123. When using R123 as ORC working fluid to recover waste heat from a CAES system, all of the pressure operating points should be at or within the region of the curve (the red line) because the left side of the curve stands for the saturated liquid state of R123, the right side of the curve stands for the saturated

vapour state of R123 (ASHRAE, 2014). Especially, the operating pressure of working fluid should be significantly considered. The operating pressure can be estimated and chosen by the temperature of working fluid heated by the evaporator. It is noticed that the maximum operating pressure cannot exceed the pressure of the highest operating point because the pressure at the highest operating point is the critical pressure of the ORC working fluid.

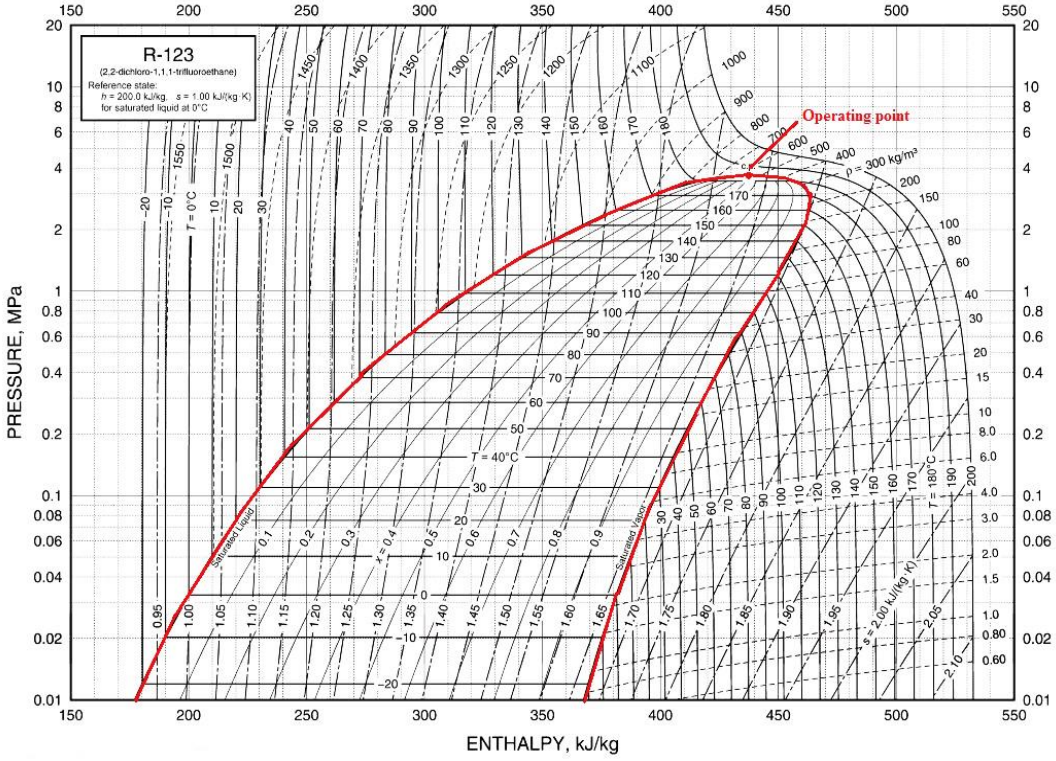

Figure 4-3. The P-h diagram for ORC working fluid (e.g. R123) (ASHRAE, 2014).

4.3 Round-trip efficiency of the integrated system

Based on equation (2-3), the general round-trip efficiency of the integrated system of the CAES system with the ORC can be described as:

$$\eta'_{CAES+ORC} = \frac{E_T + E_{ORC\_1} + E_{ORC\_2}}{E_f + E_C + E_{p\_1} + E_{p\_2}} \quad (4\text{-}1)$$

Where,

E_{ORC_1} = Power output of ORC during the charging period of the CAES system (kWh)

E_{ORC_2} = Power output of ORC during the discharging period (kWh)

E_{p_1} = Power consumption of ORC pump during the charging period (kWh)

E_{p_2} = Power consumption of ORC pump during the discharging period (kWh)

However, the power output E_{ORC_1} of the ORC during charging operation aims for reducing the electrical energy taken from the grid E_C for driving the compressors because charging operation occur in the off-peak time period. Therefore, converting Equation (4-1) to Equation (4-2) could be more accurate and acceptable for the round-trip efficiency of the integrated system based on reducing the electricity taken from the grid. Equation (4-2) can be written as:

$$\eta_{CAES+ORC} = \frac{E_T + E_{ORC\_2}}{E_f + (E_C - E_{ORC\_1}) + E_{p\_1} + E_{p\_2}} \quad (4\text{-}2)$$

Thus, the equation (4-2) will be used for the round-trip efficiency of the CAES system integrated with ORC in the following calculations.

4.4 Process analysis and technical performance evaluation of the integrated system

This section will discuss and analyse the effects of different ORC working fluids and expander inlet pressure (EIP) on the system performance. Some assumptions for the analysis of the proposed integrated system are:

- The fuel used in the CAES discharging process was assumed to be 100 vol% methane.
- The pressure drops of all the components were ignored.
- The temperature of condenser cooling water was assumed to be 10˚C.
- The working fluid at the outlet of the condenser was saturated liquid and the temperature was around 20˚C.
- The exhaust gas at the outlet of evaporator during the discharging period is 100% vapour fraction.
- The isentropic efficiencies of the ORC expander and pump were assumed to be 93% and 90% respectively (Aneke *et al.*, 2011; Cen *et al.*, 2009).
- The minimum temperature approaches of ORC evaporators (intercoolers and aftercooler) and condensers were assumed to be 3˚C (British Refrigeration Association, 2009; Tartière *et al.*, 2013; ACRG, 2005; El-Wakil, 1984).

4.4.1 Effects of the ORC organic working fluids

Selection of the working fluid is important for improving the performance of the ORC (Wang *et al.*, 2013; Tchanche *et al.*, 2011; Quoilin *et al.*, 2013; Desai and Bandyopadhyay, 2016). Different working fluids would have different impacts on the power output and the round-trip efficiency. Therefore, it is essential to

investigate the effects of different organic working fluids on the ORC power output and the round-trip efficiency of the integrated system.

For this case study, the performance of the following ORC working fluids in the ORC will be compared: R123 (2, 2-dichloro-1, 1, 1-trifluoroethane), R134a (1, 1, 1, 2-tetrafluoroethane), R152a (1, 1-difluoroethane), R245fa (1, 1, 1, 3, 3-pentafluoropropane) and R600a (isobutene). The thermo-physical properties of these refrigerants listed in Table 4-1 are calculated by REFROP V9.1. The input conditions for the CAES system were shown in Table 3-4 of Section 3.2.3.

Table 4-1. Thermo-physical properties of different working fluids for ORC.

Working fluids	**Molecular Mass (kg/kmol)**	**Boiling Point (˚C)**	**Critical Pressure (bar)**	**Critical Temperature (˚C)**
R123	152.93	27.82	36.62	183.68
R134a	102.03	-26.07	40.60	101.06
R152a	66.05	-24.02	45.17	113.26
R245fa	134.05	15.14	36.51	154.01
R600a	58.12	-11.75	36.29	134.66

Table 4-2 presents the simulation results of the integrated systems using different organic working fluids in the ORC. From the results in Table 4-2, R123 gives the highest ORC power output in both charging and discharging operations of the CAES system because the higher critical temperature of the working fluid could improve the system performance (Quoilin *et al.*, 2013; Liu *et al.*, 2004). A high critical

temperature also could result in low vapour densities, this can lead to the high cost. The results showed that there are significant differences in ORC expander inlet pressure (EIP) for different ORC working fluids, the effect of the EIP on the system performance will be discussed in section 4.4.2.

Table 4-2. Simulation results of the integrated system using different ORC working fluids.

	R600a		**R245fa**		**R152a**	
Variables	**Charging**	**Discharging**	**Charging**	**Discharging**	**Charging**	**Discharging**
EIP* (bar)	17.40	24.60	10.70	18.40	30.90	45.10
EIT* (˚C)	92.90	111.58	92.93	117.79	93.14	113.17
Mass flow rate (kg/s)	515.26	36.53	883.83	61.49	689.24	58.90
E_{ORC_1} (MW)	33.25		33.24		33.97	
E_{ORC_2} (MW)		2.78		2.89		2.72

* EIP and EIT are ORC expander inlet pressure and temperature respectively.

	R134a		**R123**	
Variables	**Charging**	**Discharging**	**Charging**	**Discharging**
EIP* (bar)	34.70	40.00	6.71	11.50
EIT* (˚C)	93.07	100.31	93.19	117.85
Mass flow rate (kg/s)	1092.51	86.99	1006.80	69.76
E_{ORC_1} (MW)	32.49		34.36	
E_{ORC_2} (MW)		2.42		3.01

Figure 4-4 presents round-trip efficiencies of the standalone CAES system and the integrated system using different ORC working fluids. The round-trip efficiency of the CAES system without the ORC was 59.29% calculated by Equation (2-3). Round-trip efficiencies of the integrated system using different working fluids were 62.95% (R600a), 63.07% (R245a), 62.91% (R152a), 62.61% (R134a) and 63.24% (R123) respectively, which were calculated by Equation (4-2). It is evident from Fig. 4-4 that round-trip efficiencies of the integrated system using different working fluids increased by 3.32-3.95% when integrating with the ORC. Therefore, integrating the ORC with the CAES system as well as selecting appropriate working fluid is a reasonable approach to improve the performance of the CAES system.

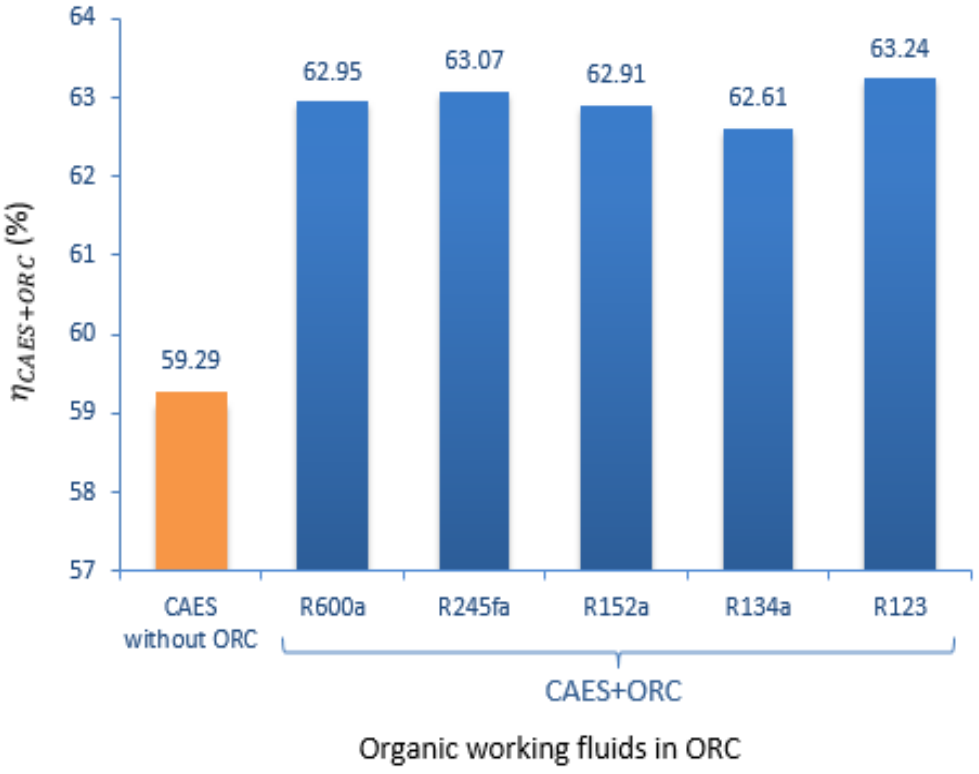

Figure 4-4. Round-trip efficiency of the standalone CAES system and the integrated system using different ORC working fluids.

When applying the ORC to recover waste heat from the CAES system to generate extra electricity for performance improvement of the integrated system, the original amount of electricity generated by the standalone CAES system would not be affected in the integrated system. Thus, the 3.32% - 3.95% efficiency improvement reported for the integrated system is from the waste heat recovery using ORC. For example, 3.95% efficiency increase (using R123 as the ORC working fluid) means the integrated system will generate 37.37 MW electricity, which is much more than that of the standalone CAES system.

4.4.2 Effects of expander inlet pressure (EIP) of the ORC

The EIP of the ORC should be considered since the pressure ratio of the expander will significantly affect the output power of the ORC. Therefore, it is essential to investigate the relationships of EIP of different working fluids and the ORC power output during charging and discharging periods.

The input conditions were same as Section 4.4.1. Figure 4-5 indicates the variation of the ORC net power output with the EIP during (a) charging and (b) discharging processes. An increase in the EIP leads to the increase of ORC power output using these five different working fluids. This is because with the fixed expander outlet pressure, a higher EIP will mean a higher pressure ratio of the expander leading to a larger enthalpy drop through the expander.

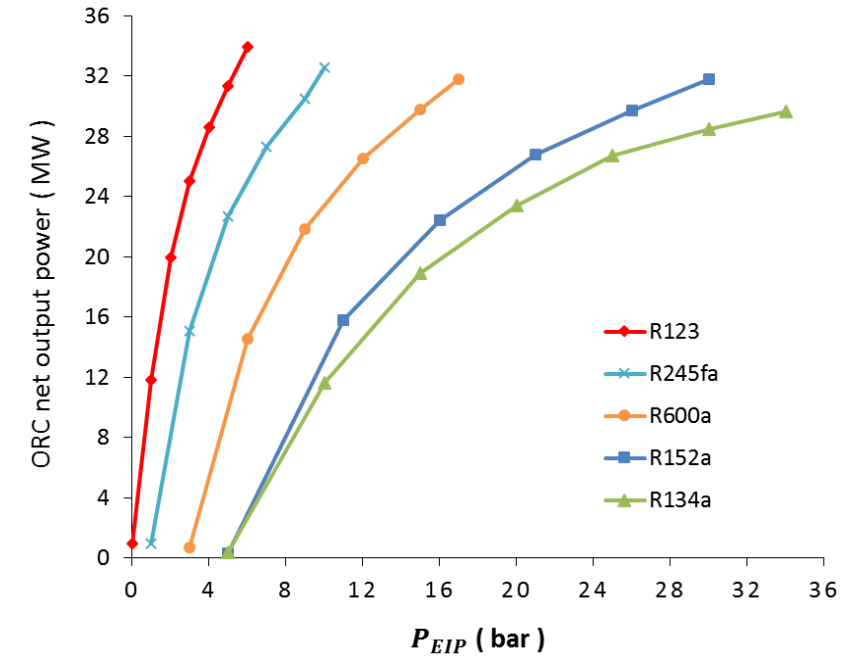

(a)

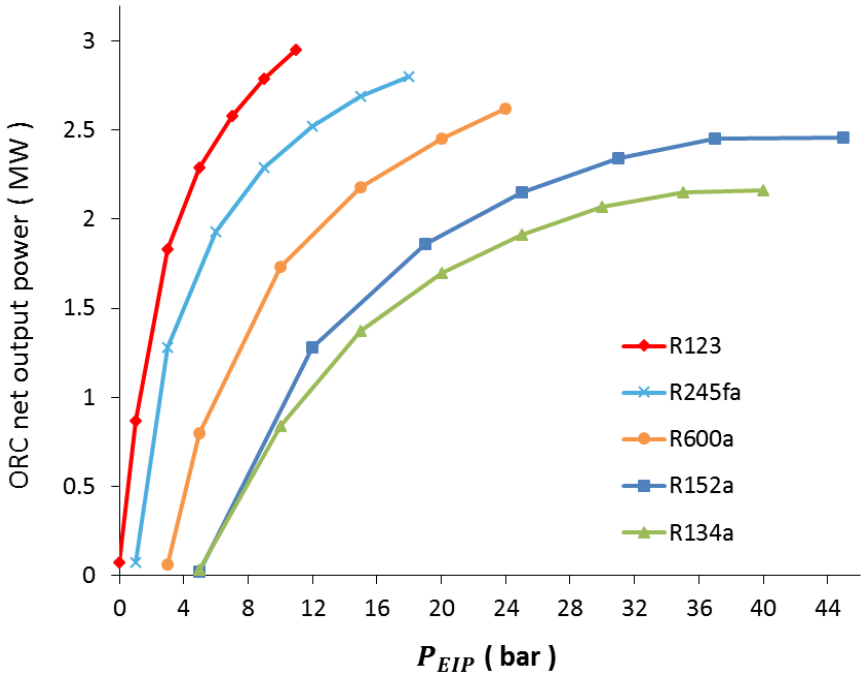

(b)

Figure 4-5. Effect of EIP on ORC net power output during (a) charging and (b) discharging processes of the CAES system.

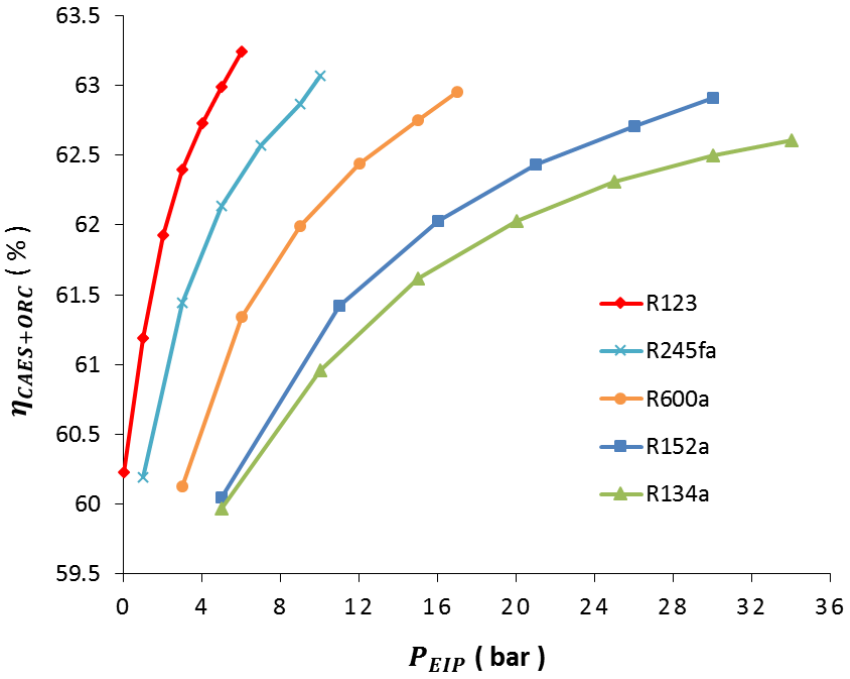

(a)

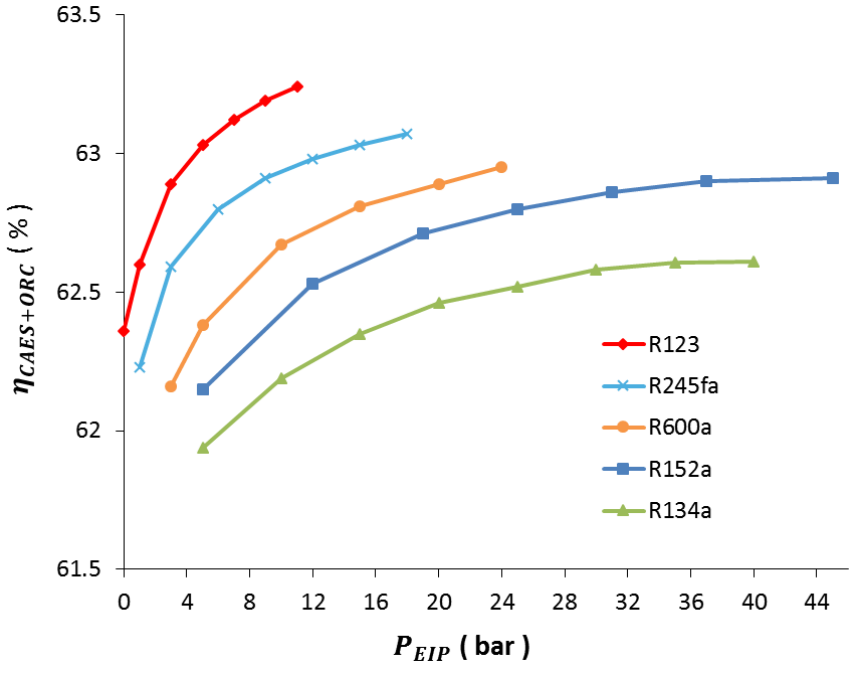

(b)

Figure 4-6. Effect of EIP on the round-trip efficiency of the integrated system during (a) charging and (b) discharging processes.

Figure 4-6 presents the variation of the round-trip efficiency of the integrated system with the EIP of the ORC during charging and discharging processes. A higher EIP will lead to an increase in the ORC net power output. The Round-trip efficiencies of both Figure 4-6 (a) and (b) were calculated by Equation (4-2). The Round-trip efficiencies in Figure 4-6 (a) were calculated by varying the EIP of the expander during the charging process while the EIP of the expander during the discharging process was fixed at the best operating point. Conversely, the round-trip efficiencies in Figure 4-6 (b) were calculated by varying the EIP of the expander during discharging process while the EIP of the expander during charging process was fixed at the best operating point.

From the results of Figure 4-5, the EIP of using R134a and R152a as ORC working fluids servicing to discharging operation of the CAES system could be not appropriate because the EIP of using them implemented to achieve the best net power output has already reached their critical pressures (refer to Table 4-1). R123 as the ORC working fluid can generate the highest net power output with the lowest EIP, but the flow rate is not low (refer to Table 4-2) which could lead to the increase of capital cost. Therefore, selecting an appropriate working fluid considers efficiency and safe operation frequently, economic evaluation is also an important factor for power plants. The Chapter 6 will investigate economic evaluation of the integrated system using different ORC working fluids.

4.5 Conclusions

As for the CAES system integrated with the ORC in this study, the steady-state process model of the proposed CAES system integrated with the ORC developed in

Chapter 3 was used for process analysis. The technical evaluation was carried out for the effects of different working fluids in the ORC. The main conclusions are summarised as follows:

- The power output and operating temperature of working fluids increase with the operating pressure, the ORC performance is also improved.
- The round-trip efficiency of the CAES system integrated with the ORC has been improved approximately by 3.32-3.95% with different working fluids in the ORC when compared with the CAES system without the ORC.
- R123 as the ORC working fluid has the best performance with a lower expander inlet pressure.

In summary, the CAES system integrated with the ORC as an energy storage technology will not only address the intermittent issue but also could decrease the electricity price for renewable energy to improve their overall economic competitiveness. The economic evaluation of the CAES system integrated with ORC using different ORC working fluids will be investigated in Chapter 6.

5. Performance Investigation of CAES System for Wind Power at Design and Off-design Conditions

5.1 Introduction

In this chapter, the process description and operation strategies of the CAES system integrated with wind power are presented. The type selection of main components including the compressor and turbine will be considered for the CAES system. The improved models for compressors, turbines and CAES system developed in Chapter 3 will be used for process analysis in this chapter. Performance analysis of the CAES system in the context of wind power at design and off-design conditions will be investigated, also two different modes (e.g. constant and variable shaft speed modes) at off-design conditions will be compared with design conditions of the CAES system. The models for wind farm and components between the CAES system and wind turbines are not included and this chapter only studies the standalone CAES system for wind power, the ORC is also not included.

5.2 Process description and operation strategies for the CAES system integrated with wind power

5.2.1 Process description of the CAES system integrated with wind power

The integrated system (as shown in Figure 5-1) includes wind turbines, a CAES system and the electricity grid. Under normal circumstance, the wind farm will transmit all the electric power generated directly to the grid. However, if the wind power output is more than the grid demand, the excess electricity can be utilised to

drive the compressors for compressing air in the charging process of the CAES system. The compressed air is injected into an underground cavern at high pressure.

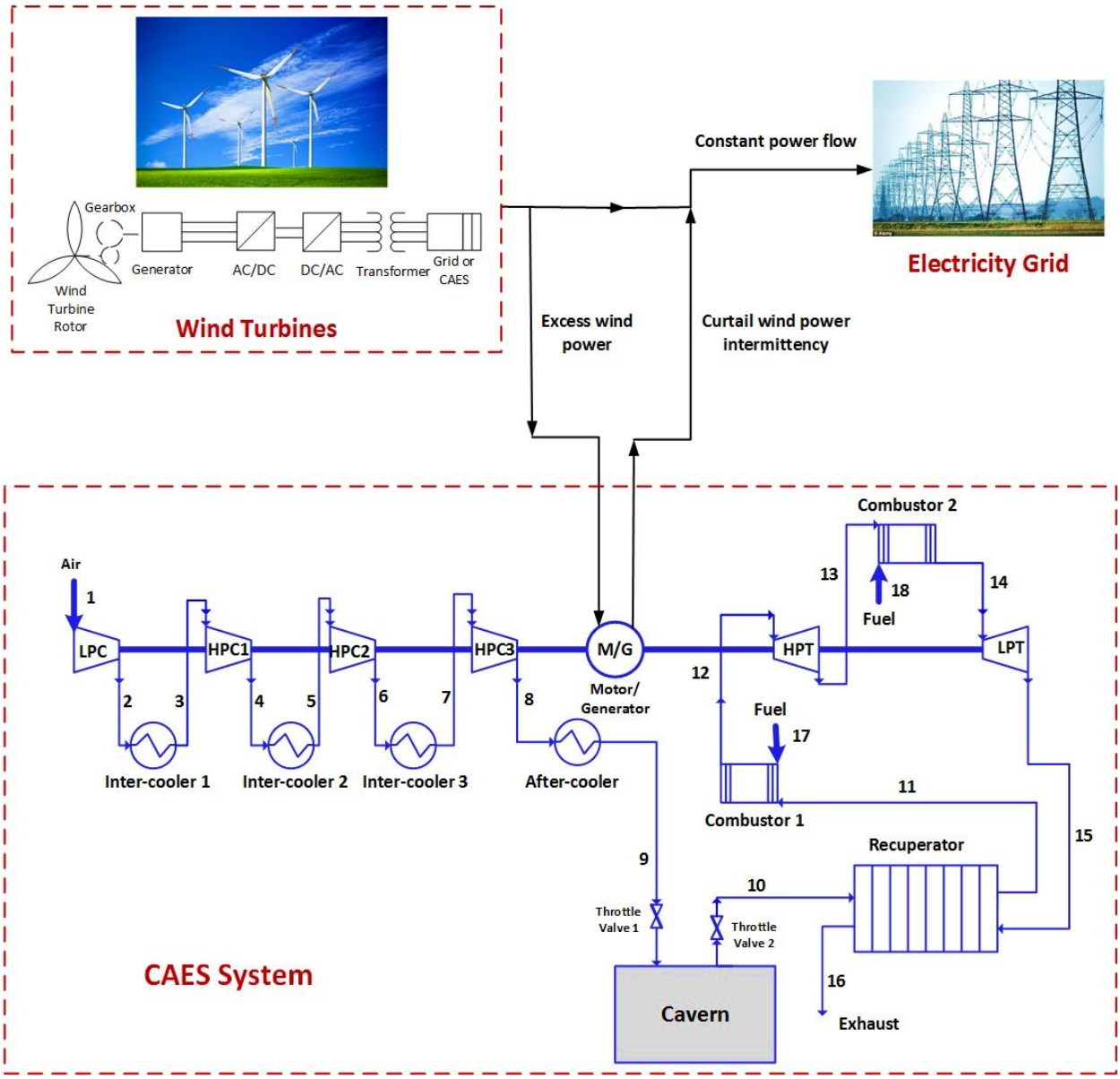

Figure 5-1. The schematic diagram of the CAES system integrated with wind turbines.

When the output power from the wind farm is below grid demand, the stored compressed air can be expanded in the turbines to generate electricity to balance the insufficient wind power output during the discharging process of the CAES system.

With a recuperator, the compressed air extracted from the cavern is preheated with the waste heat from the turbine exhaust to improve the round-trip efficiency of the CAES system. Then, the preheated air passes into the combustor, where it is mixed with fuel and combusted. The high-temperature combustion product is expanded in the turbines to generate electricity (Luo *et al.*, 2014; Chen *et al.*, 2013). Therefore, one advantage of integrating the CAES system with wind power is that the CAES system can be used to curtail the intermittency of wind power by matching the integrated system output with the grid power demand.

5.2.2 Operation strategies for the CAES system for wind power

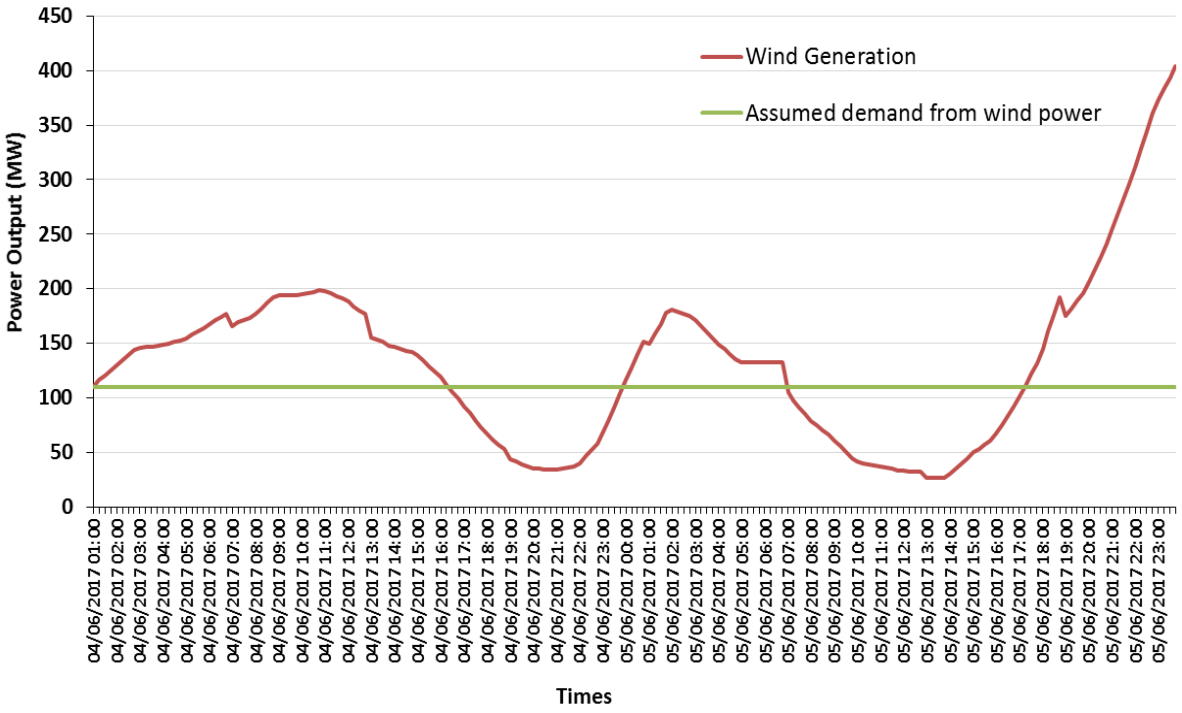

Figure 5-2. Wind power output in Northern Ireland over a 48-hour period (EIRGRID GROUP, 2017).

The wind power output in Northern Ireland over a 48-hour period is shown in Figure 5-2. The power output is seen to fluctuate between 30 MWe and 400 MWe during this period. For the purpose of this study, it is assumed that the wind power required to supply to the electricity grid is 110 MWe at all the time (as shown with the solid green line in Figure 5-2). The operation strategies of the integrated system can be summarised as:

a) Wind power output above 110 MWe (e.g. from 01:00 to 16:00 in Figure 5-2): 110 MW of electricity is supplied to the grid and the excess electricity is used in the CAES system for storing energy in the form of compressed air;

b) Wind power output below 110 MWe (e.g. from 16:00 to 24:00 in Figure 5-2): The compressed air in the CAES system is expanded to generate electricity to balance the wind power output

c) Wind power output plus the CAES system power output below 110 MWe: It is assumed that the electricity produced from other power plants (e.g. a conventional power plant) will cover the imbalance (Enis *et al.*, 2003).

5.3 Type selection for compressors and turbines of the CAES system

A combination of a low-pressure axial compressor and three high-pressure centrifugal compressors, gas turbines were used in Huntorf CAES plant (Riaz, 2010; Wang, 2017; Hoffeins, 1994). In this study, the outlet pressure of compression process of the CAES system can reach over 70 bar, so the multi-stage compressors with intercooling will be implemented. There are four compressors implemented in

the charging process of the CAES system: an axial LPC and three centrifuge HPC. As described in Section 1.1.5, the axial compressor implemented in the first stage of compression process is used for the requirement of low differential pressure, high volume air flow rate and higher efficiency, but the big weight, complex structure and high starting power requirements of the axial compressors are its drawbacks (EnggCyclopedia, 2012). The wide range of pressure rise is from about 6 bar to 70 bar after the first stage of compression. The wide range of pressure rise is determined by the high rotational speed of impeller and size. Nevertheless, the maximum allowable speed will be limited by the strength of structural materials of the impeller blades. Thus, the limitation on maximum achievable pressure rise can be overcome using high shaft speed centrifugal compressors, which is able to compress air to desirable pressure using multi-stage centrifugal compressors operating in series (EnggCyclopedia, 2012). It is noticed that the wind speed varies randomly over a wide range to result in wind power output fluctuated in a large magnitude. The operational range of the CAES system under off-design condition could be limited by the surge and choke margins of the centrifugal and axial compressors (Zhang *et al.*, 2017).

In the discharging process, there are two turbines HPT and LPT implemented for two expansion stages. The gas inlet condition of the first expansion stage in the CAES system for the high-pressure turbine of 43 bar at 550°C is the common feature of the steam turbine construction (Hoffeins, 1994). The steam turbine can work at temperatures between 500 and 650 °C and high, medium and low pressure and the general gas turbine was not compatible with the expansion pressure range from 43 bar to 11 bar (Kraftwerk, 2018; Barnes and Levine, 2011). Therefore, the HPT used

in the first expansion stage is designed by the engineering principle of the steam turbine (Hoffeins, 1994). The LPT designed by the engineering principle of the gas turbine is used in second expansion stage for the hot combustion gases and available operated at high temperature up to 1500 °C and a pressure drop of 11 bar to 1 bar (Kraftwerk, 2018; Hoffeins, 1994).

5.4 Performance analysis of the CAES system in the context of wind power

This section will investigate the technical performance of the CAES system in the context of wind power at design and off-design conditions.

5.4.1 Performance evaluation of the CAES system at design condition

In this case, the performance of the CAES system at design condition will be investigated based on the condition of wind power output in Northern Ireland (refer to Figure 5-2) and it will be viewed as a base case for the performance analysis at off-design conditions.

During the charging period, assuming continuous high wind speed, the wind power output is assumed to be constant at 170 MWe and the power requirement from electricity grid is 110 MWe. Therefore, the 60 MWe electricity from the wind farm will be used by the CAES system. During the discharging period, assuming continuous weak wind speed, the wind power output is assumed to be constant at 34.5 MWe. Thus, the 75.5 MWe electricity generated from the CAES system needs to be delivered to the grid. Table 5-1 lists the wind power condition and input parameters for the CAES system for this case study.

Table 5-1. The wind power condition and input parameters at design condition for the CAES system.

Process parameters		**Values**
Ambient air temperature (˚C)		20
Ambient air pressure (bar)		1.01325
Regular operation pressure of the cavern (bar) (Crotogino *et al.*, 2001; Hoffeins, 1994)		43 – 66
Air temperature in the cavern (˚C)		50
Air mass flowrate in charging process (kg/s)		108
LP / HP compressor ratio		5.6436 / 2.37
HP / LP turbine ratio		3.7313 / 10.5263
Air mass flowrate in the discharging process (kg/s)		99.60
The inlet pressure of combustor 1 (bar)		43
The inlet temperature of combustor 1 (˚C)		50
The inlet temperature of HP / LP turbines (˚C)		550 / 825
Exhaust gas temperature (˚C)		110
Wind power to compressors (Motor)	Rated power (MW)	60
	Frequency (Hz)	50
	Voltage (kV)	21
	Speed (min^{-1})	3000

Some assumptions about the CAES system are also made as follows:

- The pressure drops in the intercoolers and aftercooler are assumed to be 1.5% of the inlet pressure (Briola *et al.*, 2016).

- The pressure drops of the two combustors are 2% of the inlet pressure (Briola *et al.*, 2016).
- The fuel used in the CAES discharging process is pure methane.
- The isentropic efficiencies of the compressors and turbines are assumed to be 84% and 90% respectively (Briola *et al.*, 2016; Cen *et al.*, 2009).
- The volume of the cavern is assumed to be 140,000 m^3.
- The temperature of the compressed air in the cavern is assumed constant at 50 ˚C.

Simulation results of the CAES system based on the aforementioned parameters and assumptions are shown in Tables 5-2 and 5-3. Table 5-2 shows the values of the stream variable at each point in the system (refer to Figure 5-1 for the stream numbering). The simulation results of performance of the CAES system at design condition is given in Table 5-3. The total charging electricity of all compressors is 60MW and total discharging electricity output by the turbines is around 75.5MW. The fuel consumed to preheat the compressed air is 83.65MJ/s during the discharging process. The charging time (around 8.94 hours) and discharging time (around 9.70 hours) were calculated by the Equation (3-1) of the pseudo-dynamic model of the cavern in Section 3.4.4. The round-trip efficiency of the CAES system at design condition is carried out to be 54.34%. This is around 12.34% higher than round-trip efficiency of the Huntorf CAES plant (about 42%) due to the use of a recuperator to recover waste heat from the LPT exhaust to preheat the compressed air during the discharging operation.

Table 5-2. The simulation results of the CAES system at design condition.

Stream Numbers	Pressure (bar)	Temperature (°C)	Flowrate (kg/s)
1	1.01325	20.00	108.00
2	5.72	237.01	108.00
3	5.63	50.00	108.00
4	13.35	155.21	108.00
5	13.15	50.00	108.00
6	31.16	155.32	108.00
7	30.70	50.00	108.00
8	72.57	155.40	108.00
9	71.66	50.00	108.00
10	43.00	50.00	99.60
11	43.00	334.11	99.60
12	42.14	550.00	100.09
13	11.29	332.56	100.09
14	11.06	825.00	101.27
15	1.05	384.90	101.27
16	1.05	110.00	101.27

Table 5-3. The simulation results of performance of the CAES system for wind power at design condition.

Output variables	Values
Total charging electricity of the compressors (MW)	60.00
Total electricity output (MW)	75.50
Total fuel consumption (MJ/s)	83.65
Charging time (Hours)	8.94
Discharging time (Hours)	9.70
Round-trip efficiency (%)	54.34

5.4.2 Off-design analysis of the CAES system for wind power

It is difficult to maintain a steady operation (i.e. constant design condition) for the CAES system in the context of wind power due to the continuous fluctuation of wind power output and the charging electricity of the CAES system. Thus, the CAES system would mostly be operated at off-design conditions during the periods of charging and discharging operation.

In the off-design analysis, two operation modes will be investigated including constant shaft speed mode and variable shaft speed mode of the compressors. In both cases, the turbines' speeds will be maintained at the electricity grid synchronous speed of 3000 rpm (Hoffeins, 1994).

5.4.2.1 Constant shaft speed mode

The constant shaft speed of the compressors is considered since fluctuating wind power output will significantly affect the mass flow rate of compressed air, which will also have a significant impact on the pressure ratio and isentropic efficiency of compressors (as shown in Figure 5-3) in the CAES charging process.

For this case study, the wind power output condition within 24 hours has been presented in Table 5-4. The average value of wind power output for each hour was calculated based on the wind power output in Figure 5-2. The power demand is 110 MWe required from wind power output. The input parameters of the CAES system was listed in Table 5-1.

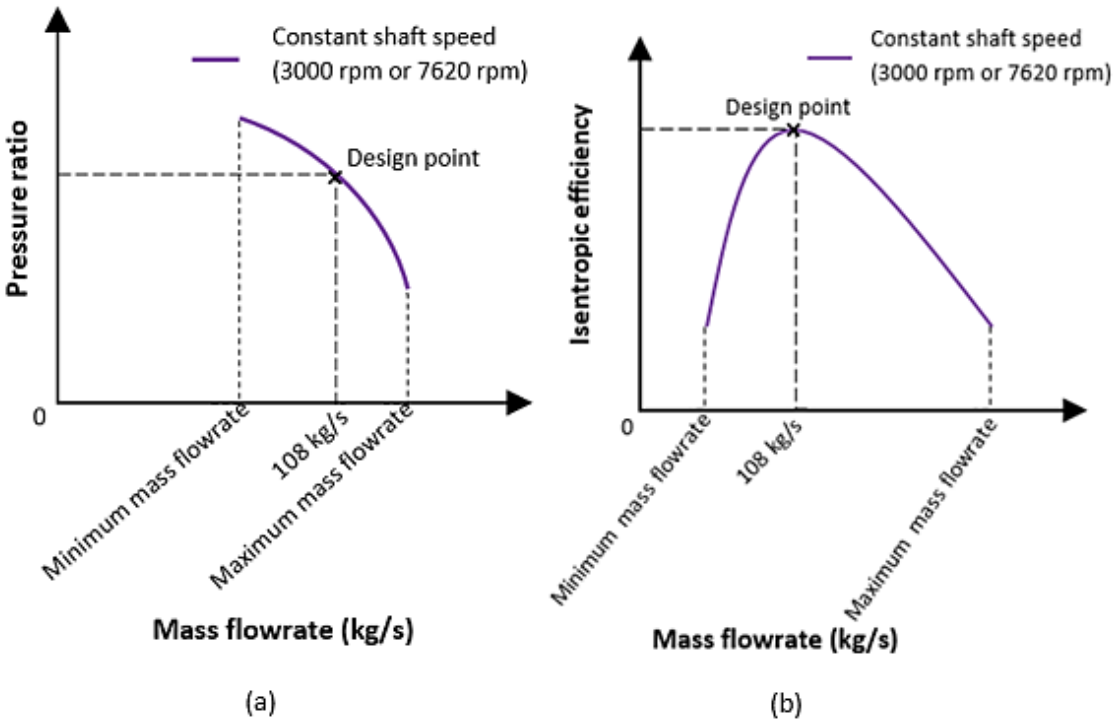

Figure 5-3. The sketch map of the relationship between both (a) pressure ratio and (b) isentropic efficiency with mass flowrate for LPC and HPC compressors at constant shaft speed mode.

The constant shaft speeds of LPC and HPC which are connected by using a gearbox are operated at 3000 rpm and 7620 rpm respectively. The different operating points from the characteristic curves of the compressors and the turbines at design condition (refer to Figure 3-4 (a) (b) v=1 and Figure 3-5 (a) (b) v=1) were used to obtain their corresponding performance data which were added into the models of the compressors and turbines developed in Aspen Plus® through *Performance Rating.*

Table 5-4. The conditions of wind power output within 24 hours.

Time (Hour)	Wind power output (MW)	Excess or insufficient wind power (MW)
00:00:00	114.50	4.50
01:00:00	118.00	8.00
02:00:00	136.75	26.75
03:00:00	147.00	37.00
04:00:00	150.50	40.50
05:00:00	159.25	49.25
06:00:00	172.50	62.50
07:00:00	169.75	59.75
08:00:00	184.50	74.50
09:00:00	194.00	84.00
10:00:00	196.75	86.75
11:00:00	194.00	84.00
12:00:00	182.25	72.25
13:00:00	151.75	41.75
14:00:00	144.25	34.25
15:00:00	131.50	21.50
16:00:00	108.75	- 1.25
17:00:00	82.50	- 27.50
18:00:00	59.75	- 50.25
19:00:00	40.50	- 69.50
20:00:00	34.50	- 75.50
21:00:00	35.50	- 74.50
22:00:00	49.00	- 61.00
23:00:00	85.25	- 24.75

The simulation results in Figure 5-4 show the charging and discharging power of the CAES system in the context of wind power at constant shaft speed mode within 24 hours. Figure 5-5 shows the air mass flowrate change of the CAES system for wind power at constant shaft speed mode. From the results, the charging process of the CAES system can be operated to utilise excess wind power and store compressed air for only 7 hours because the constant shaft speed of LPC limits the flow rate range of the compressed air between 106.40 kg/s and 120.5 kg/s.

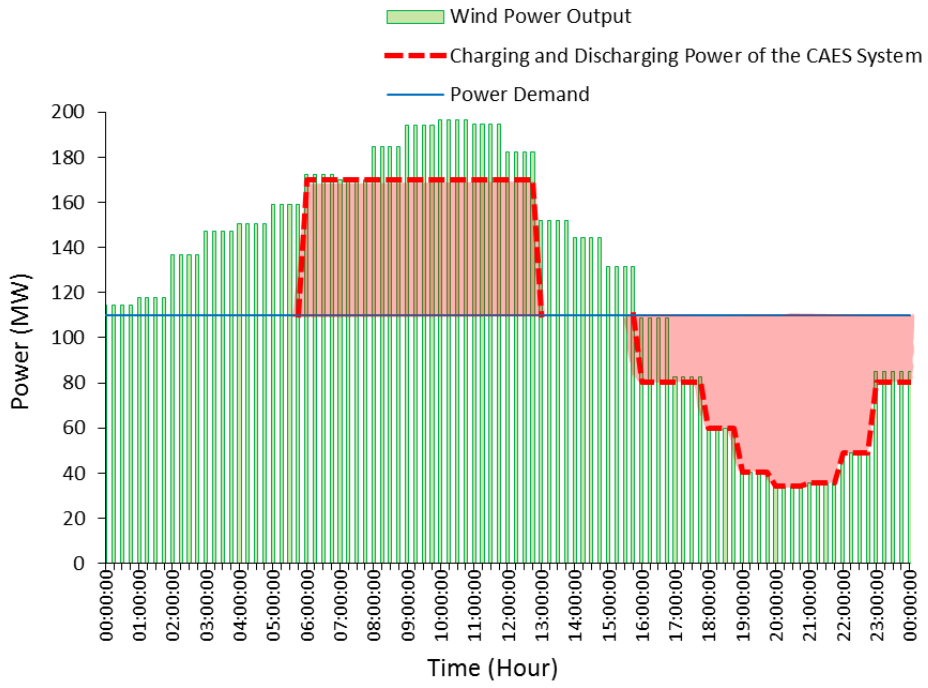

Figure 5-4. The simulation results of charging and discharging power of the CAES system for wind power at constant shaft speed mode within 24 hours.

If the flow rate is less than 106.4 kg/s, this could cause a surge condition of the LPC compressor. The rated mass flow rate of the CAES system at design condition is 108 kg/s. This will result in a limitation in the utilisation range of electricity taken from wind power, the electricity taken from the wind power for driving the compressors

will be limited to the range between 57.62 MW (106.40kg/s) and 60 MW (108 kg/s). In the discharging process, the constant shaft speed of the turbines limits flowrate range of the compressed air to be between 55.00 kg/s and 99.60 kg/s. Thus, the discharging power of the CAES system will be between 29.77 MW and 75.50 MW.

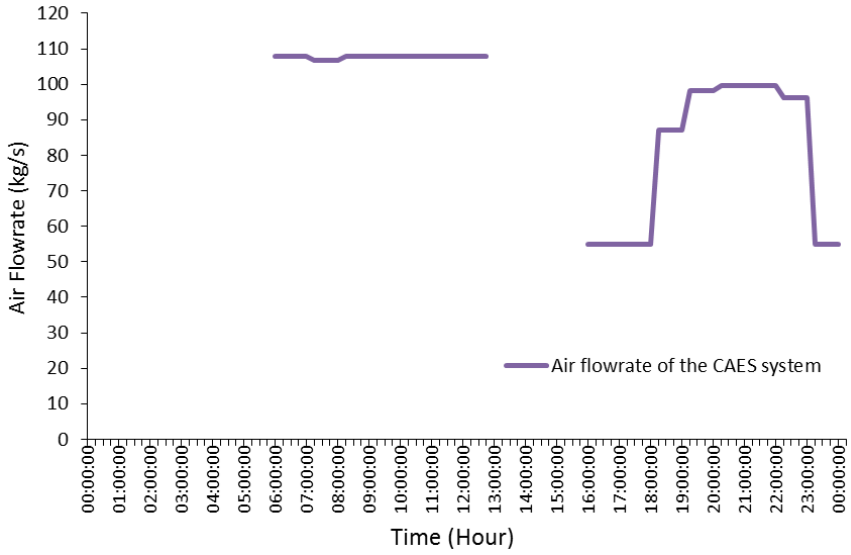

Figure 5-5. The air mass flowrate of the CAES system for wind power at constant shaft speed mode within 24 hours.

As for the charging and discharging time, the charging process of the CAES system taken from excess wind power is limited and operated from 6 am to 12 pm for 7 hours, the discharging process of the CAES system for generating electricity is operated from 4 pm to 11 pm for 8 hours. Figures 5-6 and 5-7 indicate the mass change of compressed air and pressure change of the cavern. The pressure of the cavern is an important factor considered in the operation process of the CAES system for wind power because the pressure of the cavern should be kept within the range of the regular operation pressure in the charging and discharging processes. Additionally, the round-trip efficiency of the CAES system for wind power at the constant shaft speed mode is calculated to be 47.15%. After 24 hours in Figures 5-

6 and 5-7, it is found that the mass of compressed air is remaining and the pressure of the cavern is higher than the minimum operation requirement of the cavern. Therefore, the CAES system can continue to generate more electricity, which will improve the round-trip efficiency of the CAES system for wind power from 47.15% to 50.98%.

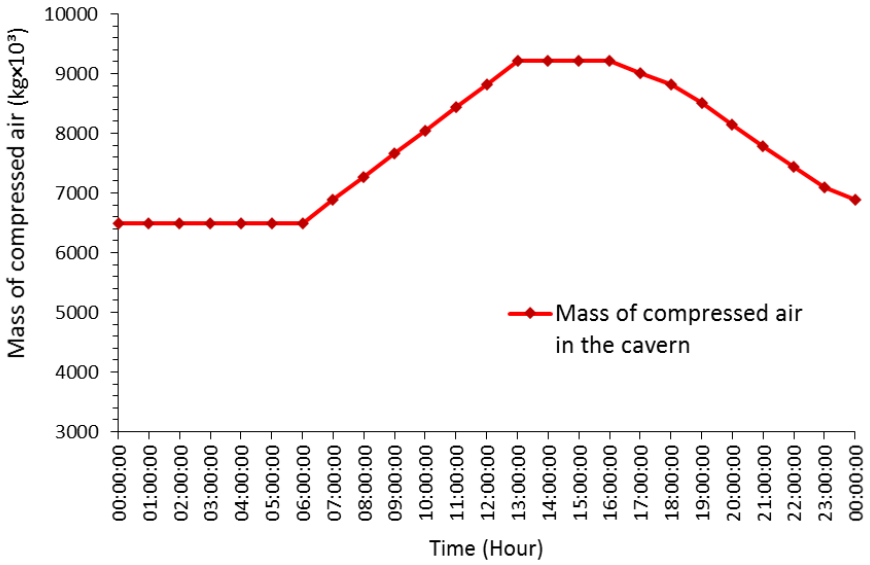

Figure 5-6. The mass change of the compressed air in the cavern at constant shaft speed mode within 24 hours.

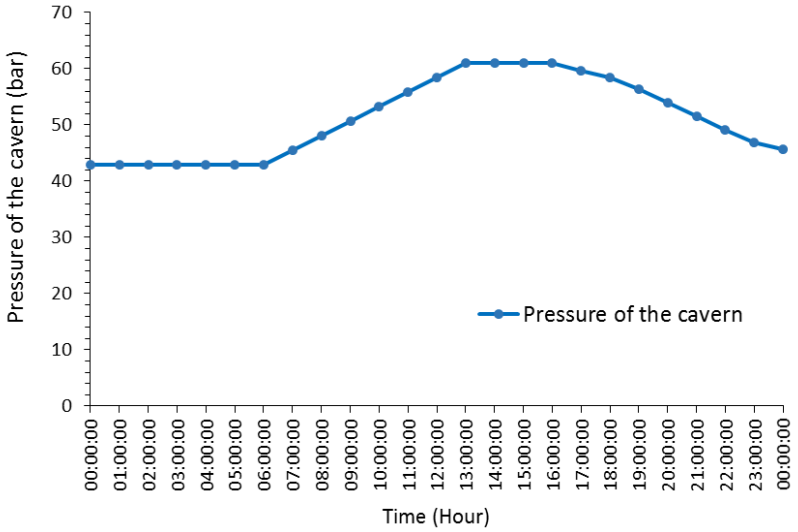

Figure 5-7. The pressure change in the cavern at constant shaft speed mode within 24 hours.

5.4.2.2 Variable shaft speed mode

The variable shaft speed of the compressors is also considered because the mass flow rate range was bounded at the constant shaft speed mode in Section 5.4.2.1. Also, the different wind power will affect the flow rate of compressed air which also has an impact on the pressure ratio and shaft speed of the LPC and HPC. Therefore, it is also essential to investigate the effects of variable shaft speed mode on the CAES system. For this case study, the wind power output condition is the same with the previous section in Table 5-4. The input conditions of the CAES system were same as Section 5.4.2.1. The characteristic curves of the compressors were used to obtain their corresponding performance data, which followed the optimal efficiency line enable LPC and HPC to operate at optimal efficiency at different shaft speeds (as shown with the solid green line in Figure 3-4 (a) and (b) 'Optimal efficiency').

From the simulation results of Figure 5-8, the simulation results of charging and discharging power of the CAES system for wind power at variable shaft speed mode were presented. Figure 5-9 shows the air mass flowrate change of the CAES system for wind power at variable shaft speed mode. Compared with the constant shaft speed mode, the CAES system at variable shaft speed mode can compress more mass of compressed air for energy storage than that at constant shaft speed mode. The charging process of the CAES system can be operated at a wider range of flow rate between 41.5 kg/s (power requirement of compressors is 7.1 MW) and 108 kg/s (60 MW).

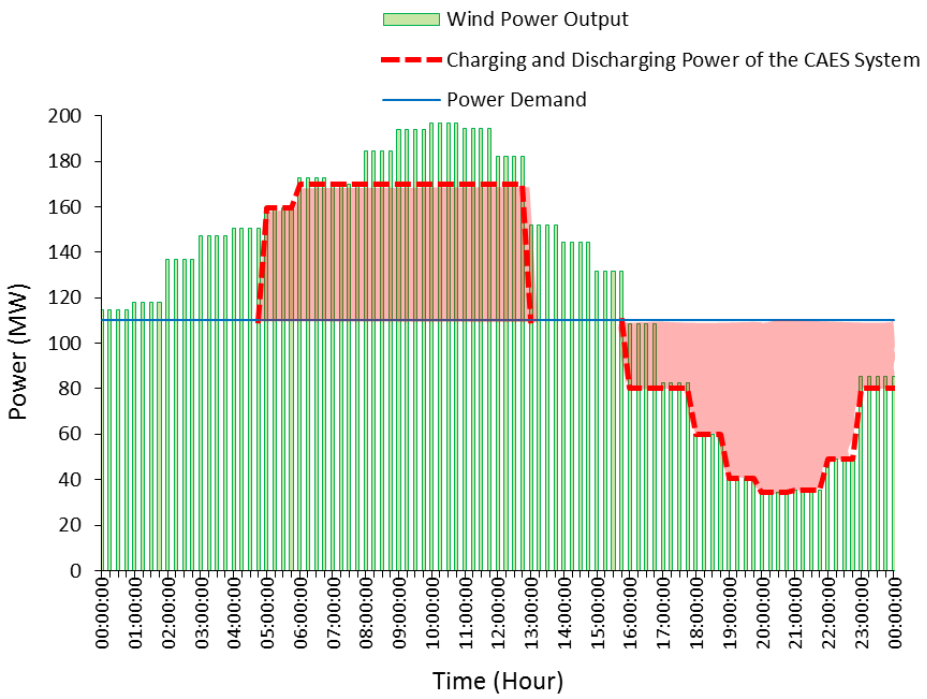

Figure 5-8. The simulation results of charging and discharging power of the CAES system for wind power at variable shaft speed mode within 24 hours.

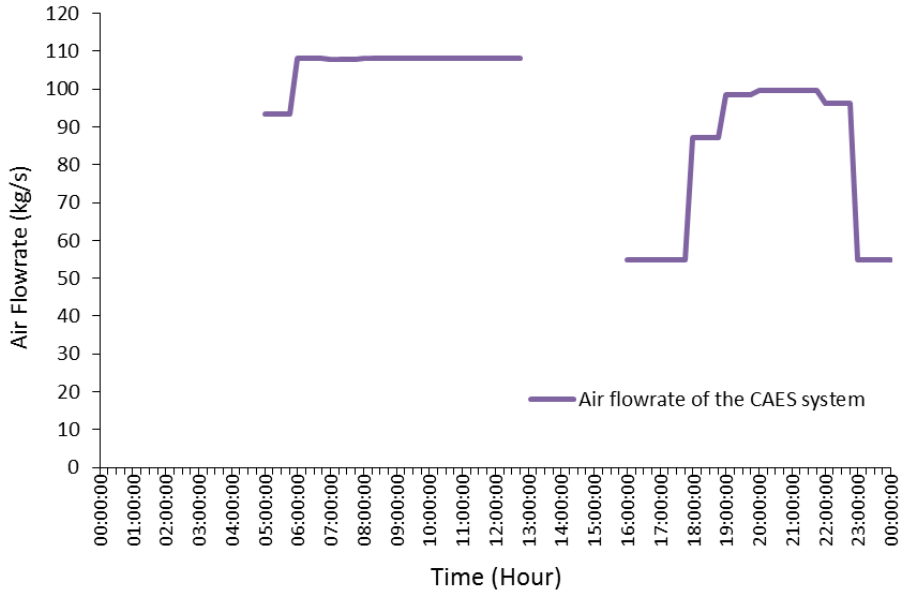

Figure 5-9. The air mass flowrate of the CAES system for wind power at variable shaft speed mode within 24 hours.

However, it is noticed that the outlet pressure of the aftercooler through a throttle valve should be considered and this pressure should be higher than existing pressure of the cavern. Otherwise, the compressed air cannot be injected into the cavern. Therefore, the charging time of the CAES system taken excess wind power and ensuring the inlet pressure to be higher than the existing pressure of the cavern was from at 5 am to 1 pm for 8 hours. As for the discharging process, the operation condition at variable shaft speed mode is the same as that at constant shaft speed mode due to the same condition of both modes. The round-trip efficiency of the CAES system for wind power at variable shaft speed mode is calculated to be 44.68%. From Figures 5-10 and 5-11, it is also found that the mass of compressed air is remaining and the pressure of the cavern is also higher than the minimum operation requirement of the cavern after 24 hours operation. Therefore, the system can continue to generate more electricity, which will improve the round-trip efficiency of the CAES system for wind power from 44.68% to 51.69%.

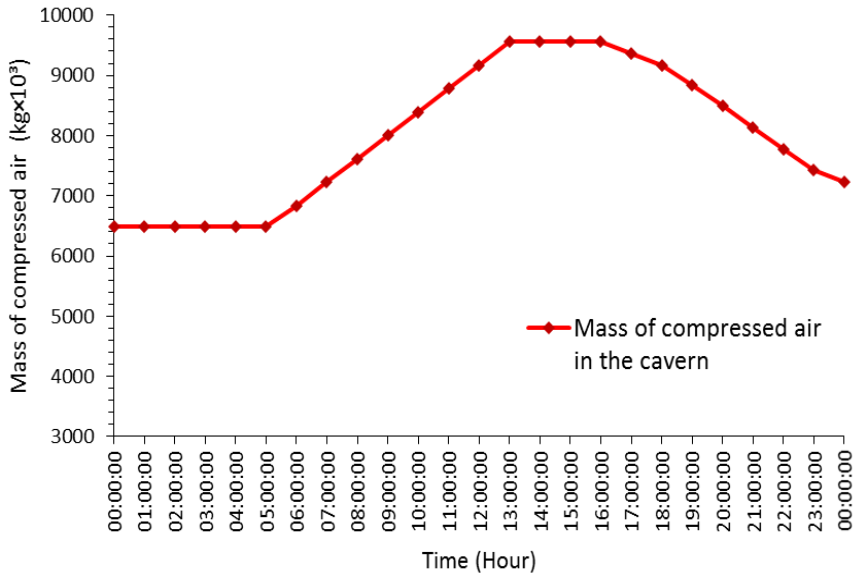

Figure 5-10. The mass change of the compressed air in the cavern at variable shaft speed mode within 24 hours.

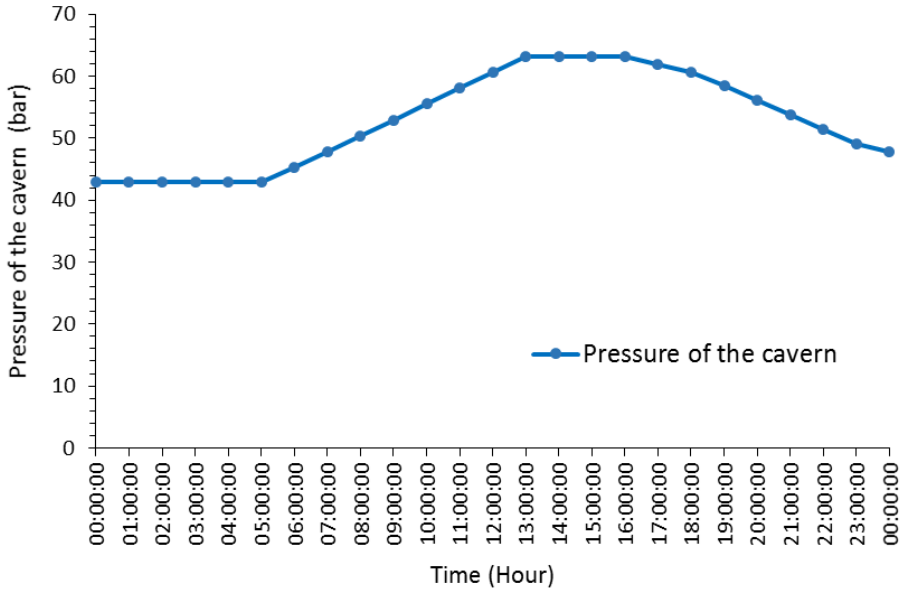

Figure 5-11. The pressure change of the compressed air of the cavern at variable shaft speed mode within 24 hours.

5.4.2.3 Comparison between the two modes

Comparing the design and off-design conditions, it is evident that the round-trip efficiency of the CAES system for wind power at design condition is higher than that at off-design conditions. The reason is that the CAES system for wind power can operate at optimal operating points at design condition. However, the CAES system operating at design condition can only be an ideal case.

Comparing both modes at off-design conditions, both modes have same electricity generation in the discharging process within 24 hours, but the charging process at variable shaft speed mode can utilise more excess wind energy for energy storage than at constant shaft speed mode. From the simulation results of Figures 5-4 and 5-8, the CAES system for wind power at variable shaft speed mode can use more excess wind energy (49.25 MWh) than constant shaft speed mode. From the

remaining mass of compressed air and pressure of the cavern at both modes in Figures 5-6 and 5-10, the CAES system for wind power at variable shaft speed mode can store more compressed air (51.55×10^3 kg) in the cavern than that at constant shaft speed mode. When the discharging process of the CAES system for wind power at both modes continue to operate for generating electricity in discharging process after 24 hours, the CAES system for wind power at variable shaft speed mode can generate more electricity (76.00 MWh) and provide longer discharging time than that at constant shaft speed mode. In this case, when the mass of the compressed air in the cavern at both modes can be utilised until to the same minimum operating pressure of the cavern (43 bar), the round-trip efficiency of the CAES system for wind power at variable shaft speed mode (51.69%) is higher than that at constant shaft speed mode (50.98%).

Moreover, the variable shaft speed compressor will save more electricity consumption than constant shaft speed compressor because the constant shaft speed compressor only can be very efficient when operating at design condition, it cannot be changed the shaft speed for lower mass flow rate. The variable shaft speed compressor can change the shaft speed with the different air mass flow rates, which can reduce energy consumption by about 35% (Atlas Copco, 2018). Therefore, the CAES system for wind power at variable shaft speed mode could be a better choice than constant shaft speed mode, due to higher round-trip efficiency, more utilisation of excess wind power and more power output.

5.5 Conclusions

In this chapter, the performance analysis of the CAES system in the context of wind power at design and off-design conditions was carried out. The improved models of the compressors, turbines and cavern were used for the CAES system in the context of wind power. The main conclusions are summarized as follows:

- The CAES system for wind power at constant and variable shaft speed modes can utilise excess wind electricity to store the compressed air and it can expand compressed air to generate electricity to smooth the fluctuating wind power with proposed different operating strategies.
- In the process analysis of off-design conditions, the range of air mass flow rate in the charging process of the CAES system at constant shaft speed mode was limited, which results in a limitation of the utilisation range of electricity taken from wind power. The range of air mass flow rate of the CAES system for wind power at variable shaft speed mode has a much wider range of the mass flow rate than that at constant shaft speed mode.
- The CAES system for wind power at variable shaft speed model has better performance than that at constant shaft speed. This is because the CAES system at variable shaft speed mode utilise more excess wind energy (49.25 MWh), store more compressed air (51.55×10^3 kg), generate more electricity (76.00 MWh) and provide longer discharging time than at constant shaft speed mode.

The CAES system could be an effective solution and promising approach for operating and utilising wind power to supply power for the grid flexibly.

Additionally, economics evaluation as an important factor for a power plant should be also considered. The economic evaluation of the CAES system for wind power at design and off-design conditions will be investigated in Chapter 6.

6. Economic Evaluation

6.1 Introduction

The economic evaluation should be one of vital factors considered for a system or plant. In this chapter, the methodology of economic evaluation is presented in Section 6.2. The economic evaluations for the CAES system integrated with ORC and the CAES system in the context of wind power will be investigated in Sections 6.3.1, 6.3.2 and 6.4 respectively. The comparison of LCOE between the CAES system and different power sources will be also considered in Sections 6.3.3 and 6.4.

6.2 Methodology of economic evaluation

Economic evaluations were implemented in APEA V8.4. APEA has become a professional and industrial standard Engineering tool. It is considered to be more accurate than correlation-based economic evaluation methods (Luo *et al.*, 2014). APEA can be used for engineering design and evaluation of different types of projects because it consists of design procedures and price data for many types of project materials and components and considers engineering contingency (5%). A bottom-up method is applied through the APEA. The unit operations were mapped to individual equipment cost model that can be designed manually due to some special components when the simulation model is imported into APEA.

The LCOE can calculate present value of the total cost of building and operating a power plant over an assumed lifetime, it can allow the comparison of different power sources, plant size, capital cost, capacities (USDOE, 2015). As for the expenditures, the LCOE of a system was calculated by dividing total annual cost (TAC) by the net

power output annually (E_{output}), as expressed in Equation (6-1) (Luo and Wang, 2017). TAC is a sum of annualised capital expenditure (ACAPEX), fixed operation expenditure (FOPEX) and variable operational expenditure (VOPEX), as described in Equation (6-2) (Luo *et al.*, 2014; McGrail *et al.*, 2013; Luo and Wang, 2017). CAPEX involves the costs of equipment materials and installation, engineering and management, labour generated during the plant construction. The ACAPEX is the total CAPEX multiplying by capital recovery factor (CRF), as written by Equations (6-3) and (6-4) (Luo and Wang, 2017; McGrail *et al.*, 2013). FOPEX involves the costs of long term service agreement, operating and maintenance and other fixed costs which could be generated during the periods of full load or shutdown. VOPEX of this system includes fuel cost and the cost of electricity consumption for the compressors.

$$LCOE = \frac{TAC}{E_{output}} \tag{6-1}$$

$$TAC = ACAPEX + FOPEX + VOPEX \tag{6-2}$$

$$ACAPEX = CAPEX \times CRF \tag{6-3}$$

$$CRF = \frac{i(1+i)^n}{(1+i)^n - 1} \tag{6-4}$$

CRF is determined by n (specifying the CAES plant life) and i (discount rate). Some parameters summarised in Table 6-1 were used for the LCOE model. Capacity factor is the total time of power output expected in one year. Regarding to the aforementioned equations, a simplified model can be used to calculate the LCOE of the integrated system, described in Equation (6-5) (McGrail *et al.*, 2013):

$$\textbf{\textit{LCOE}} = \{(CAPEX \times CRF + FOPEX) / (365days \times 24hours \times Capacity\ factor)\} + Fuel\ cost/kWh + Electricity\ consumption\ cost/kWh \quad (6\text{-}5)$$

Table 6-1. Parameters for LCOE model (McGrail *et al.*, 2013).

Description	Value
CAES plant lifetime (years)	20
Discount rate (%)	4
CRF	0.074
Capacity factor (%)	25
Fuel cost ($/Thousand Cubic Feet) (UEI, 2016)	3.426
Engineering contingency	5%

6.3 Economic evaluation for the CAES system integrated with ORC

6.3.1 Economic evaluation of effects of different working fluids of the ORC

For the CAES system integrated with ORC, the investigation of the LCOE with a different selection of ORC working fluids is important for comparing their economic advantages. Selection of the working fluid will not only affect the power output and round-trip efficiency, but also affect the cost of the equipment and the plant. Therefore, it is essential to investigate the economic impacts of the different ORC working fluids.

The compressors of the charging process will consume electricity to compress air for storing energy. In general, the CAES system uses excess and cheaper electricity

to compress air at the off-peak time, due to economical consideration. The electricity price 2.927 cents/kWh at the off-peak time in the winter was assumed for this case study (Pacific Power, 2017).

Table 6-2. Comparison of costs of CAES system integrated with ORC using different working fluids.

Costs	R134a	R123	R152a	R245fa	R600a
CAPEX (cents/kWh)	4.880	4.898	4.872	4.910	4.934
FOPEX (cents/kWh)	0.725	0.713	0.722	0.714	0.716
Fuel cost (cents/kWh)	0.0463	0.0462	0.0463	0.0462	0.0463
Electricity consumption cost (cents/kWh)	1.414	1.377	1.397	1.388	1.395
LCOE (cents/kWh)	7.066	7.035	7.037	7.058	7.091

This economic evaluation of the APEA model is based on Aspen Plus® model developed in Chapter 3. Table 6-2 illustrates the simulation results of different costs of the CAES system integrated with ORC using different working fluids. FOPEX and Fuel cost are almost the same for the five working fluids because all the components and flow rate of fuel are the same. However, the CAPEX is different because the EIP and EIT of ORC for the different working fluids are different. Hence, the size and capital cost of the components are different. Costs of electricity consumption for five different working fluids are different because power outputs for the different working fluids during charging and discharging operations are different. LCOE was lowest with R123 as the working fluid and that of R152a was almost the same as R123. However, the round-trip efficiencies of the integrated system for them are different (refer to Figure 4-4). Therefore, the round-trip

efficiency of a system is not the only factor that should be considered, economic evaluation of the system is also important.

6.3.2 Economic evaluation of effects of different power sources

The CAES system integrated with the ORC is not an independent system and it has to be associated with power plants such as coal-fired, wind, nuclear, solar photovoltaic (PV) power plants (Chen *et al.*, 2009). Therefore, considering and comparing the effects of the power sources on the price of electricity is essential.

The CAES system without the ORC will be implemented and compared with the integrated system associated with different power sources including charge free, commercial power (off-peak), wind power, nuclear power and solar PV power. Electricity prices of these power sources are different. Therefore, it is more persuasive that LCOEs of the integrated system using different working fluids associated with different power sources was investigated.

Table 6-3 shows the LCOE of the CAES system without ORC and the CAES system integrated with the ORC associated with different power sources. From the results, if the charging electricity is free, LCOE of the CAES system without the ORC is only 5.247 cents/kWh which is cheaper than that of the integrated system using working fluid, because it is uneconomical to recover waste heat during charging operation of the CAES system when electricity is free. When adopting off-peak commercial electricity for energy management strategy, the LCOE of the CAES system is still cheaper than residential electricity price (12.75 cents/kWh (EIA, 2016)) and the CAES system integrated with the ORC running in the summer is more economical than the CAES system without the ORC. When the CAES system

is supplied with expensive renewable energy, it is evident that LCOE of the CAES system integrated with the ORC is much cheaper than renewable energy except onshore wind power, and the LCOE of the CAES system integrated with ORC associated with renewable energy is cheaper than that of the CAES system without ORC.

Table 6-3. LCOE of the standalone CAES system and the integrated system associated with different power sources.

		Charge free	**Commercial power** (Pacific Power, 2017)		**Wind power** (OpenEI, 2015)		**Nuclear power** (OpenEI, 2015)	**Solar PV power** (OpenEI, 2015; LAZARD, 2014)
			Off-peak (Summer)	Off-peak (Winter)	Onshore	Offshore		
Power price (cents/kWh)		0	7.912	2.927	7.2	13	10.2	16.85
		LCOE (cents/kWh)						
Case 1: CAES without ORC		5.247	9.673	6.885	9.275	12.520	10.953	14.674
Case 2: CAES with ORC	R134a	5.652	9.474	7.066	9.130	11.932	10.579	13.792
	R123	5.658	9.380	7.035	9.045	11.774	10.456	13.585
	R152a	5.640	9.416	7.037	9.077	11.845	10.508	13.682
	R245fa	5.671	9.422	7.058	9.084	11.834	10.507	13.659
	R600a	5.696	9.466	7.091	9.127	11.891	10.557	13.726

The results for solar PV power and offshore wind power cases show the LCOE from the CAES system with the ORC is even lower than the power price supplied directly by solar PV and offshore wind power plant. This indicates one important benefit of the CAES system with the ORC, which is that the total amounts of electricity

generated from discharging process of the CAES system is almost double with the input rate of electricity during the charging process. The excess part actually is generated by combusting cheap fossil fuel such as natural gas. In this way, integrating the CAES system with the ORC could decrease the expensive prices of electricity from renewable energy such as offshore wind farm and solar power plant.

6.3.3 Comparison of LCOEs for different power sources

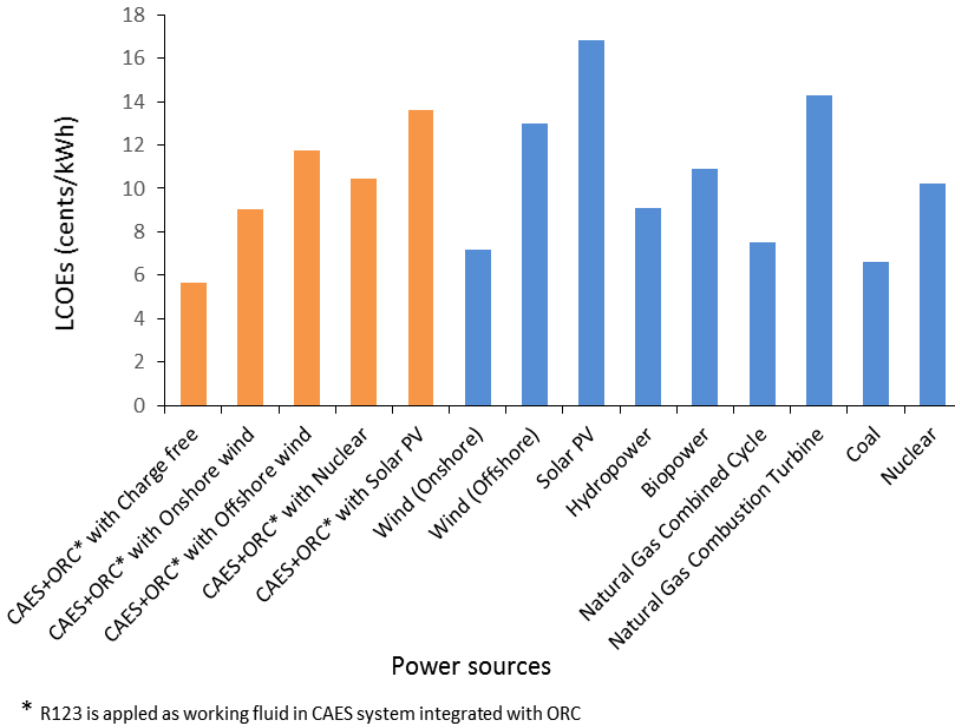

Figure 6-1. Comparative LCOEs for different power sources.

Figure 6-1 illustrates a comparison of LCOEs for different types of power sources. The CAES system integrated with the ORC associated with different power sources can provide the price of electricity that could be competitive with wind power, hydropower and nuclear power, even also some conventional coal power (OpenEI, 2015; LAZARD, 2014). The CAES system integrated with the ORC is capable of

solving intermittence of renewable energy and system level needs (such as off-peak oversupply, peak power generation, balancing supply-demand), its functions could have more potential value than reasonable LCOEs (McGrail *et al.*, 2013).

Additionally, the integrated system of the CAES system with the ORC has significant environmental benefits in the reduction of carbon emissions. The simulation results showed that the CO_2 emission of this integrated system is 0.1337 kg/kWh. Compare with other power plants, the CO_2 emission from brown-coal-fired and hard coal-fired power plants are 1.183 kg/kWh and 1.142 kg/kWh respectively, and that from Natural gas power plants is 0.572 kg/kWh (WINGAS, 2017). Hence, the CAES system integrated with ORC also releases much less CO_2 emission than other power sources.

6.4 Economic evaluation for the CAES system for wind power

Table 6-4 presents the LCOE of the CAES system for wind power at design and off-design conditions. From the results, the LCOE of the CAES system in the context of wind power at design condition (4.94 cents/kWh) is the cheapest of all. At off-design conditions, the LCOE of the CAES system for wind power within 24 hours is higher than that at the minimum operation pressure (43 bar) of the cavern because the stored compressed air was not fully discharged within 24 hours in this study and the CAES system can continue to produce more electricity after 24 hours. When both modes were operated within 24 hours, the LCOE at constant shaft speed mode is cheaper than that at variable shaft speed mode. However, the LCOE at constant shaft speed mode is higher than that at variable shaft speed mode, when both modes were operated at the same operating pressure of the cavern (43 bar). Moreover, the

LCOEs at these three modes are lower than the residential electricity price (12.75 cents/kWh (EIA, 2016)).

Table 6-4. Comparison of costs of CAES system for wind power at design and off-design conditions.

Cost (cents/kWh)	Design condition	Off-design conditions[1]		Off-design conditions[2]	
		Constant shaft speed mode[1]	Variable shaft speed mode[1]	Constant shaft speed mode[2]	Variable shaft speed mode[2]
ACAPEX	3.335	5.695	5.695	4.820	4.180
FOPEX	1.548	2.125	2.300	1.894	1.857
Fuel cost	0.058	0.0588	0.0588	0.0587	0.0586
LCOE	4.94	7.88	8.05	6.77	6.10

1. The CAES system for wind power was operated within only 24 hours of this study.
2. The CAES system for wind power was operated until to the minimum operation pressure (43 bar) of the cavern.

Figure 6-2 shows a comparison of LCOE between the CAES system and different types of power generation technologies. The CAES system can provide the price of electricity that could be cheaper than some renewable energies (e.g. offshore wind power and solar power), hydropower and nuclear power, even also some conventional power (Natural gas combustion turbine) (OpenEI, 2015; LAZARD, 2014). The CAES system integrated with the wind power is capable of balancing supply and demand of the grid. This function of the CAES system integrated with wind power could have more potential value than the reasonable LCOE (McGrail *et al.*, 2013).

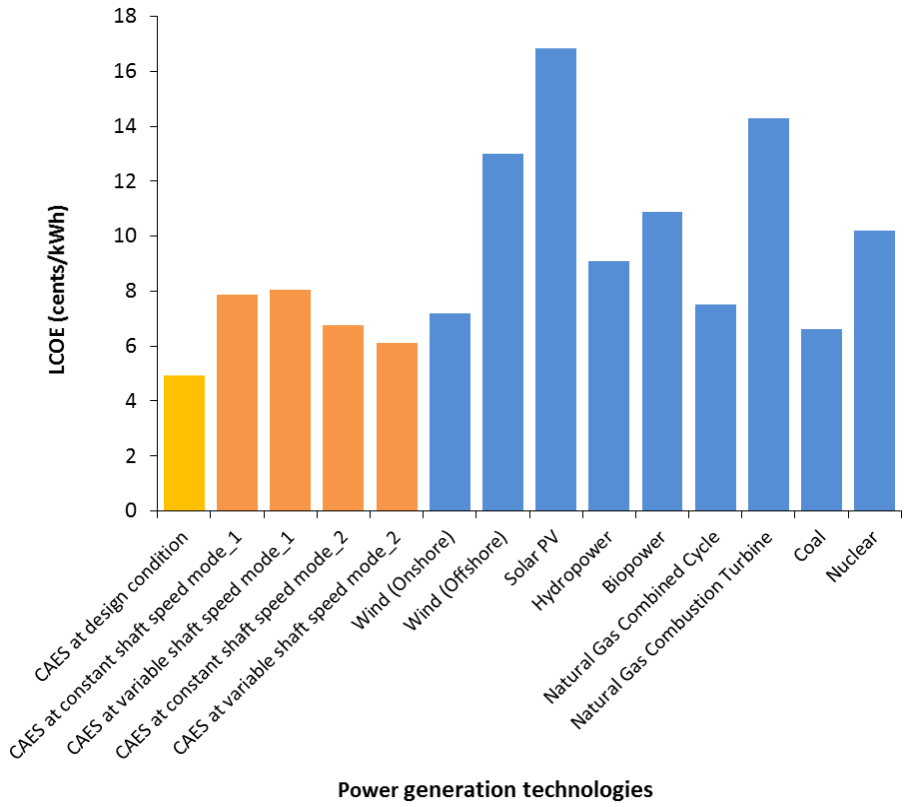

Figure 6-2. Comparative LCOE between the CAES system integrated with wind power and different power sources (OpenEI, 2015; LAZARD, 2014).

6.5 Conclusions

In this chapter, the economic evaluations of the CAES system integrated with the ORC and the CAES system for wind power were carried out by APEA. The main conclusions are summarized as follows:

- With free or low price off-peak electricity input for the charging process of the CAES system integrated with ORC, the LCOE for CAES plant is lower than the residential electricity price. The integrated system of the CAES

system with ORC further decreases the LCOE. That could be an effective solution for flexible operating for residential power supply.

- When the offshore wind farm or solar power plants are used in the CAES system integrated with ORC, their LCOEs could decrease which leads to a lower electricity sale price.
- R123 as the ORC working fluid has the best performance investigated in Chapter 4 and the lowest LCOE. The reason is that R123 with a lower expander inlet pressure. Hence, R123 as working fluid has a lower capital cost which leads to a lower LCOE.
- The LCOE for the CAES system for wind power at variable shaft speed mode is lower than that at constant shaft speed mode and the LCOE at both modes are lower than some renewable energies (e.g. offshore wind power and solar power), hydropower, nuclear power, some conventional powers (natural gas combustion turbine) and the residential electricity price.

Thus, the CAES system as one of grid-scale energy storage technologies will not only address the issue of intermittency of fluctuating wind power, but also can decrease the electricity price for renewable energy sources to improve their overall economic competitiveness.

7. Conclusions and Recommendations for Future Work

7.1 Conclusions

The CAES system has the potential for load shifting and curtailing the intermittency problem of wind electricity. A critical review and assessment for the CAES system were carried out. The review assessed different research fields of CAES systems including lab experimental rigs, pilot CAES plants, commercial and planned commercial CAES plants, performance improvement and system optimisation, CAES system integrated with renewable energy sources, economic evaluation and environmental impacts and final performance criteria for CAES system. A full scope of this study including the model development and validations, the process performance analysis for the CAES system integrated with the ORC to recover waste heat for efficiency improvement, performance investigation of the CAES system for wind power at design and off-design conditions to smooth the power flow of the grid. Furthermore, economic evaluations were performed for the integrated systems of the CAES system with ORC and the CAES system for wind power.

7.1.1 Model development and model validations

The study has been performed for model development in Aspen Plus® for the CAES system, ORC, compressors and turbines. The model validations were carried out with input parameters based on industrial operation considerations. The steady-state models for the charging and discharging processes of the CAES system were developed. The model validation and model comparison for the CAES system were carried out based on the real plant and reference system. A steady-state model for

ORC was developed for integrating with the model of the CAES system. The improved models for compressors and turbines developed based on the characteristic curves and model validations were also carried out. The pseudo-dynamic model for the cavern was developed in the Excel. These improved models were implemented for the process analysis of the CAES system in the context of the fluctuating wind power at design and off-design conditions.

7.1.2 The CAES system integrated with ORC

A technical performance analysis for the CAES system integrated with ORC was carried out to investigate the effects of different ORC work fluids and EIP of the ORC. The steady-state process model of the proposed CAES system integrated with the ORC was developed in Aspen Plus® with input parameters based on industrial operation considerations. The power output and operating temperature of ORC working fluids increase with the operating pressure, the ORC performance is also improved. The round-trip efficiency of the CAES system integrated with the ORC has been improved approximately by 3.32-3.95% with different working fluids in the ORC when compared with the CAES system without the ORC. R123 as the ORC working fluid has the best performance, the reason is R123 with a lower expander inlet pressure. Thus, the choice of an appropriate ORC working fluid should consider the factors of efficiency and safe operation for the integrated system, economics should be also considered as an essential factor for the power plants.

7.1.3 The CAES system for wind power

This study has also been performed for the CAES system for the fluctuating wind power. The CAES system at constant and variable shaft speed modes can utilise

excess wind electricity to store the compressed air and it can expand compressed air to generate electricity to smooth the fluctuating wind power with proposed different operating strategies. The range of air mass flow rate in the charging process of the CAES system at constant shaft speed mode was limited to be between 106.40 kg/s and 108 kg/s, which also results in a limitation of the utilisation range of electricity taken from wind power. The mass flow rate range of the compressed air at variable shaft speed mode was limited between 41.5 kg/s and 108 kg/s, which has a much wider range of the mass flow rate than that at constant shaft speed mode. The CAES system for wind power at variable shaft speed mode has better performance than at constant shaft speed mode. This is because the CAES system at variable shaft speed mode can utilise more excess wind power to store more compressed air into the cavern and generate more electricity for longer discharging time. The CAES system will be a promising approach for smoothing the fluctuating wind power.

7.1.4 Economic Evaluation

The economic evaluations for the CAES system integrated with the ORC and the CAES system for wind power were carried out by APEA. With free or low price off-peak electricity input, the LCOE for CAES plant is lower than the residential electricity price. The integrated system of the CAES system with ORC further decreases the LCOE. When the offshore wind farm or solar power plants are integrated with the CAES system integrated with ORC, their LCOEs could decrease which leads to a lower electricity sale price. As for the economic evaluation for the CAES system for wind power, the LCOE for the CAES system for wind power at variable shaft speed mode is lower than that at constant shaft speed mode and the

LCOE at both modes are lower than some renewable energies (e.g. offshore wind power and solar power), hydropower, nuclear power, some conventional powers (natural gas combustion turbine) and the residential electricity price. Thus, the CAES system not only addresses the problem of intermittency of fluctuating wind power, but also it can decrease the electricity price for renewable energy sources.

7.2 Recommendations for future work

The following points are recommended for future research of the CAES system:

- Presently, the technical performance analysis of the CAES system is based on the first law of thermodynamics. The exergetic analysis should be investigated to study exergy destruction, compare different CAES plants to design and operate and identify the equipment for efficiency improvement.
- As for the efficiency improvement of the CAES system, this study adopted the ORC to recover waste heat from the CAES system. Other approaches should be studied. For example, the TES system is discussed in many literatures with the round-trip efficiency, heat storage materials and modelling.
- The CAES models of this study have been limited to steady-state models and the steady-state performance analysis. In the future work, the dynamic models of the CAES systems and dynamic performance analysis should be considered.
- The preliminary design of a CAES system for wind power has been carried out based on the theoretical characteristic curves of the compressors and

turbines. Experimental study of the performance, dynamic modelling of the compressors and turbines should be further investigated, which can assure the reliability of the compressors and turbines.

- The improved model of the CAES system can be integrated with both ORC and wind power. The integrated system can not only improve the round-trip efficiency of the standalone CAES system, but also can curtail the intermittency problem of wind power.
- The recuperator of the CAES system is only implemented in the modelling and simulation with the consideration of temperature difference between the cold and hot fluids and pinch point. Further work about the design of the recuperator should be considered with the pressure loss, flow area (e.g. length and the number of tubes) for further optimisation.

References

Abbaspour, M., Satkin, M., Mohammadi-Ivatloo, B., Hoseinzadeh Lotfi, F., Noorollahi, Y. (2013). Optimal operation scheduling of wind power integrated with compressed air energy storage (CAES). *Renewable Energy*. **51**, 53–59.

Abedin, A.H., Rosen, M.A. (2012). Closed and open thermochemical energy storage: Energy- and exergy-based comparisons. *Energy*. **41**(1), 83–92.

ACRG (2005). Water cooled chiller. *Air Conditioning and Refrigeration Guide*. [online]. Available from: http://www.air-conditioning-and-refrigeration-guide.com/water-cooled-chiller.html [Accessed March 20, 2017].

AIRCAV (2008). Compressor Section. *AIRCAV*. [online]. Available from: http://www.aircav.com/gencompr.html [Accessed September 2, 2018].

Akhil, A.A., Huff, G., Currier, A.B., Hernandez, J., Bender, D.A., Kaun, B.C., Rastler, D.M., Chen, S.B., Cotter, A.L., Bradshaw, D.T., Gauntlett, W.D., Eyer, J., Olinsky-Paul, T., Ellison, M., Schoenung, S. (2016). *Electricity Storage Handbook in Collaboration with NRECA*. Albuquerque, NM, and Livermore, CA (United States).

Al-Malah, K.I.M. (2016). Introducing Aspen Plus. In *Aspen Plus®*. Hoboken, NJ, USA: John Wiley & Sons, Inc., pp. 1–47.

Amiryar, M., Pullen, K. (2017). A review of flywheel energy storage system technologies and their applications. *Applied Sciences*. **7**(3), 1–21.

Aneke, M., Agnew, B., Underwood, C. (2011). Performance analysis of the Chena binary geothermal power plant. *Applied Thermal Engineering*. **31**(10), 1825–1832.

Aneke, M., Wang, M. (2016). Energy storage technologies and real life applications – A state of the art review. *Applied Energy*. **179**, 350–377.

ApexCAES (2017). Bethel Energy Center. [online]. Available from:

http://www.apexcaes.com/project [Accessed April 22, 2018].

Arepalli, S., Fireman, H., Huffman, C., Moloney, P., Nikolaev, P., Yowell, K., Kim, K., Kohl, P.A., Higgins, C.D., Turano, S.P., Ready, W.J. (2005). Carbon-nanotube-based electrochemical double-layer capacitor technologies for spaceflight applications. *JOM*. **57**(12), 26–31.

Arfalk, E. (2014). How it works: centrifugal compressors. *The Compressed Air Blog*. [online]. Available from: https://www.thecompressedairblog.com/how-it-works-centrifugal-compressors [Accessed September 2, 2018].

Arfalk, E. (2017). Principles of the axial compressor. *The Compressed Air Blog*. [online]. Available from: https://www.thecompressedairblog.com/principles-of-the-axial-compressor [Accessed September 2, 2018].

Arsie, I., Marano, V., Rizzo, G., Moran, M. (2009). Integration of wind turbines with compressed air energy storage. In *AIP Conference Proceedings*. pp. 11–18.

ASHRAE (2014). Thermophysical properties of refrigerants. [online]. Available from: http://www.tmt.ugal.ro/crios/Support/IFPC1/Misc/SI_F09_Ch30.pdf.

AspenTech (2018a). Aspen Plus. [online]. Available from: https://www.aspentech.com/products/engineering/aspen-plus [Accessed September 10, 2018].

AspenTech (2018b). Aspen Process Economic Analyzer. [online]. Available from: https://www.aspentech.com/en/products/pages/aspen-process-economic-analyzer [Accessed September 10, 2018].

Atlas Copco (2018). So many types of air compressor. What's the difference? *Atlas Copco*. [online]. Available from: https://www.atlascopco.com/en-uk/compressors/compressed-air-tips/types-of-air-compressors [Accessed September 15, 2018].

Baker, J. (2008). New technology and possible advances in energy storage. *Energy Policy*. **36**(12), 4368–4373.

Barbour, E., Mignard, D., Ding, Y., Li, Y. (2015). Adiabatic compressed air energy storage with packed bed thermal energy storage. *Applied Energy*. **155**, 804–815.

Barnes, F.S., Levine, J.G. (2011). Compressed air enegy storage. In *Large energy storage systems handbook*. Boca Raton: CRC Press.

Beaudin, M., Zareipour, H., Schellenberg, A., Rosehart, W. (2014). Energy storage for mitigating the variability of renewable electricity sources. In *Energy Storage for Smart Grids: Planning and Operation for Renewable and Variable Energy Resources (VERs)*. pp. 1–33.

Bosio, F., Verda, V. (2015). Thermoeconomic analysis of a Compressed Air Energy Storage (CAES) system integrated with a wind power plant in the framework of the IPEX Market. *Applied Energy*. **152**, 173–182.

Bouman, E.A., Øberg, M.M., Hertwich, E.G. (2016). Environmental impacts of balancing offshore wind power with compressed air energy storage (CAES). *Energy*. **95**, 91–98.

Bouman, E.A., Øberg, M.M., Hertwich, E.G. (2013). Life cycle assessment of compressed air energy storage (CAES). In *6th international conference on life cycle management*. Gothenburg, Sweden.

Briola, S., Di Marco, P., Gabbrielli, R., Riccardi, J. (2016). A novel mathematical model for the performance assessment of diabatic compressed air energy storage systems including the turbomachinery characteristic curves. *Applied Energy*. **178**, 758–772.

British Refrigeration Association (2009). Guide to good commercial refrigeration practice part 2 system design and component selection. [online]. Available from: https://www.ior.org.uk/app/images/pdf/2-SystemDesignandComponentSelection.pdf.

Bronicki, L.Y., Elovic, A., Rettger, P. (1996). Experience with organic Rankine cycles in heat recovery power plants. In *American Power Conference*. Chicago, USA.

Budt, M., Wolf, D., Span, R., Yan, J. (2016). A review on compressed air energy storage: Basic principles, past milestones and recent developments. *Applied Energy*. **170**, 250–268.

Bullough, C. (2004). AA-CAES: integration of wind energy. [online]. Available from: https://www.slideserve.com/colin/aa-caes-integration-of-wind-energy-dr-chris-bullough [Accessed April 23, 2018].

Butcher, di C. (2010). L'utilizzo su larga scala dell'energia rinnovabile potrebbe dipendere dalla capacità di immagazzinare l'elettricità. [online]. Available from: https://lucaniaelettrica.wordpress.com/2010/05/11/immagazzinare-le-energie-rinnovabili/ [Accessed June 7, 2017].

Canepa, R., Wang, M., Biliyok, C., Satta, A. (2013). Thermodynamic analysis of combined cycle gas turbine power plant with post-combustion CO2 capture and exhaust gas recirculation. *Proceedings of the Institution of Mechanical Engineers, Part E: Journal of Process Mechanical Engineering*. **227**(2), 89–105.

Carrasco, J.M., Franquelo, L.G., Bialasiewicz, J.T., Galvan, E., PortilloGuisado, R.C., Prats, M.A.M., Leon, J.I., Moreno-Alfonso, N. (2006). Power-electronic systems for the grid integration of renewable energy sources: a survey. *IEEE Transactions on Industrial Electronics*. **53**(4), 1002–1016.

Castillo, A., Gayme, D.F. (2014). Grid-scale energy storage applications in renewable energy integration: A survey. *Energy Conversion and Management*. **87**, 885–894.

Cavallo, A. (2007). Controllable and affordable utility-scale electricity from intermittent wind resources and compressed air energy storage (CAES). *Energy*. **32**(2), 120–127.

Cen, K., Chi, Y., Yan, J. (2009). *Challenges of power engineering and*

environment: proceedings of the International Conference on Power Engineering 2007. Springer Science & Business Media.

Chan, C.W., Ling-Chin, J., Roskilly, A.P. (2013). Reprint of "A review of chemical heat pumps, thermodynamic cycles and thermal energy storage technologies for low grade heat utilisation". *Applied Thermal Engineering*. **53**(2), 160–176.

Chen, H., Cong, T.N., Yang, W., Tan, C., Li, Y., Ding, Y. (2009). Progress in electrical energy storage system: A critical review. *Progress in Natural Science*. **19**(3), 291–312.

Chen, H., Goswami, D.Y., Stefanakos, E.K. (2010). A review of thermodynamic cycles and working fluids for the conversion of low-grade heat. *Renewable and Sustainable Energy Reviews*. **14**(9), 3059–3067.

Chen, H., Tan, C., Liu, J., Zhang, X. (2013). Compressed air energy storage. In *Energy Storage -Technologies and Applications*. INTECH, pp. 101–112.

Chen, M., Sofia, M.S., Afshin, I. (2016). Torque-assisting Compressed Air Energy Storage hydraulic wind drivetrains. In *2016 IEEE Power and Energy Conference at Illinois (PECI)*. IEEE, pp. 1–5.

Crotogino, F., Mohmeyer, K.-U., Scharf, R. (2001). Huntorf CAES: More than 20 years of successful operation. *Orlando, Florida, USA*.

Dai, Y., Wang, J., Gao, L. (2009). Parametric optimization and comparative study of organic Rankine cycle (ORC) for low grade waste heat recovery. *Energy Conversion and Management*. **50**(3), 576–582.

Denholm, P., Holloway, T. (2005). Improved accounting of emissions from utility energy storage system operation. *Environmental science & technology*. **39**(23), 9016–9022.

Denholm, P., Kulcinski, G.L. (2004). Life cycle energy requirements and greenhouse gas emissions from large scale energy storage systems. *Energy Conversion and Management*. **45**(13–14), 2153–2172.

Denholm, P., Kulcinski, G.L., Holloway, T. (2005). Emissions and energy efficiency assessment of baseload wind energy systems. *Environmental science & technology*. **39**(6), 1903–1911.

Denholm, P., Sioshansi, R. (2009). The value of compressed air energy storage with wind in transmission-constrained electric power systems. *Energy Policy*. **37**(8), 3149–3158.

Desai, N.B., Bandyopadhyay, S. (2009). Process integration of organic Rankine cycle. *Energy*. **34**(10), 1674–1686.

Desai, N.B., Bandyopadhyay, S. (2016). Thermo-economic comparisons between solar steam Rankine and organic Rankine cycles. *Applied Thermal Engineering*. **105**, 862–875.

Díaz-González, F., Sumper, A., Gomis-Bellmunt, O., Villafáfila-Robles, R. (2012). A review of energy storage technologies for wind power applications. *Renewable and Sustainable Energy Reviews*. **16**(4), 2154–2171.

DM Energy (2011). *Wind turbine grid connection and interaction*. Lewes, UK.

DOE (2018). How do wind turbines work. *Department of Energy*. [online]. Available from: https://www.energy.gov/eere/wind/how-do-wind-turbines-work [Accessed September 3, 2018].

Dreißigacker, V., Zunft, S., Müller-Steinhagen, H. (2013). A thermo-mechanical model of packed-bed storage and experimental validation. *Applied Energy*. **111**, 1120–1125.

EIA (2016). Electric Power Monthly. *U.S. Energy Information Administration*. [online]. Available from: https://www.eia.gov/electricity/monthly/epm_table_grapher.cfm?t=epmt_5_6_a [Accessed January 20, 2017].

EIRGRID GROUP (2017). Northern Ireland - actual and forecast wind. [online]. Available from: http://www.eirgridgroup.com/how-the-grid-works/system-

information/ [Accessed June 7, 2017].

El-Wakil, M.M. (1984). *Powerplant technology*. Tata McGraw-Hill Education.

Elmegaard, B., Brix, W. (2011). Efficiency of compressed air energy storage. In *24th International Conference on Efficiency, Cost, Optimization, Simulation and Environmental Impact of Energy Systems*.

Elmegaard, B., Szameitat, N., Brix, W. (2005). Compressed air energy storage (CAES) - possibilities in Denmark. In *Proceedings of ECOS 2005*.

Enerdata (2017). World Power consumption. [online]. Available from: https://yearbook.enerdata.net/electricity/electricity-domestic-consumption-data.html [Accessed June 25, 2018].

Energy Storage R&D Center, C.A. of S. (2016). 10MW advanced compressed air energy storage system. [online]. Available from: http://english.iet.cas.cn/Institute/6/ [Accessed February 1, 2018].

EnggCyclopedia (2012). Axial and centrifugal-type compressors. [online]. Available from: http://www.enggcyclopedia.com/2012/03/axial-centrifugal-type-compressors/ [Accessed May 30, 2018].

Enis, B.M., Lieberman, P., Rubin, I. (2003). Operation of hybrid wind-turbine compressed-air system for connection to electric grid networks and cogeneration. *Wind Engineering*. **27**(6), 449–459.

ESA (2017). Compressed Air Energy Storage (CAES). *Energy Storage Association*. [online]. Available from: http://energystorage.org/compressed-air-energy-storage-caes [Accessed September 1, 2018].

Escalante, E., Junior, J. de C., Balestieri, J. (2017). Effect of working fluids on organic Rankine cycle for the recovery of low-grade waste heat. In *The 12th Latin-American Congress on Electricity Generation and Transmission*.

Espinar, B., Mayer, D. (2011). *The Role of Energy Storage for Mini-Grid*

Stabilization.

Ferreira, H.L., Garde, R., Fulli, G., Kling, W., Lopes, J.P. (2013). Characterisation of electrical energy storage technologies. *Energy*. **53**, 288–298.

FirstEnergy Generation Corp (2009). FirstEnergy acquires rights to norton energy storage project. [online]. Available from: https://www.nrc.gov/docs/ML1036/ML103620057.pdf [Accessed April 18, 2018].

Freeman, J., Hellgardt, K., Markides, C.N. (2015). An assessment of solar-powered organic Rankine cycle systems for combined heating and power in UK domestic applications. *Applied Energy*. **138**, 605–620.

Gaelectric (2011) Project-CAES Larne, NI. [online]. Available from: http://www.project-caeslarne.co.uk/ [Accessed April 19, 2018].

Grazzini, G., Milazzo, A. (2008). Thermodynamic analysis of CAES/TES systems for renewable energy plants. *Renewable Energy*. **33**(9), 1998–2006.

Greenblatt, J.B., Succar, S., Denkenberger, D.C., Williams, R.H., Socolow, R.H. (2007). Baseload wind energy: modeling the competition between gas turbines and compressed air energy storage for supplemental generation. *Energy Policy*. **35**(3), 1474–1492.

Guo, C., Xu, Y., Zhang, X., Guo, H., Zhou, X., Liu, C., Qin, W., Li, W., Dou, B., Chen, H. (2017). Performance analysis of compressed air energy storage systems considering dynamic characteristics of compressed air storage. *Energy*. **135**, 876–888.

Guo, H., Xu, Y., Chen, H., Zhou, X. (2016). Thermodynamic characteristics of a novel supercritical compressed air energy storage system. *Energy Conversion and Management*. **115**, 167–177.

Hadjipaschalis, I., Poullikkas, A., Efthimiou, V. (2009). Overview of current and future energy storage technologies for electric power applications. *Renewable and Sustainable Energy Reviews*. **13**(6–7), 1513–1522.

Hartmann, N., Vöhringer, O., Kruck, C., Eltrop, L. (2012). Simulation and analysis of different adiabatic Compressed Air Energy Storage plant configurations. *Applied Energy*. **93**, 541–548.

Hasan, N.S., Hassan, M.Y., Majid, M.S., Rahman, H.A. (2012). Mathematical model of compressed air energy storage in smoothing 2MW wind turbine. In *Power Engineering and Optimization Conference*. pp. 339–343.

Haugen, D. (2012). Scrapped Iowa project leaves energy storage lessons. *Midwest Energy News*. [online]. Available from: https://energynews.us/midwest/scrapped-iowa-project-leaves-energy-storage-lessons/ [Accessed April 10, 2018].

He, W., Luo, X., Evans, D., Busby, J., Garvey, S., Parkes, D., Wang, J. (2017). Exergy storage of compressed air in cavern and cavern volume estimation of the large-scale compressed air energy storage system. *Applied Energy*. **208**, 745–757.

Hoffeins, H. (1994). Huntorf air storage gas turbine power plant. *Energy supply, Brown Boveri Publication DGK*. **90**, 1–14.

Holloway, M. (2016). The Texas energy storage market: a four-part examination. [online]. Available from: https://www.emergingenergyinsights.com/2016/10/texas-energy-storage-market-four-part-examination-3/ [Accessed April 22, 2018].

Huang, Y., Keatley, P., Chen, H.S., Zhang, X.J., Rolfe, A., Hewitt, N.J. (2017). Techno-economic study of compressed air energy storage systems for the grid integration of wind power. *International Journal of Energy Research*. **42**, 559–569.

Ibrahim, H., Ilinca, A., Perron, J. (2008). Energy storage systems—Characteristics and comparisons. *Renewable and Sustainable Energy Reviews*. **12**(5), 1221–1250.

Ibrahim, H., Younès, R., Ilinca, A., Dimitrova, M., Perron, J. (2010). Study and design of a hybrid wind-diesel-compressed air energy storage system for

remote areas. *Applied Energy*. **87**(5), 1749–1762.

IEA (2017). Energy snapshot. *International Energy Agency*. [online]. Available from: https://www.iea.org/newsroom/energysnapshots/oecd-electricity-production-by-source-1974-2016.html [Accessed August 29, 2018].

ITACA (2018). How lead-acid batteries work. [online]. Available from: http://www.itacanet.org/a-guide-to-lead-acid-battries/part-1-how-lead-acid-batteries-work/ [Accessed July 4, 2018].

Jubeh, N.M., Najjar, Y.S.H. (2012). Green solution for power generation by adoption of adiabatic CAES system. *Applied Thermal Engineering*. **44**, 85–89.

Kahrobaee, S., Asgarpoor, S. (2013). Optimum planning and operation of compressed air energy storage with wind energy integration. In *North American Power Symposium (NAPS)*. pp. 1–6.

Kaiser, F. (2015). Steady state analyse of existing compressed air energy storage plants. *Power and Energy Student Summit (PESS) 2015, January 13th-14th, Dortmund Germany*.

Kala, B. (2011). model aircraft: the axial flow compressor. [online]. Available from: http://aeromodelbasic.blogspot.com/2011/12/axial-flow-compressor.html [Accessed September 2, 2018].

Kalhammer, F.R., Schneider, T.R. (1976). Energy storage. *Annual Review of Energy*. **1**(1), 311–343.

Kalyani, V.M., Nithya, C., Roselyn, J.P., Ramana, P.V. (2016). Performance of grid connected dfig wind turbine with PI and fuzzy controllers along with crowbar control for enhancing fault ride through capability. *IJCTA*. **9**(15), 7119–7135.

Karellas, S., Tzouganatos, N. (2014). Comparison of the performance of compressed-air and hydrogen energy storage systems: Karpathos island case study. *Renewable and Sustainable Energy Reviews*. **29**, 865–882.

Kluiters, E.C., Schmal, D., ter Veen, W.R., Posthumus, K.J.C.. (1999). Testing of a sodium/nickel chloride (ZEBRA) battery for electric propulsion of ships and vehicles. *Journal of Power Sources*. **80**(1–2), 261–264.

Kondoh, J., Ishii, I., Yamaguchi, H., Murata, A., Otani, K., Sakuta, K., Higuchi, N., Sekine, S., Kamimoto, M. (2000). Electrical energy storage systems for energy networks. *Energy Conversion and Management*. **41**(17), 1863–1874.

Kosi, F.F., Zivkovic, B., Komatina, M., Antonijevic, D., Galil, M.A., Milovancevic, U. (2015). Cold thermal energy storage. In *Handbook of Research on Advances and Applications in Refrigeration Systems and Technologies*. IGI Global.

Kousksou, T., Bruel, P., Jamil, A., El Rhafiki, T., Zeraouli, Y. (2014). Energy storage: Applications and challenges. *Solar Energy Materials and Solar Cells*. **120**, 59–80.

Kraftwerk, F. (2018). The difference between steam and gas turbines. [online]. Available from: http://kraftwerkforschung.info/en/quickinfo/basic-concepts/the-difference-between-steam-and-gas-turbines/ [Accessed May 30, 2018].

Krupke, C., Wang, J., Clarke, J., Luo, X. (2017). Modeling and experimental study of a wind turbine system in hybrid connection with compressed air energy storage. *IEEE Transactions on Energy Conversion*. **32**(1), 137–145.

Kutscher, C. (2001). Small-scale geothermal power plant field verification projects. *Transactions-Geothermal Resources Council*, 577–580.

LAZARD (2014). LAZARD's levelized cost of energy analysis — version 8.0. [online]. Available from: https://www.lazard.com/media/1777/levelized_cost_of_energy_-_version_80.pdf [Accessed April 20, 2018].

Li, S., Dai, Y. (2015). Design and Simulation Analysis of a Small-Scale Compressed Air Energy Storage System Directly Driven by Vertical Axis

Wind Turbine for Isolated Areas. *Journal of Energy Engineering*. **141**(4), 1–11.

van der Linden, S. (2007). Review of CAES systems development and current innovations. In *Electrical Energy Storage Applications & Technology (EESAT) Conference*. San Franncisco.

Liu, B.-T., Chien, K.-H., Wang, C.C. (2004). Effect of working fluids on organic Rankine cycle for waste heat recovery. *Energy*. **29**(8), 1207–1217.

Liu, C., He, C., Gao, H., Xie, H., Li, Y., Wu, S., Xu, J. (2013). The environmental impact of organic Rankine cycle for waste heat recovery through life-cycle assessment. *Energy*. **56**, 144–154.

Liu, W., Liu, L., Zhou, L., Huang, J., Zhang, Y., Xu, G., Yang, Y. (2014). Analysis and optimization of a compressed air energy storage—combined cycle system. *Entropy*. **16**(6), 3103–3120.

Liu, X., Chen, J., Luo, X., Wang, M., Meng, H. (2015). Study on heat integration of supercritical coal-fired power plant with post-combustion CO2 capture process through process simulation. *Fuel*. **158**, 625–633.

Liu, Y., Woo, C.K., Zarnikau, J. (2017). Wind generation's effect on the ex post variable profit of compressed air energy storage: Evidence from Texas. *Journal of Energy Storage*. **9**, 25–39.

Lobera, D., Foley, A. (2012). Modelling gas storage with compressed air energy storage in a system with large wind penetrations. In *7th Conference on Sustainable Development of Energy, Water and Environment Systems*. pp. 1–13.

Lund, H., Salgi, G. (2009). The role of compressed air energy storage (CAES) in future sustainable energy systems. *Energy Conversion and Management*. **50**(5), 1172–1179.

Luo, X. (2016). Process modelling, simulation and optimisation of natural gas combined cycle power plant integrated with carbon capture, compression

and transport. *PhD Thesis*, University of Hull, UK.

Luo, X., Wang, J., Dooner, M., Clarke, J. (2015). Overview of current development in electrical energy storage technologies and the application potential in power system operation. *Applied Energy*. **137**, 511–536.

Luo, X., Wang, J., Dooner, M., Clarke, J., Krupke, C. (2014). Overview of current development in compressed air energy storage technology. *Energy Procedia*. **62**, 603–611.

Luo, X., Wang, J., Krupke, C., Wang, Y., Sheng, Y., Li, J., Xu, Y., Wang, D., Miao, S., Chen, H. (2016). Modelling study, efficiency analysis and optimisation of large-scale Adiabatic Compressed Air Energy Storage systems with low-temperature thermal storage. *Applied Energy*. **162**, 589–600.

Luo, X., Wang, M. (2017). Study of solvent-based carbon capture for cargo ships through process modelling and simulation. *Applied Energy*. **195**, 402–413.

Luo, X., Wang, M., Oko, E., Okezue, C. (2014). Simulation-based techno-economic evaluation for optimal design of CO2 transport pipeline network. *Applied Energy*. **132**, 610–620.

Macaoenergy (2013). Macaoenergy Industry. *Macaoenergy Industry Park Development Co. Ltd*. [online]. Available from: http://www.macaoenergy.com/ [Accessed April 11, 2018].

Marano, V., Rizzo, G., Tiano, F.A. (2012). Application of dynamic programming to the optimal management of a hybrid power plant with wind turbines, photovoltaic panels and compressed air energy storage. *Applied Energy*. **97**, 849–859.

Mason, J.E., Archer, C.L. (2012). Baseload electricity from wind via compressed air energy storage (CAES). *Renewable and Sustainable Energy Reviews*. **16**(2), 1099–1109.

McGrail, B.P., Cabe, J.E., Davidson, C.L., Knudsen, F.S., Bacon, D.H., Bearden,

M.D., Charmness, M.A., Horner, J.A., Reidel, S.P., Schaef, H.T., Spane, F.A., Thorne, P.D. (2013). *Technoeconomic Performance Evaluation of Compressed Air Energy Storage in the Pacific Northwest*. Washington.

mech4study (2017). Centrifugal compressor: principle, construction, working, types, advantages, disadvantages with its application. [online]. Available from: http://www.mech4study.com/2017/11/centrifugal-compressor.html [Accessed September 2, 2018].

Mohammadi, A., Ahmadi, M.H., Bidi, M., Joda, F., Valero, A., Uson, S. (2017). Exergy analysis of a Combined Cooling, Heating and Power system integrated with wind turbine and compressed air energy storage system. *Energy Conversion and Management*. **131**, 69–78.

Mozayeni, H., Negnevitsky, M., Wang, X., Cao, F., Peng, X. (2017). Performance study of an advanced adiabatic compressed air energy storage system. *Energy Procedia*. **110**, 71–76.

Najjar, Y.S.H., Jubeh, N.M. (2006). Comparison of performance of compressed-air energy-storage plant with compressed-air storage with humidification. *Proceedings of the Institution of Mechanical Engineers, Part A: Journal of Power and Energy*. **220**(6), 581–588.

Nakashima, M., Kato, H., Takaoka, E. (1992). Development of real-time pseudo dynamic testing. *Earthquake Engineering & Structural Dynamics*, 21(1), 79-92.

Ni, W., Chen, Z. (2011). Synergistic utilization of coal and other energy — Key to low carbon economy. *Frontiers in Energy*. **5**(1), 1–19.

Nikolaidis, P., Poullikkas, A. (2017) A comparative review of electrical energy storage systems for better sustainability. *Journal of Power Technologies*. **97**(3), 220–245.

OpenEI (2015). Transparent cost database. [online]. Available from: http://en.openei.org/apps/TCDB/#blank [Accessed May 10, 2018].

Pacific Power (2017). Time of use hours & pricing. [online]. Available from: https://www.pacificpower.net/ya/po/otou/ooh.html [Accessed January 20, 2017].

Pan, Z., Lin, G., Wang, J., Dai, Y. (2016). Energy efficiency analysis and off-design analysis of two different discharge modes for compressed air energy storage system using axial turbines. *Renewable Energy*. **85**, 1164–1177.

Pardo, P., Deydier, A., Anxionnaz-Minvielle, Z., Rougé, S., Cabassud, M., Cognet, P. (2014). A review on high temperature thermochemical heat energy storage. *Renewable and Sustainable Energy Reviews*. **32**, 591–610.

Pena-Alzola, R., Sebastian, R., Quesada, J., Colmenar, A. (2011). Review of flywheel based energy storage systems. In *2011 International Conference on Power Engineering, Energy and Electrical Drives*. IEEE, pp. 1–6.

Pezzuolo, A., Benato, A., Stoppato, A., Mirandola, A. (2016) .The ORC-PD: A versatile tool for fluid selection and Organic Rankine Cycle unit design. *Energy*. **102**, 605–620.

Pickard, W.F., Hansing, N.J., Shen, A.Q. (2009). Can large-scale advanced-adiabatic compressed air energy storage be justified economically in an age of sustainable energy? *Journal of Renewable and Sustainable Energy*. **1**(3).

Pimm, A.J. (2011). *Analysis of flexible fabric structures*. The University of Nottingham.

Poling, B.E., Prausnitz, J.M., O 'connell, J.P., York, N., San, C., Lisbon, F., Madrid, L., City, M., New, M., San, D., Singapore, J.S., Toronto, S. (2001). *The Properties of Gases and Liquids Mcgraw-Hill*.

PowerSouth Electric Cooperative (2017). Compressed air energy storage. *PowerSouth Electric Cooperative*. [online]. Available from: http://www.powersouth.com/wp-content/uploads/2017/07/CAES-Brochure-FINAL.pdf [Accessed April 23, 2018].

Quoilin, S., Broek, M. Van Den, Declaye, S., Dewallef, P., Lemort, V. (2013).

Techno-economic survey of Organic Rankine Cycle (ORC) systems. *Renewable and Sustainable Energy Reviews*. **22**, 168–186.

Radcliffe, J. (2013). Energy storage technologies. *Ingenia*, Issue 54: 27-32.

Ragheb, M. (2014). *Components of wind machines*. Urbana, USA.

Riaz, M.A. (2010). *Feasibility of compressed air energy storage to store wind on monthly and daily basis*. Iowa State University.

Rice, A.T., Li, P.Y. (2011). Optimal efficiency-power tradeoff for an air motor/compressor with volume varying heat transfer capability. In *ASME 2011 Dynamic Systems and Control Conference and Bath/ASME Symposium on Fluid Power and Motion Control, Volume 1*. ASME, pp. 145–152.

Robb, D. (2011). The CAES for wind. *Renewable Energy Focus*. **12**(1), 18–19.

Roy, P., Srivastava, S.K. (2015). Nanostructured anode materials for lithium ion batteries. *Journal of Materials Chemistry A*. **3**(6), 2454–2484.

Ruiz, I.B. (2016). Hydrogen and wind: Allies for sustainable energy. *DW*. [online]. Available from: https://www.dw.com/en/hydrogen-and-wind-allies-for-sustainable-energy/a-19330382 [Accessed July 6, 2018].

RWE (2013). ADELE–adiabatic compressed-air energy storage for electricity supply. *RWE Power AG, Essen/Koln*.

Ryan, C. (2017). Hydrostor launches new Terra bulk energy storage system. *Energy Storage News*. [online]. Available from: https://www.energy-storage.news/news/hydrostor-launches-new-terra-bulk-energy-storage-system [Accessed July 2, 2018].

Saadat, M., Shirazi, F.A., Li, P.Y. (2015). Modeling and control of an open accumulator Compressed Air Energy Storage (CAES) system for wind turbines. *Applied Energy*. **137**, 603–616.

Safaei, H., Keith, D.W., Hugo, R.J. (2013). Compressed air energy storage (CAES) with compressors distributed at heat loads to enable waste heat

utilization. *Applied Energy*. **103**, 165–179.

Salgi, G., Lund, H. (2008). System behaviour of compressed-air energy-storage in Denmark with a high penetration of renewable energy sources. *Applied Energy*. **85**(4), 182–189.

Schoenung, S.M. (2001). *Characteristics and Technologies for Long- vs. Short-Term Energy Storage: A Study by the DOE Energy Storage Systems Program*. Albuquerque, NM, and Livermore, CA: Sandia National Laboratories.

Schulte, R.H., Critelli Jr, N., Holst, K., Huff, G. (2012). Lessons from Iowa: development of a 270 megawatt compressed air energy storage project in Midwest independent system operator. *Sandia National Laboratories, Albuquerque*.

Schüth, F. (2012). Energy storage strategies. In *Chemical Energy Storage*. pp. 35–48.

Sciacovelli, A., Li, Y., Chen, H., Wu, Y., Wang, J., Garvey, S., Ding, Y. (2017). Dynamic simulation of Adiabatic Compressed Air Energy Storage (A-CAES) plant with integrated thermal storage – Link between components performance and plant performance. *Applied Energy*. **185**, 16–28.

Sedighnejad, H. (2011). Performance evaluation of a hybrid wind-diesel-compressed air energy storage system. In *Electrical and Computer Engineering (CCECE), 2011 24th Canadian Conference*. IEEE, pp. 270–273.

Seltzer, M.A. (2017). Why salt is this power plant's most valuable asset. [online]. Available from: https://www.smithsonianmag.com/innovation/salt-power-plant-most-valuable-180964307/ [Accessed April 23, 2018].

Sharma, A., Tyagi, V.V., Chen, C.R., Buddhi, D. (2009). Review on thermal energy storage with phase change materials and applications. *Renewable and Sustainable Energy Reviews*. **13**(2), 318–345.

Simpore, S., Garde, F., David, M., Marc, O., Castaing-Lasvignottes, J. (2016). Design and dynamic simulation of a compressed air energy storage system (CAES) coupled with a building, an electric grid and photovoltaic power plant. In *CLIMA 2016*. Aalborg, Denmark.

Sioshansi, R., Denholm, P., Jenkin, T. (2011). A comparative analysis of the value of pure and hybrid electricity storage. *Energy Economics*. **33**(1), 56–66.

Skea, J., Nishioka, S. (2008). Policies and practices for a low-carbon society. *Climate Policy*. **8**(sup1), S5–S16.

Smith, S.C., Sen, P.K., Kroposki, B. (2008). Advancement of energy storage devices and applications in electrical power system. In *2008 IEEE Power and Energy Society General Meeting - Conversion and Delivery of Electrical Energy in the 21st Century*. IEEE, pp. 1–8.

Succar, S., Williams, R.H. (2008). Compressed air energy storage: theory, resources, and applications for wind power. *Princeton environmental institute report*. **8**.

Sulaiman, N.S. (2018). Scale-up of chemical engineering process. [online]. Available from: http://ocw.ump.edu.my/pluginfile.php/6764/mod_resource/content/4/Chapter 1.pdf [Accessed September 15, 2018].

Sun, H., Luo, X., Wang, J. (2015). Feasibility study of a hybrid wind turbine system–Integration with compressed air energy storage. *Applied Energy*. **137**, 617–628.

Sun, H., Luo, X., Wang, J. (2011). Management and control strategy study for a new hybrid wind turbine system. In *Decision and Control and European Control Conference (CDC-ECC), 50th IEEE Conference*. IEEE, pp. 3671–3676.

Sundararagavan, S., Baker, E. (2012). Evaluating energy storage technologies for wind power integration. *Solar Energy*. **86**(9), 2707–2717.

Swider, D.J. (2007). Compressed air energy storage in an electricity system with significant wind power generation. *IEEE Transactions on Energy Conversion*. **22**(1), 95–102.

Tartière, T., Obert, B., Sanchez, L. (2013). Thermo-economic optimization of subcritical and transcritical ORC systems. In *ASME ORC 2013–International seminar on ORC power systems*.

Tchanche, B.F., Lambrinos, G., Frangoudakis, A., Papadakis, G. (2011). Low-grade heat conversion into power using organic Rankine cycles – A review of various applications. *Renewable and Sustainable Energy Reviews*. **15**(8), 3963–3979.

The Engineering Toolbox (2018). Ideal Gas Law. [online]. Available from: https://www.engineeringtoolbox.com/ideal-gas-law-d_157.html [Accessed November 26, 2018].

UEI (2016). Natural gas. *Administration, U.S Energy Information*. [online]. Available from: https://www.eia.gov/dnav/ng/hist/n3035us3M.htm [Accessed January 20, 2017].

USDOE (2015). Levelized cost of energy (LCOE). U.S. Department of Energy. [online]. Available from: https://www.energy.gov/sites/prod/files/2015/08/f25/LCOE.pdf [Accessed November 29, 2018]

Vélez, F., Segovia, J.J., Martín, M.C., Antolín, G., Chejne, F., Quijano, A. (2012). A technical, economical and market review of organic Rankine cycles for the conversion of low-grade heat for power generation. *Renewable and Sustainable Energy Reviews*. **16**(6), 4175–4189.

Venkataramani, G., Parankusam, P., Ramalingam, V., Wang, J. (2016). A review on compressed air energy storage – A pathway for smart grid and polygeneration. *Renewable and Sustainable Energy Reviews*. **62**, 895–907.

Wang, J. (2017). Overview of compressed air energy storage and technology development. *Energies*. **10**(7), 1–22.

Wang, J., Yan, Z., Wang, M., Ma, S., Dai, Y. (2013). Thermodynamic analysis and optimization of an (organic Rankine cycle) ORC using low grade heat source. *Energy*. **49**, 356–365.

Wang, M., Wang, J., Zhao, Y., Zhao, P., Dai, Y. (2013). Thermodynamic analysis and optimization of a solar-driven regenerative organic Rankine cycle (ORC) based on flat-plate solar collectors. *Applied Thermal Engineering*. **50**(1), 816–825.

Wang, S., Zhang, X., Yang, L., Zhou, Y., Wang, J. (2016). Experimental study of compressed air energy storage system with thermal energy storage. *Energy*. **103**, 182–191.

WINGAS (2017). Natural gas is the most climate-friendly fossil fuel in electricity production. [online]. Available from: https://www.wingas.com/fileadmin/Wingas/WINGAS-Studien/Energieversorgung_und_Energiewende_en.pdf [Accessed July 9, 2017].

Wolf, D. (2011). *Methods for Design and Application of Adiabatic Compressed Air Energy: Storage Based on Dynamic Modeling*. Laufen.

Wolf, D., Budt, M. (2014). LTA-CAES – A low-temperature approach to Adiabatic Compressed Air Energy Storage. *Applied Energy*. **125**, 158–164.

Yoshimoto, K., Nanahara, T. (2005). Optimal daily operation of electric power systems with an ACC-CAES generating system. *Electrical Engineering in Japan*. **152**(1), 15–23.

Zaloudek, F.R., Reilly, R.W. (1982). An assessment of second-generation compressed-air energy-storage concepts. *NASA STI/Recon Technical Report*.

Zhang, Y., Xu, Y., Zhou, X., Guo, H., Zhang, X., Chen, H. (2017). Compressed air energy storage system with variable configuration for wind power generation. *Energy Procedia*. **142**, 3356–3362.

Zhang, Y., Yang, K., Li, X., Xu, J. (2013). The thermodynamic effect of thermal energy storage on compressed air energy storage system. *Renewable Energy*. **50**, 227–235.

Zhao, H., Wu, Q., Hu, S., Xu, H., Rasmussen, C.N. (2015). Review of energy storage system for wind power integration support. *Applied Energy*. **137**, 545–553.